UNIVERSITÉ DE SHERBROOKE
Faculté de génie
Département de génie mécanique

Analyse et optimisation d'un cycle organique de Rankine Intégré avec un éjecteur monophasé

Analysis and Optimization of an Organic Rankine Cycle Integrated with One-Phase Ejector

Thèse de doctorat
Spécialité: génie mécanique

Doctoral Thesis
Specialty: Mechanical Engineering

Payam Haghparast

Jury :
Mikhail Sorin (Supervisor)
Sébastien Poncet (Examiner)
Mathieu Picard (Examiner)
Mehdi Falsafioon (Examiner)

Sherbrooke (Québec) Canada December 2018

RÉSUMÉ

L'intérêt pour la récupération de chaleur à faible temperature a augmenté au cours des dix dernières années en raison de la préoccupation croissante face à la pénurie d'énergie et au réchauffement climatique. Etant donné que les cycles de production de vapeur classiques ne permettaient pas souvent de récupérer efficacement de la chaleur perdue de faible qualité, de nombreuses solutions nouvelles ont été suggérées afin de produire de l'électricité à partir des sources de chaleur à basse température, telles que le biogaz, la géothermie, le solaire, les gaz d'échappement, etc.
Parmi ceux-ci, les cycles de Rankine organiques (ORC) semblent être les procédés les plus prometteurs et les plus largement appliqués. Dans un tel système, le fluide de travail est un composant organique, mieux adapté que l'eau pour les faibles températures de source de chaleur. Contrairement aux cycles de puissance traditionnels, cette technologie permet aussi de générer de l'électricité à petite échelle. D'autre part, la faible efficacité du cycle de Rankine organique (ORC) avec une source de chaleur de faible teneur (LGHS) a limité son utilisation dans l'industrie. Afin d'augmenter la capacité et la performance de la puissance de sortie, une nouvelle structure du cycle de Rankine organique intégré à un éjecteur (EORC) a été proposée dans le cadre de ce projet. Les éjecteurs sont des dispositifs simples dans lesquels l'énergie d'un flux est utilisée pour entraîner et augmenter la pression d'un flux secondaire par mélange direct. Ils sont utilisés en raison de leur fonctionnement simple, de leur faible entretien et de l'absence de pièces mobiles. Étant donné que l'impact des caractéristiques de fonctionnement de l'éjecteur et de sa géométrie est important pour optimiser la conception d'un système EROC, trois documents publiés ont examiné en détail l'amélioration des performances de l'éjecteur. Dans un premier lieu, un modèle 1D d'éjecteur complet a été préparé en considérant la meilleure hypothèse de choc normal et le choix de l'efficacité locale qui constituent deux des plus grandes sources d'erreur dans les modèles 1D. Un grand nombre de simulations CFD ont été effectuées. Les résultats ont été validés et comparés avec d'autres modèles 1D et des données expérimentales, dans le but d'analyser les flux d'exergie interne d'un éjecteur et pour extraire les valeurs des efficacités isentropiques, polytropiques, une contre-pression critique et un rapport d'entraînement. Des études numériques et expérimentales sur les éjecteurs ont révélé que le remplacement des efficacités isentropiques par des efficacités polytropiques dans les modèles d'éjecteurs 1D fournit des résultats plus précis. Les rendements polytropiques permettent d'accéder plus précisément aux effets de la variation du rapport de pression sur les irréversibilités des processus d'accélération et de décélération. Il a été démontré que la déviation de la longueur de conduit à surface constante, calculée en utilisant un rendement isentropique par rapport à la longueur réelle, est trois fois supérieure à celle calculée en utilisant un rendement polytropique. De plus, des résultats expérimentaux ont montré que les meilleures performances de l'éjecteur et par conséquent du cycle étaient atteintes pour le rapport de pression maximal au point critique de la température du condenseur. A cette condition, les pertes d'exergie interne de l'éjecteur sont minimes selon les études numériques effectuées. Enfin, après une étude approfondie sur le comportement des éjecteurs, dans la quatrième publication, un éjecteur approprié (fonctionnant en régime de double étranglement) est utilisé pour améliorer les performances du EORC. Il a été démontré qu'une augmentation du rapport de la surface de l'éjecteur, du débit massique secondaire ainsi qu'une diminution du diamètre de la gorge et des propriétés de l'éjecteur d'entrée ont des effets significatifs sur l'augmentation de la puissance nette. En outre, il a été constaté que la production d'électricité est indépendante des paramètres de sortie de l'éjecteur en mode On-Design.

Mots-clés: Optimisation; Cycle organique de Rankine; Éjecteur; Modèle thermodynamique; Modèle CFD; Étude expérimentale; Efficacité polytropique; Dimensions de l'éjecteur.

Abstract

The interest for low grade heat recovery has been growing for the last ten years because of the increasing concern over energy shortage and global warming. Since conventional steam power cycles cannot give a good performance to recover low grade waste heat, a large number of new solutions have been suggested to produce electricity from low-temperature heat sources such as biological waste heat, geothermal heat, solar thermal power, engine exhaust gases, domestic boilers, etc. Among them, the Organic Rankine Cycle (ORC) system seems to be the most promising process and it is the most widely applied. In such a system, the working fluid is an organic component, better adapted than water to lower heat source temperatures. Unlike traditional power cycles, local and small-scale power generation is made possible by this technology. On the other hand, the low efficiency of the Organic Rankine Cycle (ORC) with a low-grade heat source (LGHS) has limited its use in the industry. In order to increase the power output capacity and its performance, a new structure of the Organic Rankine Cycle integrated with Ejector (EORC) is proposed in this project. Ejectors are simple devices in which the energy of a flow is used to entrain and enhance the pressure of a secondary stream by direct mixing. They are used due to their simple operation, low maintenance requirements and lack of moving parts. Since the impact of ejector working characteristics and its geometry are important to optimize the design of an EROC system, three published papers have investigated in detail the improvement of ejector performance. In the first step, a comprehensive ejector 1D model is prepared by considering the best normal shock assumption and the selection of the efficiencies that are two of the greatest sources of error in the 1D models. A large number of CFD simulations have been performed for validating and comparing with 1D models and experimental data, for ejector internal exergy analysis, and to extract ejector isentropic and polytropic efficiencies, critical back pressure and entrainment ratio. Numerical and experimental investigations on the ejectors have revealed that the replacement of isentropic efficiencies with polytropic efficiencies within 1D ejector models provides more accurate results. Polytropic efficiencies access more precisely the effects of the pressure ratio variation on the irreversibilities of the acceleration and deceleration processes. It is demonstrated that the deviation in the constant area duct length, calculated by using an isentropic efficiency from the real length is three times greater than the one calculated by using a polytropic efficiency. Furthermore, from experimental results, it is found that the best performance of the ejector and consequently the cycle were achieved for the maximum pressure ratio at the critical condenser temperature point. At this condition, ejector internal exergy losses are minimal according to the carried out numerical studies. Finally, after a comprehensive study on the ejector behavior, in the fourth journal publication, an appropriate ejector (working in the double-choking regime) is employed to enhance the EORC performance. It is shown that a rise in the ejector area ratio, secondary mass flow rate as well as decreasing the throat diameter and inlet ejector properties have significant effects on increasing the net power output. It is further found that power output capacity is independent of the ejector outlet parameters in the on-design mode.

Keywords: *Optimization; Organic Rankine Cycle; Ejector; Thermodynamic model; CFD model; Experimental study; Polytropic efficiency; Ejector dimensions; Power generation.*

Acknowledgments

I would like to express my deep appreciation to my supervisor Prof. Mikhail Sorin, for his continued support, valuable guidance, and the academic environment he provided during the course of research. Without his support and encouragement, this thesis would not have been possible.

I would like to thank my committee members, Prof. Sébastien Poncet, Prof. Mathieu Picard and Dr. Mehdi Falsafioon for their time to review and approve my thesis.

I would like to thank Dr. Hakim Nesreddine and Dr. Marc A. Richard as my industrial advisors at Energy Technologies Laboratory (LTE) of Hydro-Québec for their support, valuable consultation and experimental tests during my research.

I am grateful to my friends and colleagues at the Université de Sherbrooke for providing a friendly and dynamic environment in the office. I have had a great time working with you guys and have enjoyed each and every one of you.

I would like to acknowledge my parents and my brothers for the unlimited love and support you provided me throughout all these years. Without your support, I would not have made it so far.

Last but not least, I am greatly indebted to my dear wife, Sahar, who has inspired me and supported me throughout this research.

TABLE OF CONTENTS

LIST OF FIGURES

LIST OF TABLES

CHAPTER 1 : INTRODUCTION

1.1 Background and motivation

Significant growth in energy demand over the past years has caused an energy crisis in the world. On the other hand, there is a vast amount of the low-temperature waste heat generally discharged during various industrial processes which is usually released to the environment directly. Therefore, recovering these low-grade heat sources can achieve energy saving, sustainable development and also the reduction of environmental problems such as ozone depletion, global warming and air pollution. The organic Rankine cycle (ORC) is an effective method to recover the low-grade heat source by employing organic working fluids instead of water.

The ORC technology has been investigated widely during the past decades, and main efforts have been devoted to identify the working fluids in ORC systems and conduct performance optimizations. However, the low efficiency of the ORC has caused its application become limited in the industry. In this study, a new structure of the Organic Rankine Cycle integrated with an ejector (EORC) is proposed in order to increase the power output capacity and its performance.

Although an abundant literature is available on the optimization of ORCs, few papers propose a detailed modeling of the combination of this cycle with ejector. Thus because of this limited knowledge about this new ejector system, obtaining an optimum design methodology has received much attention from many researchers. Since ejector is a key component in the EORC system, it is important to quantify its performance in the cycle.

This study aims at proposing a detailed model of an ORC integrated with ejector including thermodynamic model, CFD and Experimental analysis. The validated thermodynamic model of EORC is eventually used to optimize the performance of the Cycle.

In general, this thesis will present an optimization study and detail investigation of an ORC system with ejector. A single-phase ejector model has been developed and incorporated into an ORC system to reveal the effects of various parameters such as operating conditions and ejector geometry in the whole system. A thermodynamic modeling of single-phase ejector has been used to release an optimum design. An experimental study is carried out to provide a validation of the analytical results. Furthermore, parametric study and optimization have been performed based on the obtained model to determine which design parameters have the most effects on the objective indicators.

1.2 Objectives and approach

The main objective of the project is the analysis and optimization of an ORC system integrated with ejector and compare to classical ORC system performance. To this end, the working characteristics and geometry of an ejector are investigated in order to have a more efficient design of ejector and consequently to improve the performance of the EORC system. This general objective includes the following specific objectives:

- Develop a CFD model of the one-phase ejector to analyze the behavior of streams inside the ejector as well as calculating isentropic and polytrophic efficiencies, critical back pressure, entrainment ratio , and internal exergy losses.
- Develop a 1-D thermodynamic model of a one-phase ejector to predict the performance of an ejector under different operating conditions and geometry parameters.
- Perform an experimental analysis of an Organic Rankine Cycle (ORC) to validate thermodynamic simulation of the ORC.
- Thermodynamic simulation of the ORC including heat exchangers, pump and turbine.
- Perform an experimental study of an R245fa single-phase ejector to validate the thermodynamic and CFD models of a one-phase ejector.
- Investigation on the more appropriate place of normal shock assumption and the selection of the ejector efficiencies that are two of the greatest sources of error in the ejector 1D models.
- Perform a parametric study and optimization of the EORC to define the optimal values of ejector input parameters as well as its optimal design characteristics and geometry.

1.3 Thesis outline

The present thesis is divided into seven chapters. Chapter 1 is an introduction to the study. In chapter 2 a comprehensive literature review on ORC systems, some power and refrigeration cycles which are integrated with ejector, and operation and performance characteristics of the ejectors are presented.

As previously proven, the normal shock assumption and the selection of the efficiencies are two of the greatest sources of error in the 1D models. Since, in chapters 3 and 5, the impact of these key parameters are investigated. However, in chapter 4, the main focus is only on the investigation of the internal ejector working characteristics.

In chapter 3, a 1D model is proposed that is more realistic than previous 1D models due to the application of the polytropic (or elemental) efficiency conception. In this case, the 1D model is

able to consider the effects of the pressure ratio on the entropy increase during the irreversible acceleration and deceleration processes, unlike previous models, which use isentropic (or overall) efficiencies for this purpose. CFD simulation is used for calculating the real values of the polytropic efficiencies for the 1D model. In general, a comprehensive comparison between all dimensions obtained by the 1D model based on isentropic and polytropic efficiencies is carried out against experimental data. Empirical correlations for polytropic efficacies are also proposed using a parametric study.

In chapter 4, an experimental investigation is carried out in order to study the performance of an ejector refrigeration system (ERS) under various internal ejector working characteristics for both single-choking and double-choking regimes. A geometrical optimization of the ejector for increasing the pressure ratio and ejector performance is carried out.

In chapter 5, the effects of the normal shock assumption on the ejector dimensions are evaluated. The obtained dimensions by the 1D model based on different normal shock locations are compared to experimental data in order to determine more accurate assumption.

Finally, the main objective of the thesis is investigated in chapter 6. The performance of the EORC system is evaluated. For available ORC test bench, a one-phase ejector that works in the on-design regime is designed. The influence of ejector working characteristics and its geometry on the EORC system performance is investigated in order to have a more efficient system.

A summary of important conclusions as well as the future works of this study are expressed in chapter 7. At last, all used references are given at the end of the thesis

CHAPTER 2 : STATE OF THE ART

This chapter summarizes an overall review of various articles related to the Organic Rankine Cycle (ORC), ejector and also some power and refrigeration cycles integrated with ejector. To better understanding of the previous works, it is divided into four main sections: the first section describes the organic Rankine cycle (ORC). In the second section, application of the ejector in the power cycles is investigated. In the third section, the modeling of the one-phase flow ejector is presented including CFD, experimental and thermodynamic models and lastly in the fourth section, a general definition of ejectors and some parameters which have important effects on its performance is introduced.

2.1 Organic Rankine Cycle (ORC)

Due to the scarcity of fossil fuels, environmental pollution and global warming in the past few decades, energy and environment have progressively attracted the world's attention. The interest for energy saving and renewable energy have been growing in many parts of the world. An important number of new solutions have been proposed to generate electricity from low-temperature heat sources and are now applied to many diversified fields such as solar thermal power, biological waste heat, engine exhaust gases, domestic boilers, etc. In general, more than 11% of total energy production is related to these sources [1].

The Organic Rankine Cycle (ORC) system is more common among other proposed solutions due to the simplicity and availability of its components. In the most organic Rankine cycles, a refrigerant undergoes phase transitions from a liquid to a gas and back again. Due to the lower boiling point and high heat transfer rate, the refrigerants are suitable for low-temperature heat sources.

The configuration of the Organic Rankine Cycle is somewhat simpler than that of the steam Rankine cycle: there is no water-steam drum connected to the boiler and one single heat exchanger can be used to perform the three evaporation phases (preheating, vaporization and superheating). The variations on the cycle architecture are also more limited: reheating and turbine bleeding are generally not suitable for the ORC cycle, but a recuperator can be installed as a liquid preheater between the pump outlet and the expander outlet, as illustrated in figure 2-1 [1]. The configuration of the ORC main components is based on figure 2-2.

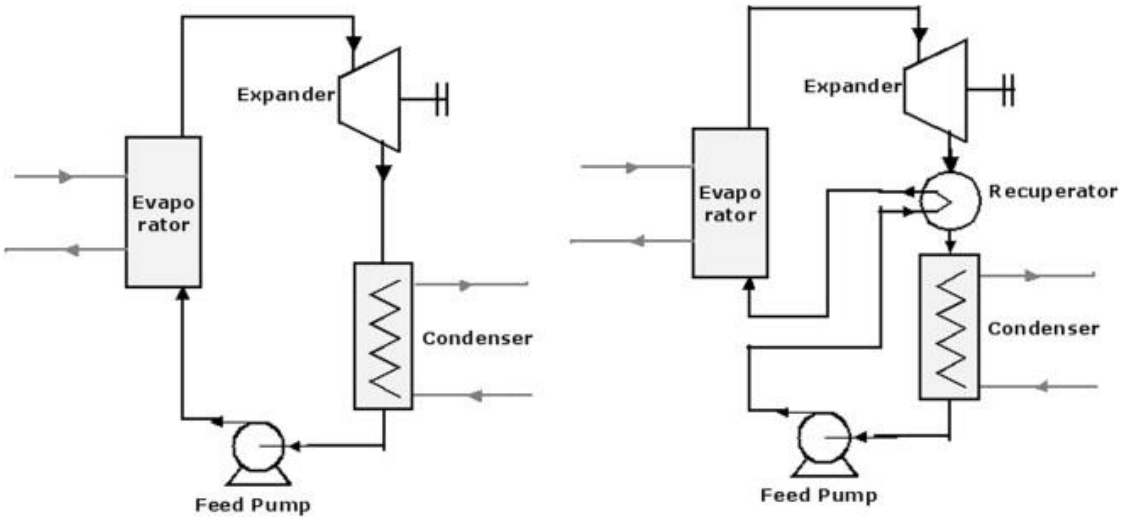

Figure 2.1 Working principle of an ORC cycle with (right) and without (left) recuperator [1]

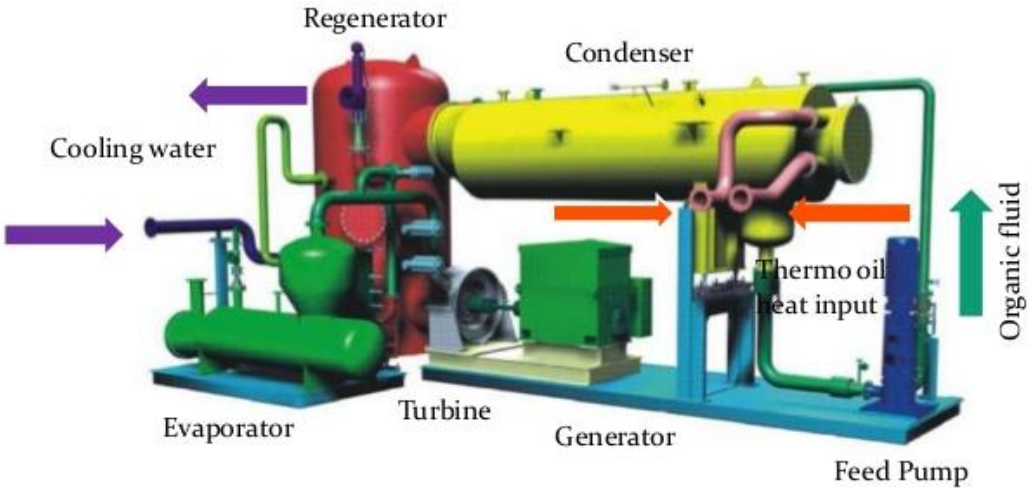

Figure 2.2 ORC main components [1]

The schematic and T-s diagram of an organic Rankine cycle is illustrated in figure 2-3.

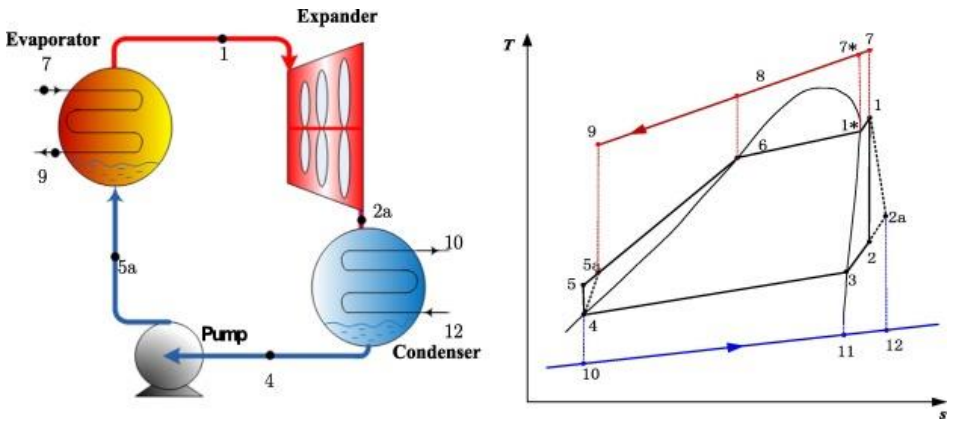

Figure 2.3 The schematic and Ts diagram of the organic Rankine cycle.

The basic cycle is very similar to the traditional steam cycle: the organic working fluid is successively pumped, vaporized, expanded and then condensed. The cycle with recuperator takes profit of the residual heat after the expansion to preheat the liquid after the pump. This operation allows reducing the amount of heat needed to vaporize the fluid in the evaporator [1].

Unlike traditional power cycles, local and small-scale power generations are made possible by this technology. A wide range of ORC applications has been investigated in the previous works [1] [2]. It should be mentioned that Organic Rankine Cycle (ORC) is a technology that can convert thermal energy at relatively low temperatures in the range of 80 to 350 °C to electricity and can, therefore, play an important role to improve the energy efficiency of new or existing applications. Figure 2-4 illustrates some applications of such a system. A survey on the progress of the ORC technology over the last decades, for commercial applications, shows that total installed capacity is about 2749.1 MWel, in 563 power plants by 2017 and new capacity planned is more than 523.6 MWel in 75 plants. Geothermal power plants contribute to 76.5% of all ORC installed capacity in the world. Biomass follows with 10.7%. Heat recovery from gas turbines (compressor stations along pipelines) and stationary diesel power plants have a similar share with 8.5%. All other heat recovery applications represent 4.2%, while solar thermodynamic remains neglectible. ORMAT is the world leader for the total installed capacity (65.7%), followed by the Italian companies Turboden (12.6%) and Exergy (9.8%) [1].

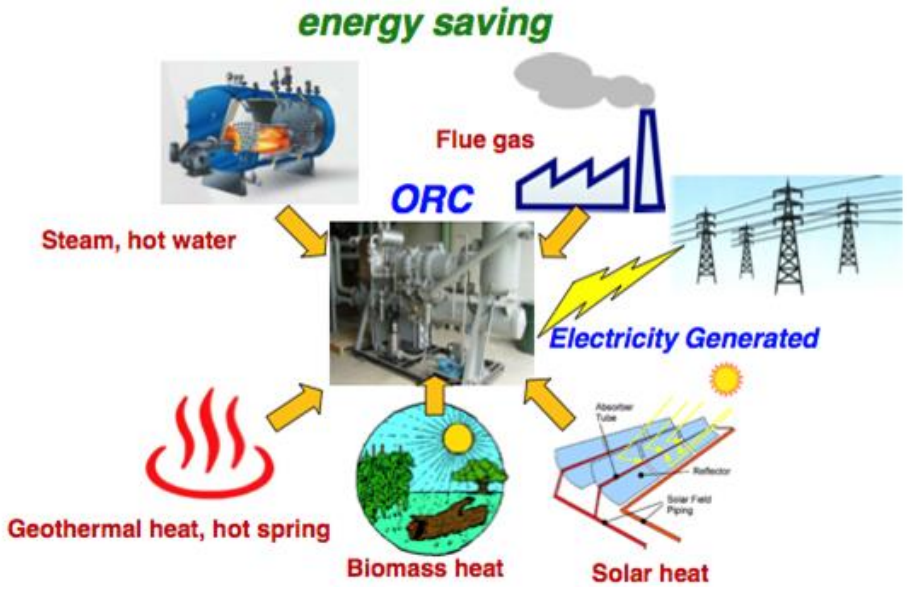

Figure 2.4 ORC applications to generate electricity from low-temperature heat sources [1].

2.1.1 Solar energy use

Integrated solar combined cycles with ORC are currently used in countries with high incident solar radiation in order to increase the net output power and decrease the specific fuel consumption. Solar power is known as a renewable free source of energy that is sustainable and totally inexhaustible, unlike fossil fuels that are limited.

Solar power is the conversion of sunlight into electricity, either directly using photovoltaics (PV), or indirectly using concentrated solar power. Concentrated solar power systems use lenses or mirrors and track systems to focus a large area of sunlight into a small beam. The sun is tracked and reflected on a linear or a punctual collector, transferring heat to a fluid at high temperature. The heat is then transferred to a power cycle generating electricity. The three main concentrating technologies are the parabolic dish, the solar tower, and the parabolic trough. Parabolic dishes and solar towers are punctual concentration technologies leading to a higher concentration factor and higher temperatures. The best-suited power cycles for these technologies are the Stirling engine (for small-scale plants), the steam cycle or even the combined cycle for solar towers [3].

Parabolic troughs work at a lower temperature (300°C to 400°C) than point-focused CSP systems. They are basically coupled to the conventional steam Rankine cycles to generate power [4].

Organic Rankine cycles are a favorable technology to reduce investment costs at small scale: they can work at lower temperatures and the total installed power can be reduced down to the kW scale. The working principle of such a system is presented in figure 2-5.

Shaaban [5] recently described a modified integrated Solar Combined Cycles (ISCC) with an Organic Rankine Cycle ORC. The ORC was used in order to intercool the compressed air and generate a net power from the received thermal energy. The performance of the proposed cycle was optimized. Fifteen working fluids were studied in the ORC. The working fluid R1234ze(z) shows a good agreement between thermodynamics, economic, safety and environmental considerations. An increase of the output power by 19.5% with solar contribution and 23.1% without solar contribution have been shown for the cycle with R1234ze(z).

Quoilin et al. [2] described the design of a solar organic Rankine cycle being installed in Lesotho for rural electrification purpose. The model allows sizing the different components of the cycle and evaluates the performance of the system. They compared different working fluid and two simulated different expansion machine configurations are simulated (single and double stage).

Technologies such as Fresnel linear concentrators [6] are particularly appropriate for solar ORCs since they require lower investment cost but work at a lower temperature.

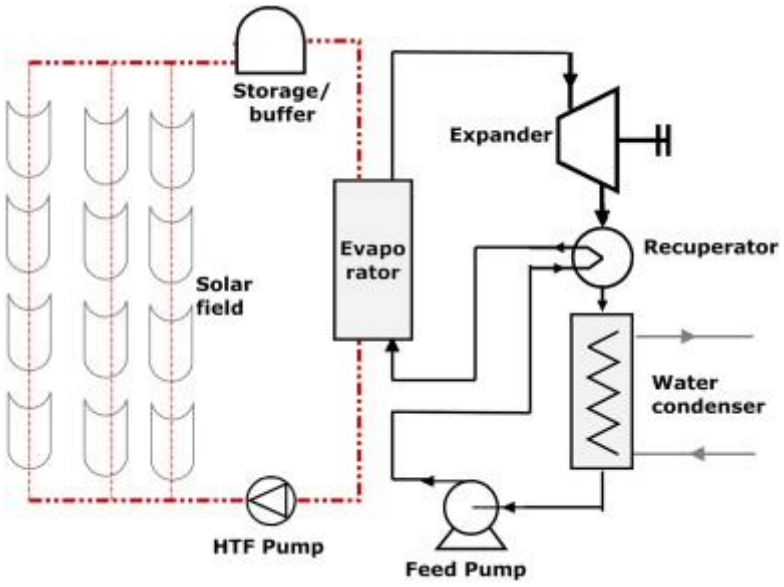

Figure 2.5 Working principle of a solar ORC system [2].

2.1.2 Geothermal systems

The ground and lakes around us represent a vast reservoir of renewable thermal energy stored from the sun. This geothermal energy is estimated to exceed all other energy sources combined by more than two thousand times. At depths below 8 to 10 feet (2.5 to 3 meters), the earth's temperature remains at or near the average annual air temperature. Geothermal heat sources are available over a broad range of temperatures, from a few tens of degrees up to 300°C. The actual technological lower bound for power generation is about 80°C. Below this temperature conversion efficiency becomes too small and geothermal plants are not economical [3].

To recover heat at an acceptable temperature, boreholes must generally be drilled in the ground, for the production well and for the injection well (fig. 2-6). The hot brine is pumped from the former and injected into the latter at a lower temperature. Depending on the geological formation, boreholes can be several thousand meters deep which are required. According to Kranz S. (2007), this leads to a high share of drilling cost in the total investment cost (up to 70%) of a geothermal ORC plant. Lazzaretto et al. [8] reported a much more moderate share of 15.6% for an Italian geothermal binary cycle.

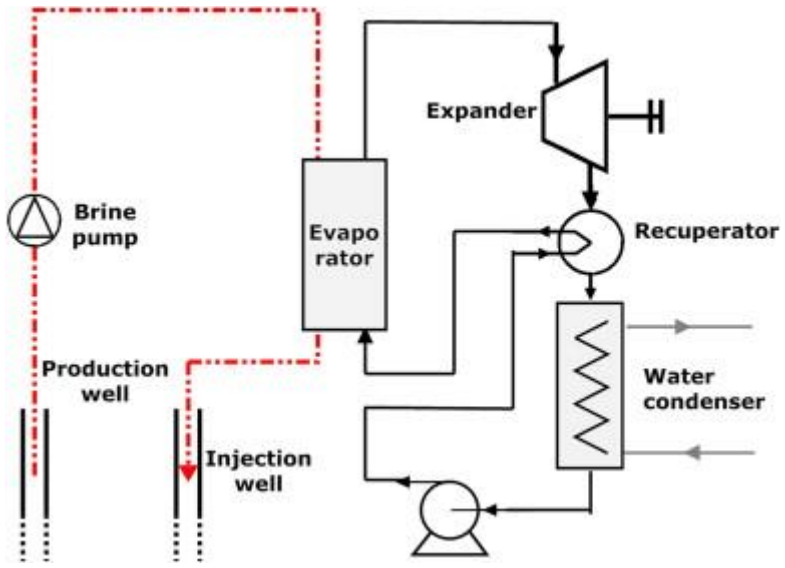

Figure 2.6 Working principle of a geothermal ORC system [1].

2.1.3 Biomass combined heat and power

Biomass is a renewable energy source not only because the energy in it comes from the sun, but also because biomass can regrow over a relatively short period of time compared with the hundreds of millions of years that it took for fossil fuels to form. Biomass is widely available in a number of agricultural or industrial processes such as wood industry or agricultural waste. Among other devices, it can be converted into electricity by combustion through a thermodynamic cycle.

In small biomass plants, the ORC is the ideal choice due to its efficiency, availability and ability to follow load dependent on fuel supply. In addition, the elimination of the steam turbine for traditional biomass solutions brings with it a number of maintenance and operational advantages.

The boiler through the combustion process converts the biomass in thermal power to feed the ORC module. The hot exhaust gas warms up the intermediate fluid in a heat exchanger. The ORC-boiler interface circuit transfers the thermal power from the boiler to the ORC evaporator. The commonly employed intermediate fluids between the boiler and ORC are thermal oil, pressurized water and steam. The interface fluid transfers heat to the organic fluid in the ORC evaporator, where the organic fluid vaporizes. The vaporized fluid then passes to the turbine. Here the expansion vapor causes the turbine to spin and creates electricity into the generator. Figure 2-7 illustrates the working principle of a biomass CHP ORC [1].

Moro et al. [9] investigated biomass CHP plants in order to achieve high energy conversion efficiency. It is shown that the biomass CHP plants are usually driven by the heat demand rather than by the electricity demand. Figure 2-8 shows energy flow as a function of the conversion temperatures in a biomass CHP ORC system.

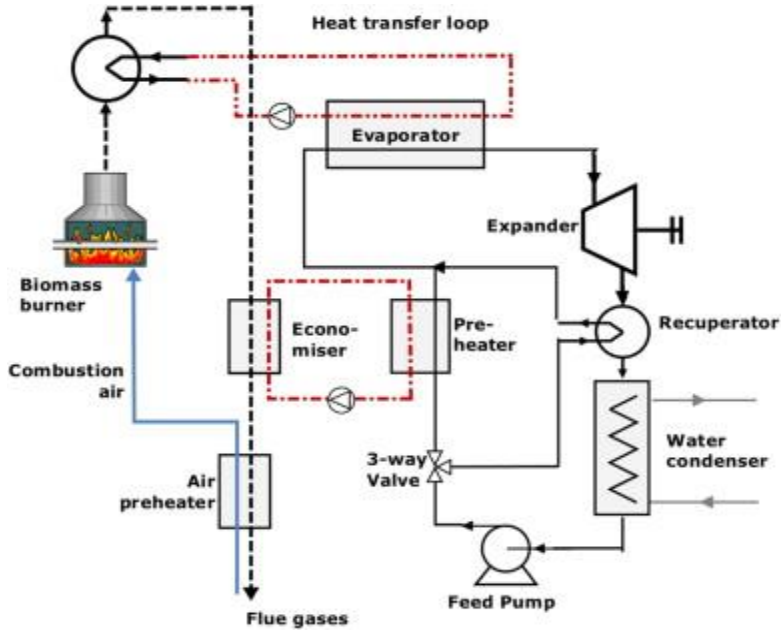

Figure 2.7 Working principle of a biomass CHP ORC[1].

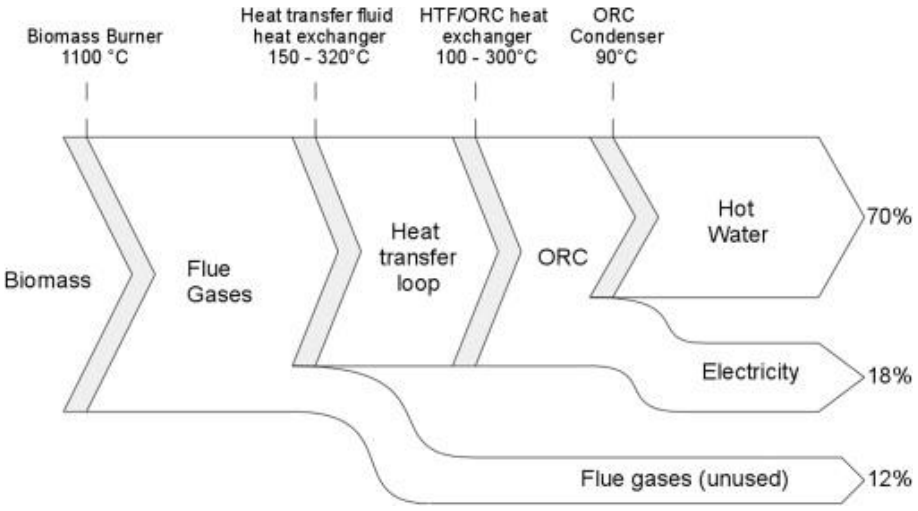

Figure 2.8 Energy flow as a function of the conversion temperatures in a biomass CHP ORC system [1].

2.1.4 Waste heat recovery

One of the most important solutions for energy production is to recover waste heats. The waste heat from industrial plants, mechanical equipment and internal combustion engines are the forms of essentially free energy which can be recovered and converted into work and electricity. Organic Rankine Cycle (ORC) is a technology ideally suited for such heat sources to generate electricity.

- Heat recovery on mechanical equipment and industrial processes

Many applications in the manufacturing industry reject heat at relatively low temperature. It is quite abundant and widely available but its quality is low compared to that of conventional fossil-fuel power-plants and cannot, therefore, be converted into electricity using water as the working fluid. On the other hand, in the most power plants and manufacturing plants, such heat doesn't reuse on-site and it is rejected to the atmosphere. But, it leads to generate health or environmental issues that are due to pollutants (CO_2, NO_x, SO_x, HC) contained in the flue gases. Besides, the heat rejection can perturb aquatic equilibrium and have a negative effect on the biodiversity. Therefore, the recovery of this heat is necessary [10].

Bailey and Worrell)2005) investigated the potential of such cycles. A potential of 750 MWe is estimated for power generation from industrial waste heat in the US, 500 MWe in Germany and 3000 MWe in Europe (EU-12) [11].

Engin and Ari (2005) presented the cement industry has a high potential among other industries for waste heat recovery because 40% of the heat is lost in flue gases. These flue gases are located after the limestone preheater or in the clinker cooler, with a temperature varying between 215 and 315 °C [12].

Minea [13] investigated on a laboratory beta-prototype, 50 kW Organic Rankine Cycle (ORC) machine using industrial waste. He showed that the power generated and the overall net conversion efficiency rate of the machine mainly depends on the inlet temperatures of the waste heat and cooling fluid as well as on the control strategy and amount of parasitic electrical power required.

- Heat recovery on internal combustion engines

The Internal Combustion Engine (ICE) has been a primary power source for automobiles, long-haul trucks, locomotives, and ships over the past century. An Internal Combustion Engine only converts about one-third of the fuel energy into mechanical power. The heat recovery Rankine cycle system is efficient means for recovering heat (in comparison with other technologies such as thermo-electricity and absorption cycle air-conditioning). The idea of associating a Rankine cycle to an ICE is not new and the first technical developments followed the 70's energy crisis. Sprouse and Depcik (2013) reviewed the history of internal combustion engine exhaust waste heat recovery focusing on Organic Rankine Cycles since this thermodynamic cycle works well with the medium-grade energy of the exhaust [14]. The choice of the working fluid and the cycle expander were the main subjects of this review due to the significant influence on system performance. The results showed a potential fuel economy improvement around 10% with modern refrigerants and advancements in the expander technology.

2.2 The application of the ejector in the power cycles

Since 1858, ejectors have been intensively studied for a large number of various applications. In the past, ejectors have mostly been used in different cycles for refrigeration purposes. In recent decades, they are widely used in the power cycles.

The number of the investigation on the ORC integrated with the ejector is very limited. While the investigation on cascade organic Rankine cycles is abundant. The review of the application of the ejector within power cycles is divided into two different sections.

2.2.1 The application of the ejector in the organic Rankine cycles

Scientific literature covering organic Rankine cycle integrated with ejector is still limited, as a few investigations have been carried out on such cycles. The research on ORC is mainly reflected in the selection of working fluids, analysis of the thermal performance, optimization of the system and transcritical cycle. The selection of the working fluids greatly affects the thermal performance of the ORC, the power output capacity and the thermal efficiency.

In order to increase the power output capacity and efficiency, some researchers have proposed an integration of ORC with ejector.

Li et al. (2012) proposed a combined ORC with ejector. In this new configuration, an ejector and a second-stage evaporator were added to the ORC [15]. Figure 2-9 (a) and figure 2-9 (b) illustrates the principle of the organic Rankine cycle with ejector (EORC) and the principle of double Organic Rankine Cycle (DORC) respectively. The vapor from the second-stage evaporator was worked as the primary fluid for the ejector to suck the exhaust from the expander to decrease the expander backpressure and increase the pressure difference through the expander which resulted in an increase of the power output capacity compared to ORC.

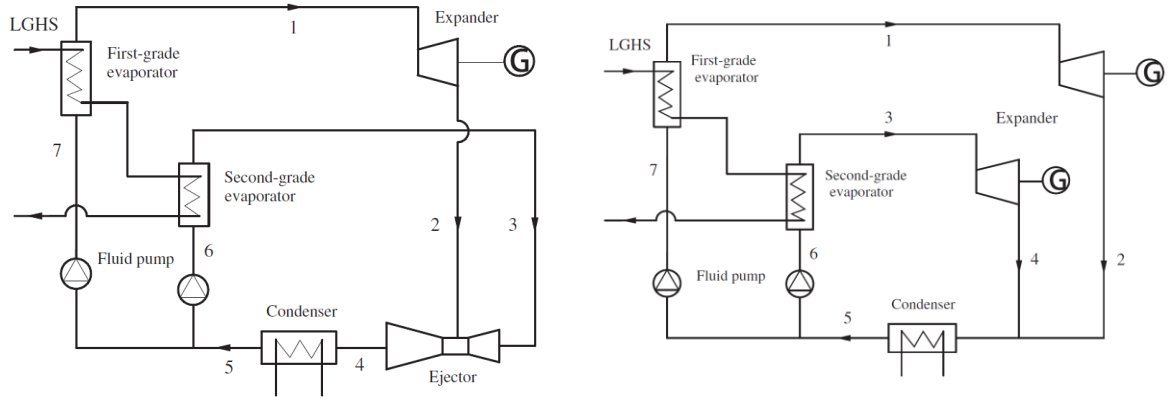

Figure 2.9 (a) Principle of Organic Rankine Cycle with Ejector (EORC) (b) Principle of double Organic Rankine Cycle (DORC) [15].

Their experiments (Figure 2-10) and theoretical analyses were carried out in the same operation conditions. The ejector in EORC made the expander's outlet pressure decreased by 0.32 bar compared to the ORC system, which meant that the output capacity was increased by 34.93%. The output efficiency of EORC was 5.93%, increased by 26.17% compared to ORC's 4.70%, but the system efficiency of EORC was lower than that of ORC.

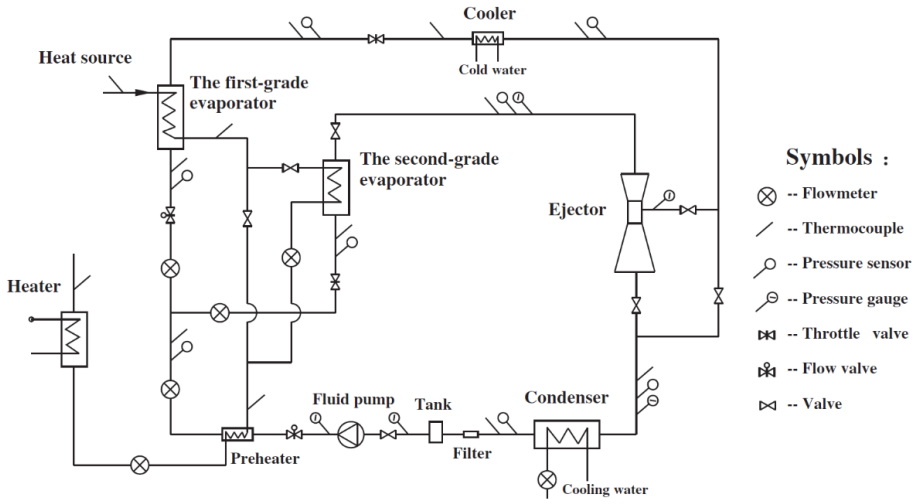

Figure 2.10 Experiment system of Organic Rankine Cycle with Ejector (EORC).

Li et al. [16] calculated the net power output and exergy destruction of three cycles (ORC, EORC, DORC). The results show that the power output is higher in the EORC and DORC compared to the ORC. The power output and thermal efficiency of the DORC are superior to the EORC, but another expander-generator and its auxiliary equipment are required for the DORC led to the increase of the investment and operation management compared to the EORC.

They also ranked the exergy loss ratio in the evaporator and the condenser of the cycles from high to low is: EORC > DORC > ORC and it is: ORC > DORC > EORC in the exhaust water. The cycle's exergy efficiency can be ranked from high to low: DORC > EORC > ORC. Another important result of their research is the most exergy losses took place in the evaporator, condenser and the exhaust water, cycle at the maximum net power output while it is the smallest in the ejector in the EORC.

Li et al. [17] also proposed a Kalina cycle with ejector. Kalina cycle and organic Rankine cycles (ORC) are potentially feasible to recover energy from the low-grade heat sources (LGHS). Results show that the net power output and thermal efficiency of the EKalina cycle are higher than that of the KCS.

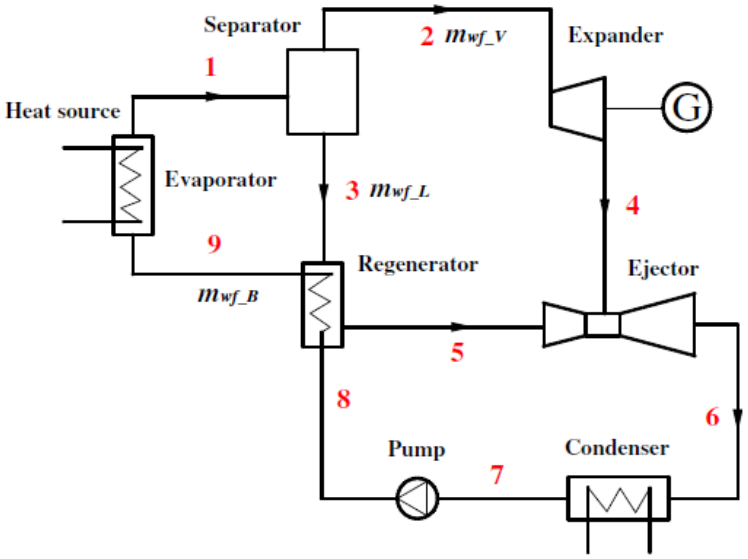

Figure 2.11 Schematic diagram of the Kalina cycle with ejector (EKalina cycle) [17].

Li et al. [18] proposed a supercritical or transcritical Rankine cycle with ejector (ESRC, ETRC) based on the basic supercritical or transcritical Rankine cycle (SRC, TRC) in order to generate electricity from low-grade sources. They increased the net power output of the cycle by decreasing the outlet pressure of the expander or increasing the pressure difference in the expander. The carbon dioxide was chosen as the working fluid for the cycles. Water was chosen as the fluid of the low-grade heat Results show that the net power output of the cycles could be ranked from high to low: ESRC > ETRC > SRC > TRC, and the thermal efficiency could be ranked from high to low: TRC > SRC > ESRC > ETRC.

2.2.2 The application of the ejector in the cascade organic Rankine cycles

Ejectors have long been used in power and cooling applications and as vacuum generators. A large number of researchers have investigated various cascade cycles. In this part will have a review of some studies related to cascade organic Rankine cycles.

Habibzadeh et al. [19] performed a thermodynamic study of a thermal system which combines an organic Rankine cycle (ORC) and an ejector refrigeration cycle (Figure 2-12). The results for refrigerants under investigation show that when the heat source temperature increases the thermal efficiency and the total exergy destruction increase while the total thermal conductance decreases. By increasing the cooling water temperature, the total exergy destruction decreases while the total thermal conductance increases. When the expansion ratio of the turbine increases the total exergy destruction and the total thermal conductance decrease.

By varying either the inlet pressure of the pump (or equivalently the evaporation temperature) or the inlet pressure of the turbine more results could be achieved. They revealed that these variables can be optimized to obtain a minimum total thermal conductance. R601a has the highest thermal efficiency and lowest total exergy destruction in both optimum cases. Among the considered working fluids, R141b has the lowest optimum pressure and smallest total thermal conductance for both these optimum conditions.

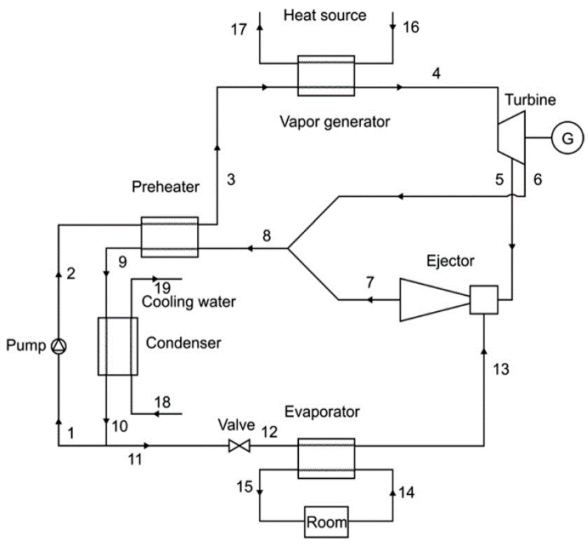

Figure 2.12 Schematic diagram of the combined ORC and refrigeration cycle [19].

In 2016, Zhang et al. [20] considered a combined ORC and ejector refrigeration cycle (figure 2-13) that is capable of producing useful power while having a simultaneous capacity for cooling. In this integrated cycle, due to unavoidable losses caused by irreversible mixing, the main exergy loss in the combined system takes place in the ejector. They found that some

operating conditions, such as a high pressure of the secondary and discharge fluid lead to higher exergy losses inside the ejector and limit the performance of the entire system. They proposed an optimal design featuring a smoothed nozzle edge and an improved nozzle position in order to obtain an improved entrainment ratio, reduced exergy losses in the ejector and better performance.

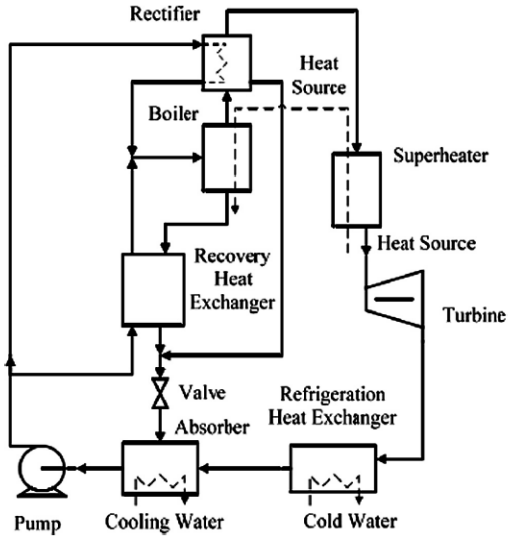

Figure 2.13 Schematic of the combined ORC and absorption refrigeration system [20].

Soroureddin et al. [21] investigated the waste heat from intercooler and pre-cooler of the gas turbine-modular helium reactor (GT-MHR) is utilized to drive organic Rankine and ejector refrigeration cycles for performance enhancement. Three efficient combined cycles are proposed and analyzed in detail. The results of optimization revealed that one of the configurations is more efficient than the other ones from the viewpoint of the first law of thermodynamics. In this configuration, at turbine inlet temperature of 850 ºC the first law efficiency is 15.86% higher than the GT-MHR cycle and the fuel energy saving ratio (FESR) could be up to 20.06%. Another configuration is found to be the most effective (among the three) from the exergy utilization perspective. In this layout, the exergy efficiency is around 2.6% higher than that of the GT-MHR.

Besides, they have studied on the influence of some important parameters such as turbine inlet temperature, pinch point temperature difference as well as the compressor pressure ratio on the systems' performance. The results show that the compressor pressure ratio is higher for the configuration with the highest first law efficiency under the optimized condition. This point can be accounted as an economic drawback for the configuration. The highest exergy destruction

for all the proposed configurations take place in the reactor. The second highest exergy destruction belongs to the compressor or recuperator.

Yari et al. [22] proposed a novel dual-evaporator system with dual-source (renewable and electrical energies) to provide negative and positive evaporator temperatures. The system is a combination of the generator–absorber heat exchange (GAX), ejector-expansion transcritical CO_2 refrigeration (EETC), Organic Rankin Cycle (ORC) and supercritical CO_2 power cycles. They analyzed the entire system thermodynamically and optimize the performance of the cycle. The results show that allocating the lower temperatures (−25 to −45 °C) for EETC evaporator and higher temperatures (5–10 °C) for GAX evaporator is more appropriate. Detailed exergy analyses reveal that ejector is the highest source of irreversibility in the system and also it found that 19.89% and 5.92% of total input exergy, are useful in EETC evaporator and GAX evaporator, respectively. Optimization results reveal that increasing the temperature of either the GAX or EETC evaporator increases the maximum COP value.

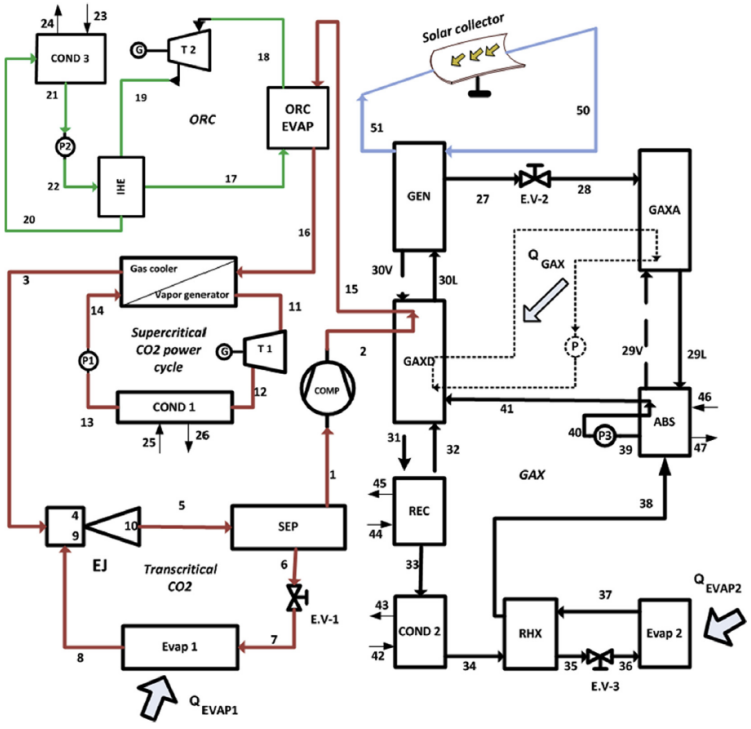

Figure 2.14 Schematic diagram of the proposed DEDS system [22].

2.3 Modeling of the one-phase flow ejector

Research studies on the ejector as a favorable device have increased since the 1950s. The performance of ejectors has been carefully considered theoretically and by experiment. Most

researchers believe that it is essential to enhance the performance of ejectors in order to make them economically more attractive. For this purpose, a numerous number of investigations on optimizing the ejector performance have been carried out.

Among these studies, comparing different refrigerants in order to achieve an appropriate working fluid under varying operating conditions and effect of the geometry on the ejector performance are considerably investigated experimentally and by numerical methods.

Chen et al. [23] and Gil and Kasperski [24] studied the effect of different refrigerants on the ejector efficiency in the refrigeration systems. Some researchers have investigated the effect of ejector geometry on its performance such as nozzle exit location, mixing chamber/nozzle area ratio and nozzle design. Banasiak et al. [25] examined different ejector configurations in order to achieve an optimum ejector geometry. They used various lengths and diameters of the mixer and various angles of divergence for the diffuser. Cizungu et al. [26] optimized the ejector geometry to achieve maximum values for either the entrainment ratio or the pressure ratio. Elbel and Hrnjak [27] experimentally studied different ejector dimensions such as the sizing of the motive nozzle and the size of the diffuser. Nakagawa et al. (2011) [28] experimentally analyzed the effect of the mixer length on ejector system performance. A Review of recent developments in advanced ejector technology can be found in Elbel and Lawrence [29].

Researchers usually use some assumptions for theoretical analyses of the ejectors. One of them is considering constant isentropic efficiencies at various parts along the ejector including a primary nozzle, secondary and diffuser in order to take into account the irreversibilities. Tyagi and Murty [30] assumed these constants arbitrarily. Aly et al. [31] and Cizungu et al. [26] took from literature. Some researchers experimentally measured ([32] [33]). Varga et al. [34] extracted from the CFD model and also Grazzini and Rocchetti [35] used a “trial and error” approach by comparing the solution from a 1D model to CFD results.

In all previous 1D models, constant isentropic efficiencies were used. However, recently Galanis and Sorin (2016) introduce the concept of the polytropic efficiency for ejectors which is used extensively in the design and analysis of compressors and turbines [37] but has only recently been applied to the study of ejectors. ([36], [38], [39]). The polytropic efficiency η_{pl} is defined as the isentropic efficiency of an elemental process. It takes into account the elemental pressure ratio and the irreversibilities occurring during the acceleration and deceleration processes, unlike isentropic efficiency.

2.4 General definition of the ejectors

Ejector is a simple, reliable and low-cost device to produce a vacuum by accelerating a gas, vapor or liquid in a nozzle. It has no moving parts. Instead, it uses a fluid or gas as a motive force. Applications of ejectors include refrigeration, air conditioning, removal of non-condensable gases, transport of solids and gas recovery. A large number of studies have been conducted on ejector working characteristics. Some of the most important features and parameters of ejectors are summarized as follows:

1- A typical ejector construction includes four distinct parts: a convergent–divergent nozzle, a suction chamber attached to a constant area duct and a diffuser. A simple picture of an ejector is shown in figure 2-15. Ejectors are considered as an excellent alternative to mechanical vacuum pumps and compressors for a number of reasons:

- No source of power is required other than the motive gas.
- They are easy to install, operate and maintain.
- They have no moving parts; thus they are reliable vacuum producers.
- Versatility with a variety of refrigerants.

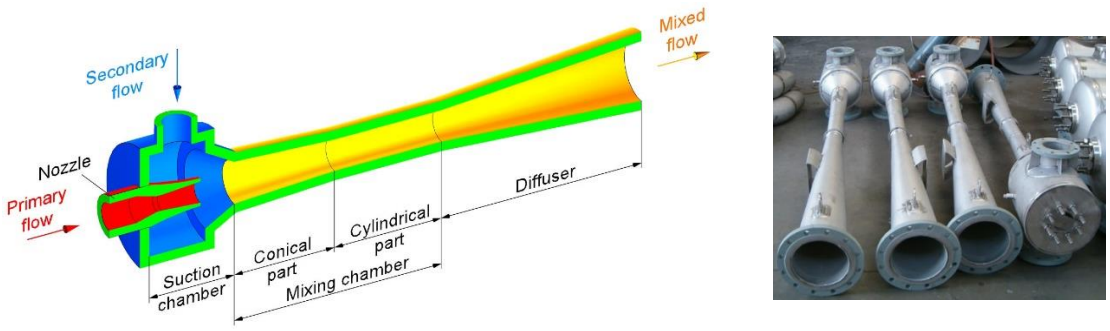

Figure 2.15 Schematic of an ejector

2- The ejector performance is defined by two global parameters [40]:
Entrainment ratio: ($\omega = \dot{m}_{sec}/\dot{m}_{pr}$) (mass of secondary flow / mass of primary flow)
Pressure ratio: ($PR = P_{out}/P_{sec}$) (static pressure at diffuser exit / static pressure at secondary inlet)

3- Compression effect: Back pressure should be higher than the secondary fluid inlet pressure.

4- Variation in stream pressure and velocity is as a function of location along the ejector.

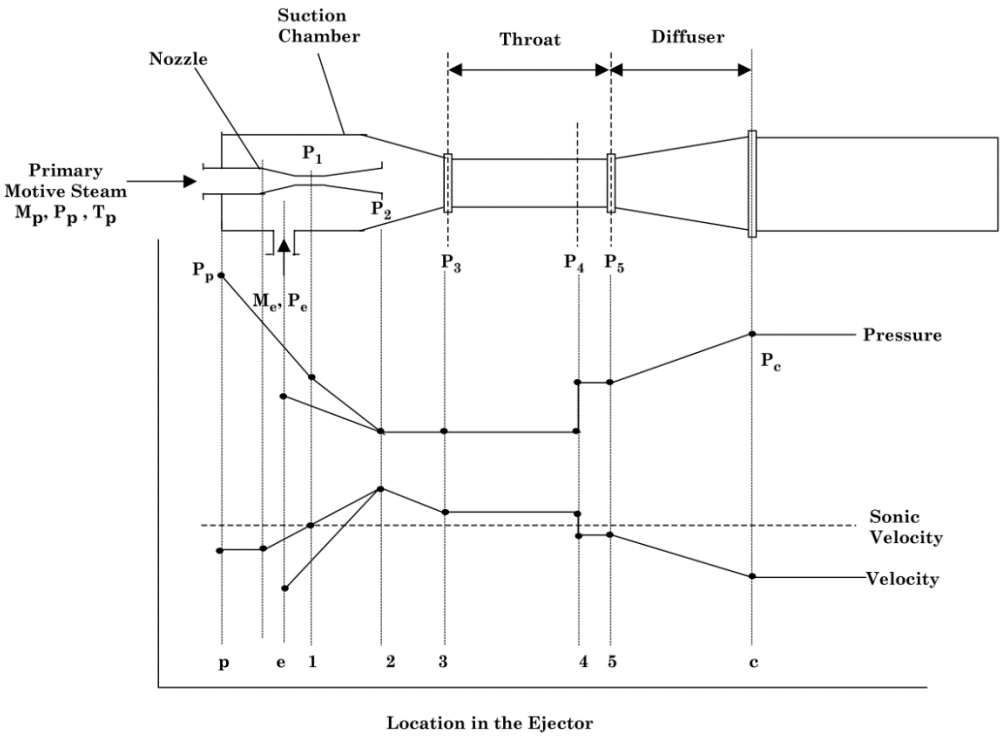

Figure 2.16 Variation in stream pressure and velocity as a function of location along the ejector [41]

5- Flow regimes consist of double choking, single choking and backflow [42]. The best performance of ejectors occurs in double-choking regime in which entrainment ratio is constant.

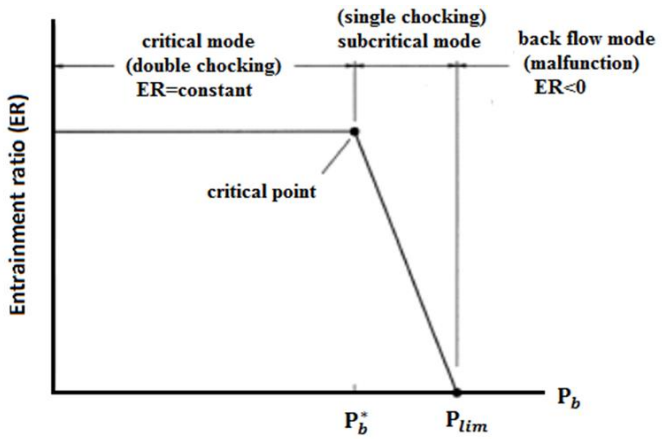

Figure 2.17 Ejector operation regimes for constant inlet conditions[42].

6- Figure 2-18 shows the typical operating map of an ejector depending on primary and secondary flow conditions, based on the experimental work of Chunnanond and Aphornratana [43].

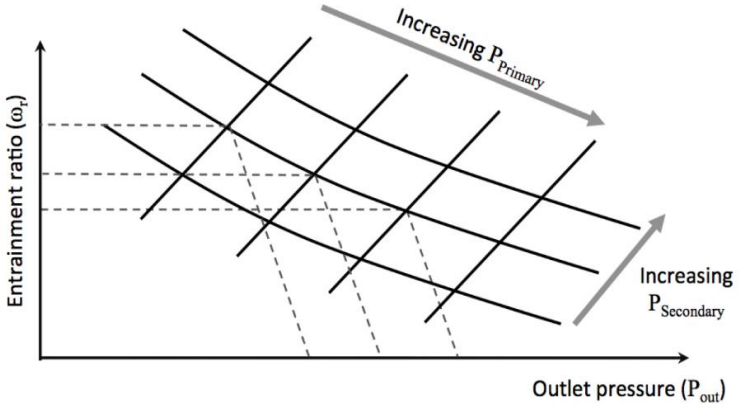

Figure 2.18 Typical ejector operating map: ω as a function of inlet and outlet pressures[43].

7- There are three general governing equations to analyze the nozzle, mixing and a diffuser section. The three governing equations are as follows:

Conservation of mass: $$\sum \rho_i V_i A_i = \sum \rho_e V_e A_e \quad (2.1)$$

Conservation of momentum: $$P_i A_i + \sum m_i V_i = P_e A_e + \sum m_e V_e \quad (2.2)$$

Conservation of energy: $$\sum m_i (h_i + {V_i^2}/{2}) = m_e (h_e + {V_e^2}/{2}) \quad (2.3)$$

where "i " is input and "*e*" is output.

8- According to the position of the nozzle exit (NXP), There are two different types of ejector namely constant-area mixing ejector and constant-pressure mixing ejector [40].

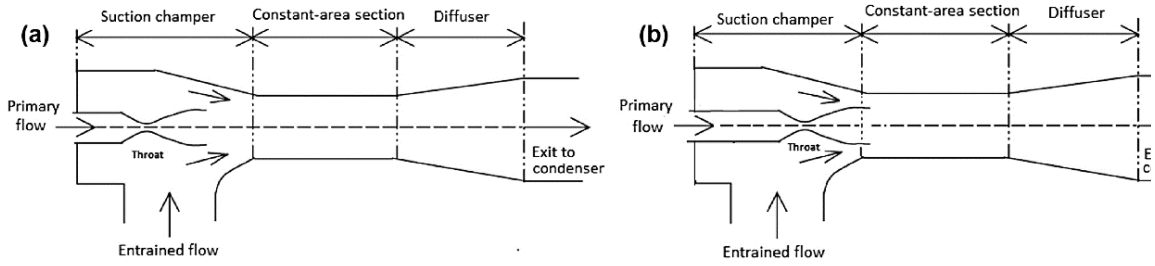

Constant-pressure mixing ejector. Constant-area mixing ejector.

Figure 2.19 Two different types of ejectors based on nozzle exit position (NXP) [40].

Some researchers previously have shown that the constant-pressure mixing ejector has a better performance than that of the constant area [40] [44]. Therefore, constant-pressure mixing ejectors are generally used in various refrigeration applications, especially in the ejector refrigeration systems.

Keenan et al. found that the constant-area mixing model offers better agreement with the experimental results than that of the constant-pressure mixing model. Also, the constant-area mixing model gives more information of the flow inside the ejector than that of the constant-pressure mixing model [45].

9- There are four efficiencies for each ejector, namely the efficiency of the primary nozzle (η_{pr}), secondary stream (η_{sec}), diffuser (η_d) and mixing (η_{mix}). The definition of isentropic efficiency of each part based on figure 2-20 is as follows: (see fig 3.3 for the ejector cross-sections)

$$\eta_{sec} = \frac{h_6 - h_{7s}}{h_6 - h_{is,7s}} \tag{2.4}$$

$$\eta_{pr} = \frac{h_4 - h_{7p}}{h_4 - h_{is,7p}} \tag{2.5}$$

$$\eta_d = \frac{h_{is,1} - h_8}{h_1 - h_8} \tag{2.6}$$

$$\eta_{mix} = 1 - \frac{F_f}{\dot{m}_p V_{7p} + \dot{m}_s V_{7s}} \tag{2.7}$$

$$F_f = \left(P_{7p}A_{7p} + \dot{m}_p V_{7p}\right) + \left(P_{7s}A_{7s} + \dot{m}_s V_{7s}\right) - P_8 A_8 - \left(\dot{m}_p + \dot{m}_s\right)V_8$$

where, "*h*" is enthalpy, subscript "*is*" is isentropic process and numbers indicate points.

10- Polytropic efficiency is an innovation recently introduced by Galanis and Sorin for ejectors. Their research group published three papers regarding the application of polytropic efficiency. ([36], [39], [38]). Definition of polytropic efficiency is as follows. (Fig. 2-20)

- The polytropic efficiency η_{pl} is defined as the isentropic efficiency of an elemental process.
- Fluid pressure changes by a small quantity dP while its entropy increases by ds.
- Overall isentropic efficiency is a function of the polytropic efficiency and depends on the overall pressure ratio.
- the polytropic, or infinitesimal stage, efficiency is used extensively in the design and analysis of compressors and turbines.
- It takes into account the elemental pressure ratio and the irreversibilities occurring during the acceleration and deceleration processes unlike isentropic.

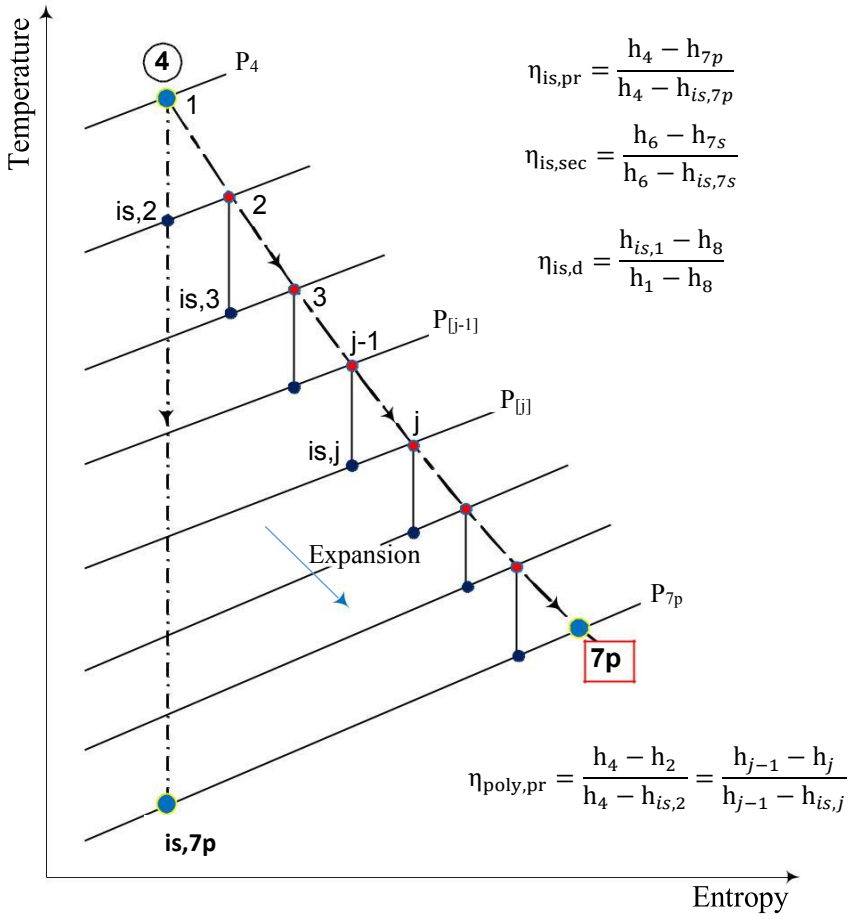

Figure 2.20 Definition of polytropic and isentropic efficiencies for the acceleration of the primary fluid [36]

11- In a real process, secondary choke does not take place exactly at the secondary stream exit. In particular, for CPM ejectors, the choke phenomena of the secondary stream approximately take place at the inlet of constant area duct. In other words, The hypothetical throat occurs inside the constant-area section of the ejector. For critical operation, two choked flows exist inside the ejector. One occurs in the primary flow through the nozzle throat, the second choke is related to the secondary flow at the "hypothetical throat" (Munday and Bagster, [46] ; Huang et al., [40]) in the mixing chamber. Munday and Bagster further assumed a constant pressure mixing in which the primary flow expands after exiting from the primary nozzle. It creates a hypothetical throat area (effective area) for the secondary flow downstream of the nozzle exit where the secondary flow reaches a sonic velocity and chocks at this point (fig. 2-23). After chocking of the secondary flow, mixing process of the two streams starts and completes at the end of the mixing chamber. Due to the supersonic flow downstream of the mixing section, there is a train of shock waves that cause a compression effect and a sudden drop in flow speed. In addition, it is

proved by CFD simulations. According to CFD results of constant pressure mixing and constant area mixing type of ejectors, the choke phenomena of primary stream takes place at the throat. The choke phenomena of the secondary stream for CPM approximately takes place at the inlet of constant area duct. In other words, The hypothetical throat occurs inside the constant-area section of the ejector. The choke phenomena of the secondary stream for CAM ejectors approximately takes place at the hypothetical throat, a small distance of exit plan of the secondary duct.

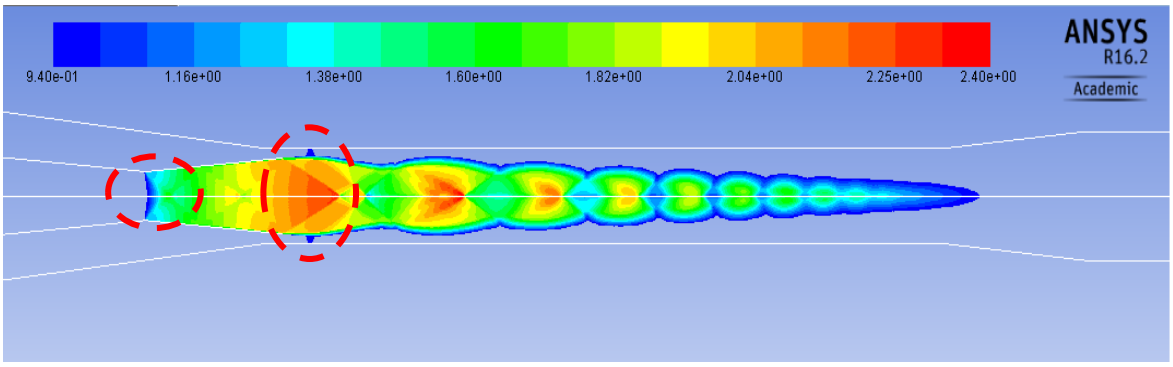

Figure2.21 Choked flows in the constant area mixing ejector (Mach contour)

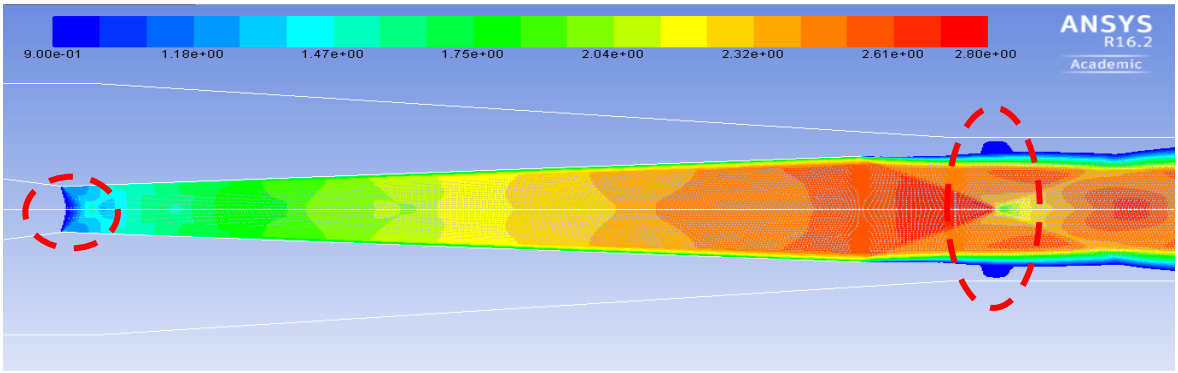

Figure2.22 Choked flows in the constant pressure mixing ejector (Mach contour)

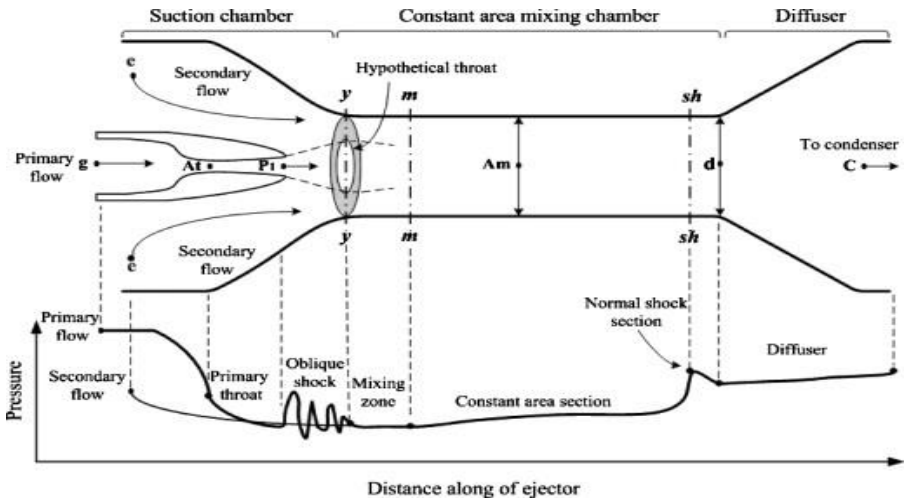

Figure 2.23 Hypothetical throat area (effective area) for the secondary flow [46].

CHAPTER 3 : Effects of component polytropic efficiencies on the dimensions of monophasic ejectors

AVANT-PROPOS

Auteurs et affiliation:

- Payam Haghparast: étudiant au doctorat, Université de Sherbrooke, Faculté de génie, Département de génie mécanique.
- Mikhail Sorin: professeur, Université de Sherbrooke, Faculté de génie, Département de génie mécanique.
- Hakim Nesreddine: Institut de recherche d'Hydro-Québec (IREQ), 600 Rue de la montagne, Shawinigan, QC, G9N 7N5, Canada

Date d'acceptation: 10 February 2018

État de l'acceptation: version finale publiée.

Revue: Energy Conversion and Management

Référence: [47]

Titre français: Effets des rendements polytropiques des composants sur les dimensions des éjecteurs monophasiques

Contribution au document: Cet article contribue à la thèse en comparant l'efficacité des composants polytropiques et isentropiques sur les cycles de réfrigération des éjecteurs pour concevoir l'éjecteur le plus thermodynamiquement efficace.

This article contributes the thesis by comparison of component polytropic and isentropic efficiencies on the ejector refrigeration cycles to design the most thermodynamically efficient ejector.

Résumé français:

Un choix inapproprié d'efficacité isentropique pour le dimensionnement des composants des éjecteurs monophasiques est l'une des plus grandes sources d'erreur dans leur conception. La présente étude montre que le remplacement des rendements isentropiques par des rendements polytropiques dans les modèles à éjecteur 1D fournit des résultats plus précis. Les rendements polytropiques permettent d'accéder plus précisément aux effets de la variation du rapport de pression sur les irréversibilités des processus d'accélération et de décélération. Il a été démontré que la déviation de la longueur de conduit à surface constante, calculée en utilisant un rendement isentropique par rapport à la longueur réelle, est trois fois supérieure à celle calculée en utilisant un rendement polytropique. Les rendements polytropiques sont extraits de la

modélisation CFD de deux types d'éjecteurs, un éjecteur à mélange à surface constante (CAM) et un éjecteur à mélange à pression constante (CPM). Un modèle thermodynamique 1D pour les éjecteurs CAM et CPM, basé sur le concept d'efficacité polytropique, est proposé et validé sur la base de données expérimentales. Des études paramétriques basées sur ce modèle ont été menées. Elles révèlent que la variation de l'efficacité polytropique de la buse primaire a l'impact le plus important sur la longueur de conduit du secteur constant. De nouvelles corrélations empiriques pour estimer les efficacités polytropiques sont également fournies.

3.1 Abstract

An inappropriate choice of isentropic efficiencies for the sizing of the component parts of monophasic ejectors is one of the greatest sources of error in their design. The present study shows that the replacement of isentropic efficiencies with polytropic efficiencies within 1D ejector models provides more accurate results. Polytropic efficiencies access more precisely the effects of the pressure ratio variation on the irreversibilities of the acceleration and deceleration processes. It is demonstrated that the deviation in the constant area duct length, calculated by using an isentropic efficiency from the real length is three times greater than the one calculated by using a polytropic efficiency. The polytropic efficiencies are extracted from the CFD modeling of two types of ejectors, a constant area mixing (CAM) ejector and a constant pressure mixing (CPM) ejector. A 1D thermodynamic model for CAM and CPM ejectors, based on the polytropic efficiency concept, is proposed and validated against experimental data. Parametric studies based on this model were completed. They reveal that the variation in polytropic efficiency of the primary nozzle has the most important impact on the constant area duct length. New empirical correlations to estimate the polytropic efficiencies are also provided.

Keywords: *1D model; Polytropic efficiency; Ejector dimensions; Parametric study*

Nomenclature

A	Cross section area (mm^2)	**Subscripts**	
D	Diameter (mm)	cp	Critical point
F	Force (N)	d	Downstream of shock
f	Friction coefficient (-)	D	Diffuser
h	Specific enthalpy ($kJ.kg^{-1}$)	e	Exit
L	Length (m)	f	Friction
$\dot{m}$	Mass flow rate ($kg.s^{-1}$)	is	Isentropic
Ma	Mach number	mix	Mixing
P	Pressure (kPa)	out	Outlet
PR	Pressure Ratio=P_1/P_6 (-)	pol	Polytropic
s	Specific entropy ($kJ.kg^{-1}\ K^{-1}$)	p	Primary nozzle
T	Temperature (K)	s	Secondary stream
Therm	Thermodynamic	th	Ejector throat
V	Velocity ($m.s^{-1}$)	tot	Total
υ	Specific volume ($m^3.kg^{-1}$)	u	Upstream of shock
X	Position of nozzle exit (mm)	1	Exit of ejector
		4	Primary inlet
Greek symbols		6	Secondary inlet
ε	Wall roughness (mm)	7	Nozzle exit
η	Efficiency	8	Inlet of diffuser
θ	Half-angle (deg)	**Acronyms**	
ω	Entrainment ratio = $\dot{m}_s.\dot{m}_p^{-1}$ (-)	CAM	Constant area mixing
ρ	Density ($kg.m^{-3}$)	CPM	Constant pressure mixing

3.2 Introduction

An Ejector is a simple, reliable and low-cost device to produce vacuum by accelerating a gas, vapor or liquid in a nozzle. Ejectors employ liquid or gas as a motive fluid without using any moving parts. Typical ejector construction includes four distinct parts: a convergent–divergent nozzle, a suction chamber attached to a constant area duct and a diffuser (Fig. 3-3).

Ejectors are considered as an alternative to compressors in refrigeration systems due to no source of power is required other than the motive gas and they are easy to install, operate and maintain. The layout of an ejector refrigeration cycle is shown in Figure 3-1.

Research studies on the ejector as a favorable device is on the increase since the 1950s to date. The performance of ejectors has been carefully considered theoretically and experimentally. Most researchers believe that it is essential to enhance the performance of ejectors in order to make them economically more attractive. For this reason, numerous investigations on optimizing the ejector performance have been carried out.

Among these studies, comparing different refrigerants in order to achieve an appropriate working fluid under varying operating conditions and effects of the geometry on the ejector performance are considerably investigated experimentally and numerically.

The effects of different refrigerants on the ejector efficiency in the refrigeration systems are studied by [48] [23] [24]. Some researchers have investigated the effect of ejector geometry on its performance, such as nozzle exit location, mixing chamber/nozzle area ratio, and nozzle design. Banasiak et al. [25] examined different ejector configurations in order to achieve optimum ejector geometry. They used various lengths and diameters of the mixing duct and various angles of divergence for the diffuser. Cizungu et al. [26] and Tang et al. [49] optimized the ejector geometry to achieve maximum values for either the entrainment ratio or the pressure ratio. Vereda et al. [50], Elbel [27] and Omidvar et al. [51] experimentally studied different ejector dimensions, such as the sizing of the motive nozzle, the diffuser and nozzle exit position. Nakagawa et al. [28] experimentally analyzed the effect of the mixer length on ejector system performance. A review of recent developments in advanced ejector technology can be found in [29] [52].

Researchers always make assumptions for theoretical analyses of the ejectors. One of the most important assumptions is assuming the appropriate component efficiencies. Some consider constant isentropic efficiencies at various parts along the ejector, including the primary nozzle, secondary nozzle, and diffuser in order to take into account the irreversibilities. Tyagi and Murty [30] assumed these constants arbitrarily. Aly et al. [31] and Cizungu et al. [26] chose values from the literature. Some researchers experimentally determined the constants [32] [33] [53]. Varga et al.

[34] and Zhang et al. [54] extracted values from a CFD model. Grazzini and Rocchetti [35] used a "trial and error" approach by comparing the solution from a 1D model to CFD results.

In all of the previously referenced 1D models, the constant isentropic efficiencies were used. Recently Galanis and Sorin [36] introduced the concept of the polytropic efficiency for the ejectors. The polytropic efficiencies are used extensively in the design and analysis of compressors and turbines [37] but has only recently been applied to the study of ejectors [38] [39] [55]. However, the authors did not present a proof that the application of the polytropic efficiency is advantageous compared to the isentropic efficiency. The polytropic efficiency is defined as the isentropic efficiency of an elemental process (Fig. 3-2). It takes into account the elemental pressure ratio and the irreversibilities occurring during the acceleration and deceleration processes, unlike isentropic efficiency.

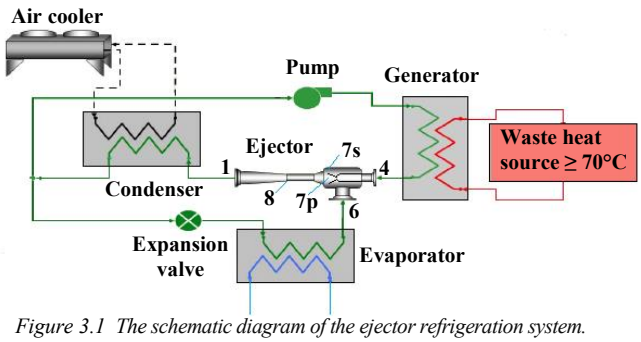

Figure 3.1 The schematic diagram of the ejector refrigeration system.

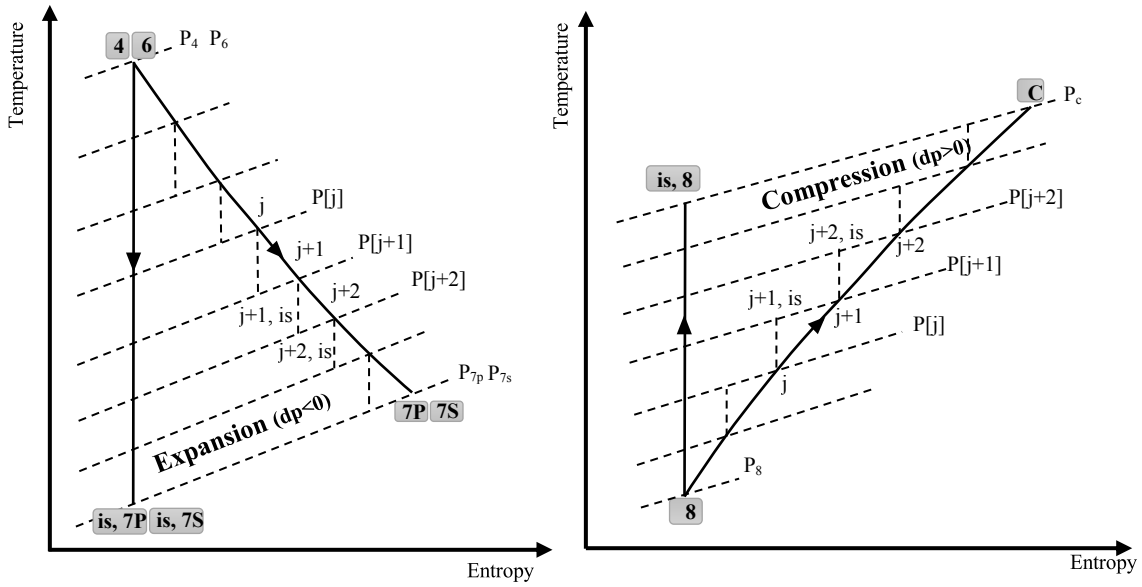

$P_{j+1} = P_j - \Delta P$
$S_{j+1,is} = S_j$
$h_{j+1,is} = f(P_{j+1}, S_{j+1,is})$
$h_{j+1} = h_j - \eta_{pol}(h_j - h_{j+1,is})$
$\boldsymbol{\eta_{pol,pr\ or\ sec}} = \dfrac{h_j - h_{j+1}}{h_j - h_{j+1,is}}$

$\boldsymbol{\eta_{is,pr}} = \dfrac{h_4 - h_{7p}}{h_4 - h_{is,7p}}$

$\boldsymbol{\eta_{is,sec}} = \dfrac{h_6 - h_{7s}}{h_6 - h_{is,7s}}$

$P_{j+1} = P_j + \Delta P$
$S_{j+1,is} = S_j$
$h_{j+1,is} = f(P_{j+1}, S_{j+1,is})$
$h_{j+1} = h_j - \dfrac{1}{\eta_D}(h_j - h_{j+1,is})$
$\boldsymbol{\eta_{pol,D}} = \dfrac{h_j - h_{j+1,is}}{h_j - h_{j+1}}$

$\boldsymbol{\eta_{is,D}} = \dfrac{h_{is,1} - h_8}{h_1 - h_8}$

3.2 Definitions of polytropic (or elemental) and isentropic (or overall) efficiencies to calculate the flow properties.

The number of papers dedicated to the thermodynamic modeling of the ejectors is considerable. This research paper has the following novelty and originality items:

(1) The proposed 1D model is more realistic than previous 1D models due to the application of the polytropic (or elemental) efficiency conception. In this case, the 1D model is able to consider the effects of the pressure ratio on the entropy increase during the irreversible acceleration and deceleration processes, unlike previous models, which use isentropic (or overall) efficiencies for this purpose.

(2) Real values of the polytropic efficiencies are calculated by CFD models for the first time. In this case, the 1D model is able to evaluate the ejector dimensions and flow properties more accurately.

(3) A comprehensive comparison between all dimensions obtained by the 1D model based on isentropic and polytropic efficiencies is carried out against experimental data. In order to make a robust comparison, two separate cases of experimental ejector data are considered, namely a constant area mixing (CAM) ejector and a constant pressure mixing (CPM)

ejector, with different known geometries, working fluids (R245fa, R141b), and operating conditions.

(4) The improved 1D model is able to evaluate all diameters and lengths of both types of ejectors, in particular, the length of the constant area duct (L_4). All Previous models only determined some dimensions, without including an explicit method for the calculation of the constant area duct length.

(5) A parametric study of the main parameters is performed to improve the ejector sizing by using the validated 1D model. The effects of the following parameters on all ejector dimensions are investigated for a base case: the primary and secondary inlet pressures, the diffuser exit back pressure, the component polytropic efficiencies, and the mass flow rates.

(6) Empirical correlations are established to estimate the polytropic efficiencies and to demonstrate the interaction between ejector parameters.

3.3 Ejector operation and geometry

In this study, two different types of ejectors are considered, based on the design nozzle exit position, namely constant area mixing (CAM) and constant pressure mixing (CPM).

In constant area mixing ejector, the nozzle exit is located within the constant area duct as the mixing of the primary and secondary streams occur inside this duct. In constant pressure mixing, the nozzle exit is located within the converging part of the suction chamber and the mixing occurs at a constant pressure [56] [57].

Fig. 3-3 illustrates the geometry, parts and main cross-sections of ejectors under investigation. For case 1, an available experimental data of test bench located at the Hydro-Québec laboratory in Shawinigan was used [58]. For case 2, the experimental data of Huang [40] was considered.

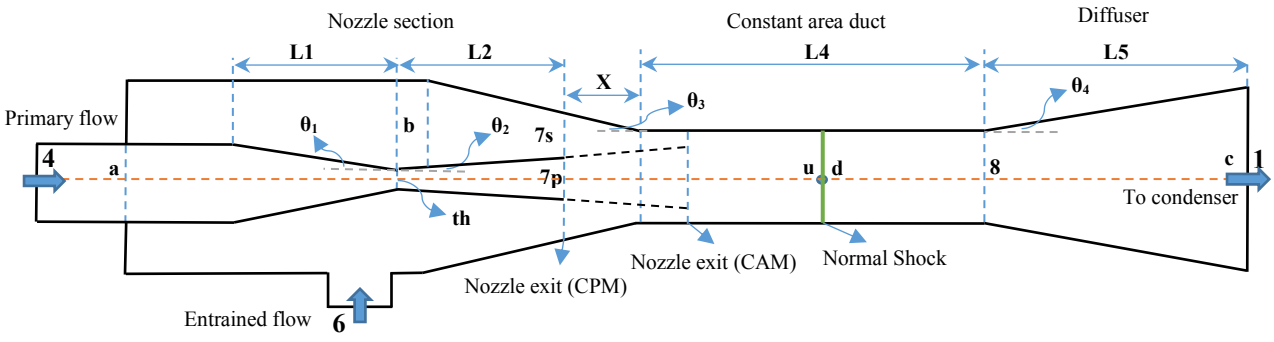

Figure 3.3 Ejector geometry, parts and main cross-sections

Operating conditions, as well as the geometry of the supersonic single-phase ejectors are presented in table 3.1 and 3.2. Furthermore, a flowchart of the main inputs and outputs of the models are introduced in fig. 3-4. This strategy is applicable for the 1D models, which calculate all dimensions of the ejectors. It should be noted that for validation of a sizing 1D model, it is necessary that polytropic efficiencies and critical back pressure point calculate by CFD model as shown in figure 3-4. However, in order to size and design an ejector for integration into a thermodynamic cycle, component efficiencies must be assumed, as well as an appropriate condenser pressure, which fixes the back pressure.

Table 3.1 Operating conditions

Parameter	Case# 1 (CAM)	Case# 2 (CPM)
Working fluid	R245fa, **Real Fluid**	R141b, **Real Fluid**
P_4, T_4 (Primary Inlet)	480.6 kPa, 352.45 K	604.9 kPa, 373.15 K
P_6, T_6 (Secondary Inlet)	100.1 kPa, 303.75 K	39.9 kPa, 283.45 K

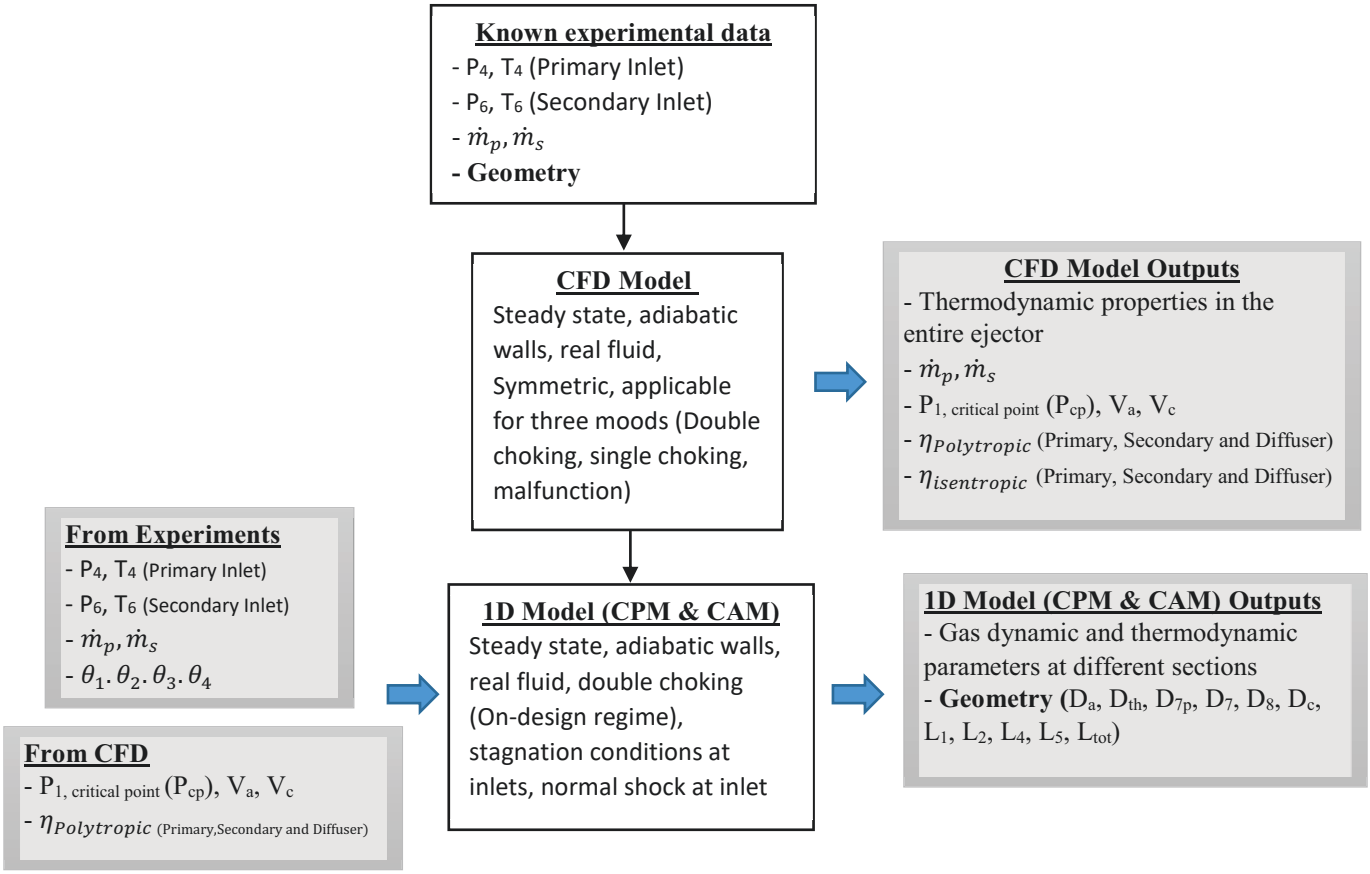

Figure 3.4 Overall procedure of inputs and outputs for calculating all ejector dimensions

Table 3.2 Geometry of the ejectors (Case# 1 & 2)

D [mm]	Case# 1	Case# 2	L, X [mm]	Case# 1	Case# 2	θ [deg]	Case# 1	Case# 2
D_a	32.08	8.251	L_1	100.9	15.4	θ_1	5	10
D_{th}	14.42	2.810	L_2	46	35.4	θ_2	5	3
D_{7p}	22.47	6.518	X	7.08	4.2	θ_3	6.99	5
D_7	28.47	9.527	L_4	223.77	146.0	θ_4	5.98	4
$D_{8, u, d}$	28.47	8.794	L_5	46	121.6			
D_c	38.10	25.803	L_{tot}	416.67	322.6			
			(L_4/D_8)	7.86	16.6			
			$(L_4+X)/D_8$	8.109	17.1			

3.4 Description of the models

According to the procedure of the inputs and outputs illustrated in Fig. 3-4, after providing required data from previous experimental studies, it is possible to make the CFD models, extract the values of the polytropic efficiencies from it and then to complete the 1D model of the ejectors. Some assumptions for both types of models are the same, i.e. steady state conditions, real fluid properties, and adiabatic walls.

3.4.1 CFD model

A detailed CFD model is carried out to simulate the fluid flow in the ejector for the two cases with different geometries and operating conditions. Some important parameters such as critical back pressure point (point cp), component polytropic efficiencies, velocity value at section “a” and “c” (see fig. 3-3) should be calculated by using the CFD models. Afterwards, the ejector sizing by using the thermodynamic model will be carried out.

3.4.1.1 Details of the CFD settings

The CFD simulation was conducted using the ANSYS commercial software package based on successful implementations reported in the literature [59] [60]. Turbulence effects in the ejector have been modeled using the k-ω SST turbulence model. Second order accurate discretization scheme coupled with a pressure-based implicit solver is used. The energy equation is solved in a second step and the density is computed through the REFPROP v9.1 database equation. The conservation equations governing the fluid flow in the ejector are of the compressible, steady state, axisymmetric form and all walls are assumed adiabatic. In conclusion, the main features of the numerical scheme can be summarized in table 3.3:

Table 3.3 CFD Settings (Case# 1 & 2)

Working fluid	R245fa, Real fluid (Case# 1) R141b, Real fluid (Case# 2)
Turbulence Model	k-w SST(HRN)
Solver Numerical schemes	Pressure based Coupled, Pressure: PRESTO! Momentum, Turbulence, Energy: 2nd order Upwind
Convergence criteria	Residuals RMS<1×10^{-5} Mass imbalances<1%

3.4.1.2 Details of the mesh grid used in the CFD calculations

Before proceeding with the main calculation, a grid convergence study was performed to ensure overall mesh independent results. To this aim, the results of four sets of grids were compared for both cases. The results with different grids reveal that the grid density has a strong influence on the convergence and stability characteristic. The Mach number along the ejector is used to detect the influence of the cell number (Fig. 3-5). From these figures, 565592 quadrilateral cells for Case# 1 and 684960 quadrilateral cells for Case# 2 were considered sufficient to give satisfactory results in terms of entrainment ratio (Fig. 3-6). This mesh is refined from the primary nozzle lips along the shear layer and also close to walls in order to achieve an acceptable value for the wall coordinate ($30\leq y^{+}\leq100$), adequate for the application of a High-Reynolds approach [61]. The standard wall function was applied near the wall and the cells close to the walls were intensive enough to capture the complicated supersonic flow.

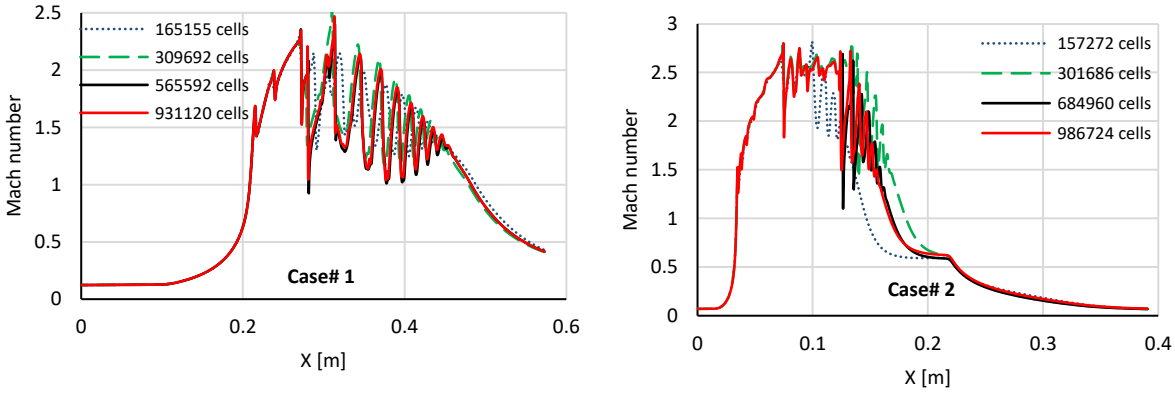

3.5 Variation of axial Mach number with different grid levels for Case# 1 & 2

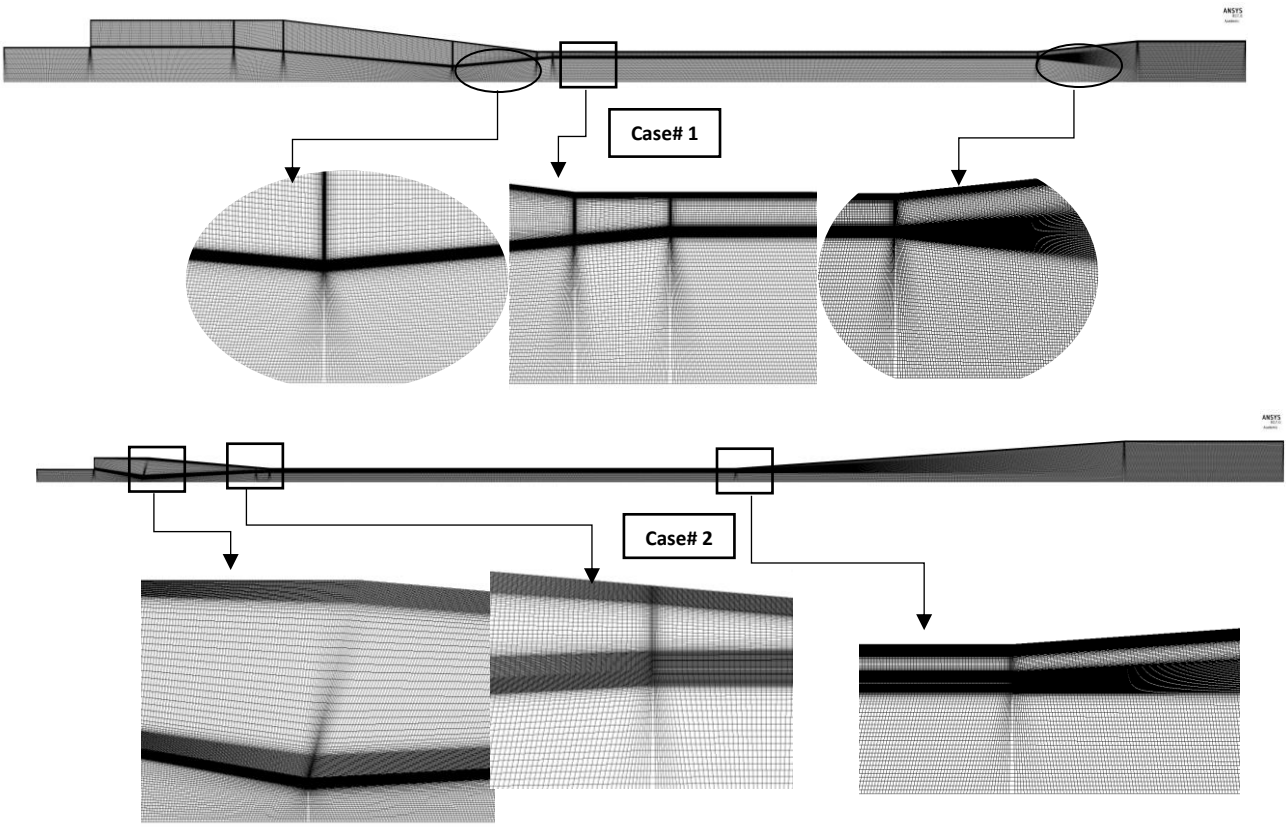

Figure 3.6 Details of the mesh grid used in the CFD calculations for Case# 1 (CAM) and Case# 2 (CPM)

3.4.1.3 Calculation of the critical back pressure point (point cp)

The critical back pressure point is one of the most important input parameters to validate a 1D model against experimental data. The calculated dimensions are extremely dependent on the value of this parameter.

Critical back pressure and secondary mass flow rate are usually as output parameters in 1D models for ejector design. However, for sizing all dimensions of an ejector, they are required as input.

It should be noted that the back pressure of the presented ejector test benches that are working in critical mode is not necessarily a critical point. Therefore, in order to obtain the critical back pressure point, it is necessary to run different CFD simulations at fixed inlet conditions. According to the performance curves of the ejectors, the critical back pressure for case# 1 is equal to 190.19 kPa (Fig. 3-7) and for case# 2 is equal to 105.5 kPa (Fig. 3-8).

To validate the CFD ejector models for two cases, comparisons with the experiments of Nesreddine et al. [58] and Huang et al. [40] are made. Fig. 3-7 and 3-8 display a comparison between the predicted entrainment ratio by the present CFD models and the experimental data. The CFD results are in good agreement with experimental data in the on-design regime. The

deviation between the calculated and the experimental entrainment ratio is found to be around -9.36 % for case 1 and similarly 6.65% for case 2. In addition, Mach number contour plots of the different back pressures along the ejector are shown in fig. 3-9 and 3-10. The pressure diagram in terms of length is also drawn for two obtained critical points, which are the transition points between double choking mode and single choking. Basically, the ejector performance can be divided into three operational modes, according to the back pressures. (1) double-choking or critical mode (2) single-choking or subcritical mode and (3) back-flow or malfunction mode.

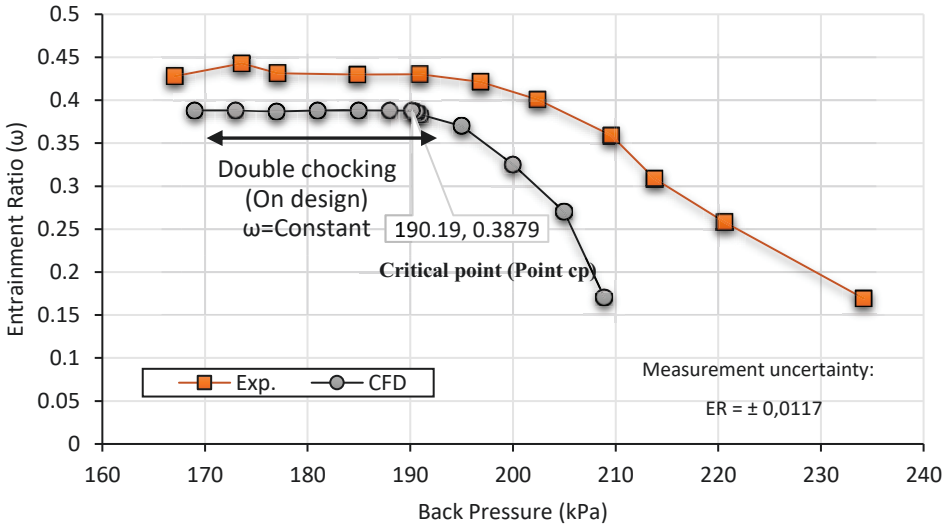

Figure 3.7 Ejector operational modes (Performance Curves) for Case# 1 (R245fa)

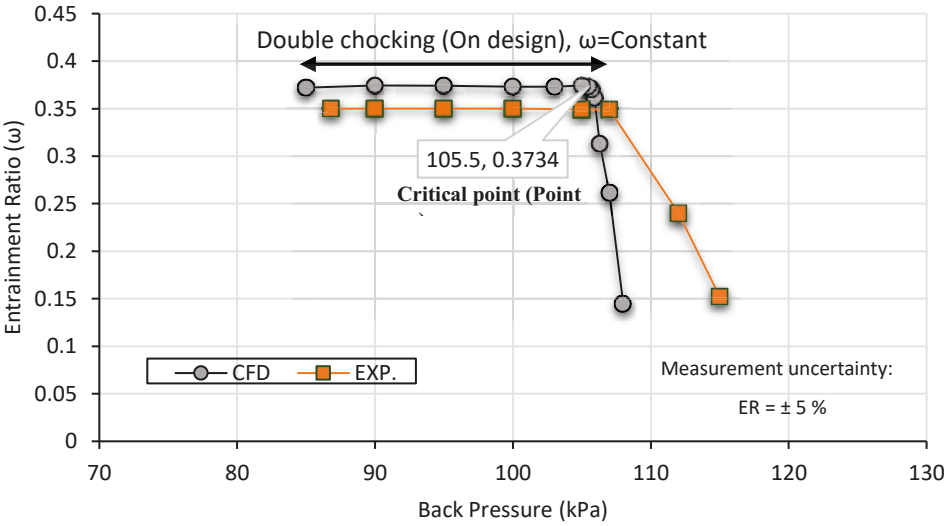

Figure 3.8 Ejector operational modes (Performance Curves) for Case# 2 (R141b)

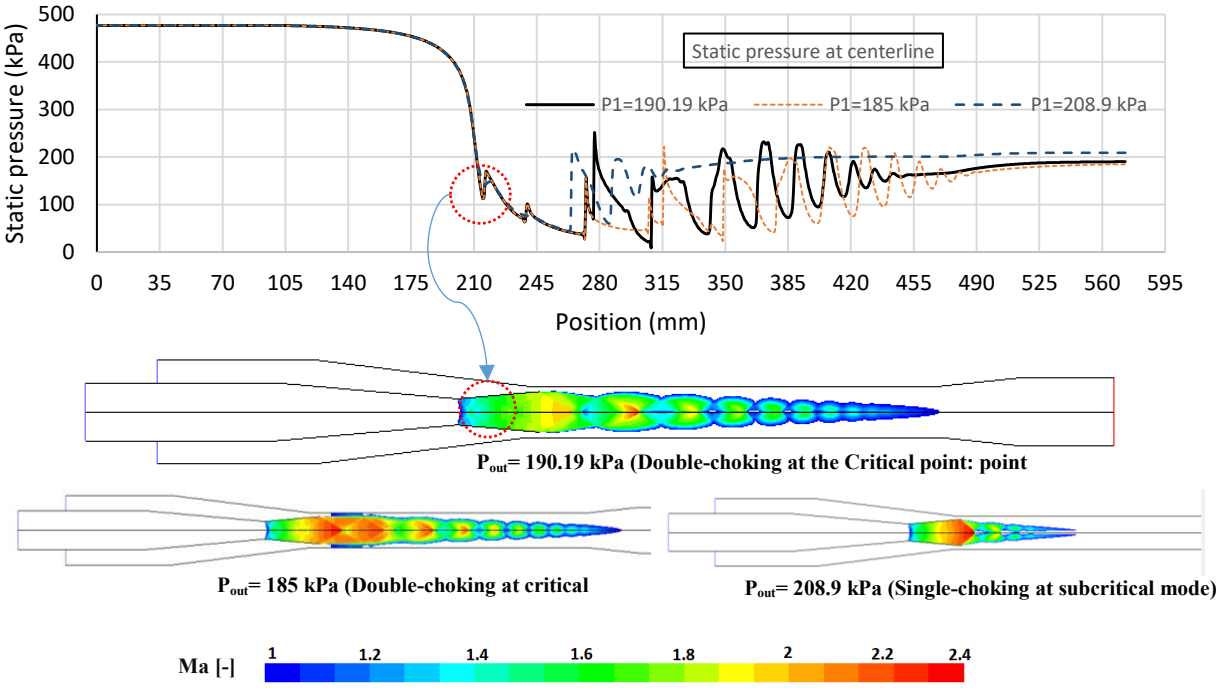

Figure 3.9 Mach number plots at three different back pressures for case# 1

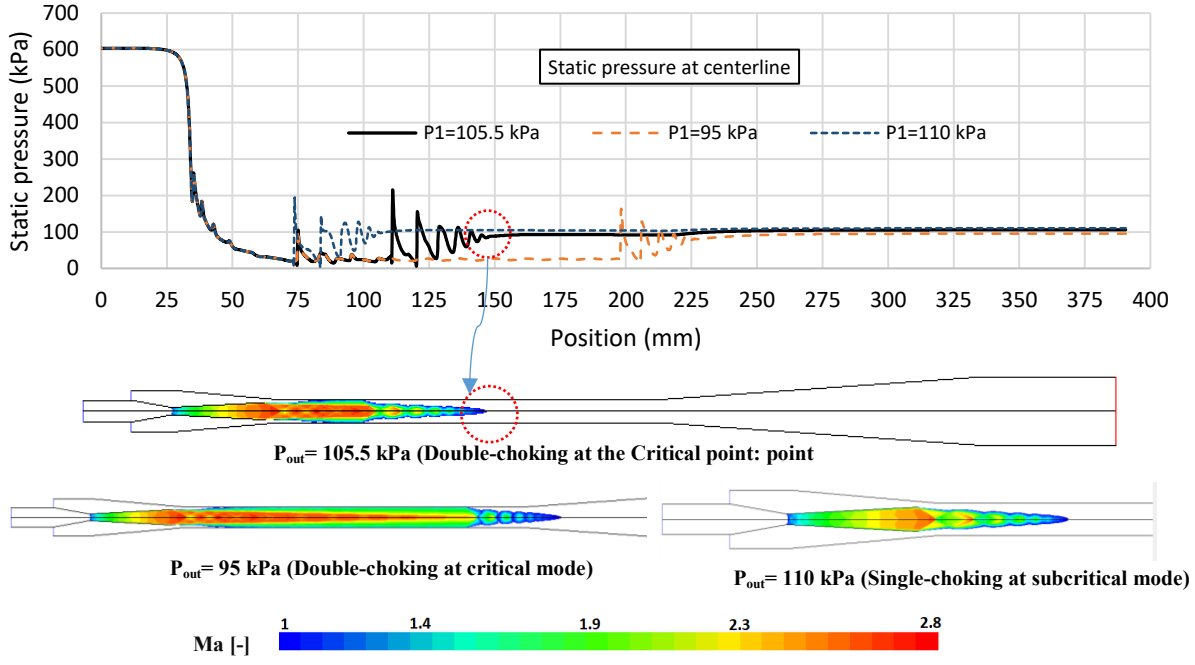

Figure 3.10 Mach number plots at three different back pressures for case# 2

3.4.1.4 Calculation of the polytropic efficiencies

Contrary to isentropic efficiencies, polytropic efficiencies take into account the effect of the pressure ratio on the corresponding entropy increase during the irreversible expansion and compression processes. In fact, they apply to a small pressure ratio while the isentropic

efficiencies apply to the pressure ratio between the beginning and end of the process. According to this definition, three parts, including the primary nozzle, secondary nozzle and diffuser, are divided into small stages based on pressure ratios in the CFD models. The correlations introduced in fig. 3-2 are used to calculate the efficiencies.

Using surface integrals, thermodynamic properties are calculated in each stage. The area-weighted average for pressure and velocity are considered, while the mass-weighted average is used for temperature. Finally, for the calculation of each polytropic efficiency, an average of the elemental efficiencies in each part is taken. Fig. 3-11 displays the definition of the elemental process (polytropic) in the CFD models for Case 1&2.

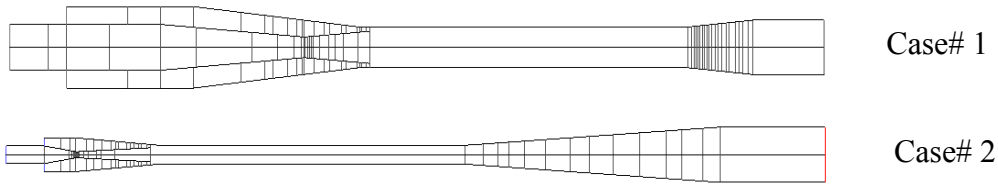

Figure 3.11 Definitions of the elemental process (polytropic) in the CFD model for Case# 1&2

Table 3.4 and 3.5 present the calculated efficiencies for varying back pressures at fixed inlet conditions. It can be observed that the η_D increased considerably with condenser pressure (P_{out}). As expected, for fixed inlet conditions the values for primary and secondary (efficiencies and fluid properties) are constant since P_{out} is changed. In addition, the value of the polytropic efficiency for the primary and secondary expansion streams is less than the corresponding isentropic efficiency while that of the diffuser compression stream is higher. These results are consistent with corresponding analytical expressions for perfect gases [62]. The mixing efficiency also decreases with the increase in the p_{out} at fixed inlet conditions.

Table 3.4 Efficiencies obtained from the CFD models for varying PR=P_1/P_6 (P_6=100.1 kPa). (Case# 1)

P_{out} (kPa)	PR	Isentropic (CFD)			Polytropic (CFD)			Mixing (CFD)
P_1	P_1/P_6	Primary	Secondary	Diffuser	Primary	Secondary	Diffuser	Mixing
191	1.908	0.9802	0.9804	0.8432	0.9757	0.9751	0.8529	0.9728
190.6	1.904	0.9802	0.9804	0.8284	0.9757	0.9751	0.8383	0.9711
190.19	1.9	0.9802	0.9805	0.8117	0.9757	0.9752	0.8211	0.9681
188	1.878	0.9802	0.9805	0.736	0.9757	0.9752	0.7461	0.9531
185	1.848	0.9802	0.9805	0.6649	0.9757	0.9752	0.6789	0.9326
181	1.808	0.9802	0.9805	0.621	0.9757	0.9752	0.6393	0.9177

Table 3.5 Efficiencies obtained from CFD models for varying PR=P_1/P_6 (P_6=39.9 kPa), (Case# 2)

P_{out} (kPa)	PR	Isentropic (CFD)			Polytropic (CFD)			Mixing (CFD)
P_1	P_1/P_6	Primary	Secondary	Diffuser	Primary	Secondary	Diffuser	Mixing
105.5	2.644	0.9463	0.9739	0.935	0.9373	0.9352	0.9436	0.9137
100	2.506	0.9462	0.9739	0.7649	0.9373	0.9352	0.7763	0.8419

3.5 1D Thermodynamic model

In this study, a model is developed which has the ability to design both types of monophasic ejectors, CPM and CAM, using the polytropic efficiency concept first proposed for ejectors evaluation by Galanis and Sorin [36]. This model is programmed in EES (Engineering Equation Solver), which includes relations for the fluid properties [63].

3.5.1 Assumptions

To simplify the analysis, some assumptions are made for the proposed thermodynamic model:

- The primary and secondary fluids are identical vapors, with real fluid properties.
- Body forces and heat transfer between the fluid streams and the ejector walls are neglected.
- Flow is one dimensional, compressible and steady state throughout the ejector.
- The inlet velocities of the primary and secondary flows are negligible (stagnation conditions).
- Pressure, temperature and mass flow are known from available experimental data for both the primary and secondary inlets. All fluid properties are uniform across their respective cross-sectional areas.
- Losses in the mixing chamber are accounted for by a dissipation coefficient.
- Mass flux maximization criterion is used at the nozzle throats. Due to the area reduction and low back pressure, flow choking occurs at the minimum cross-sectional area where the Mach number is unity.
- The pressure of the two streams at cross-section (7) is the same ($P_{7p} = P_{7s} = P_7$). This assumption implies that there are no shocks due to overexpansion or under an expansion of the primary stream.
- In constant pressure mixing type, the mixing of the two streams takes place at constant pressure and is complete at the inlet of the constant area duct.
- In constant pressure mixing type, the normal shock wave takes place at the entrance of the constant diameter duct then $P_{7p} = P_{7s} = P_u$.
- Both primary and secondary fluids are choked (critical operation).
- At the diffuser inlet (state 8) the mixed stream is always subsonic.
- For constant area mixing type (CAM), we have $A_7=A_u=A_d=A_8$. Therefore, P_u can be calculated by iteration.

- Critical back pressure point (point cp), isentropic and polytropic efficiencies are extracted from CFD models.
- The half-angles θ_1, θ_2, θ_3, θ_4 shown in fig. 3-3 are known from experimental geometry.

3.5.2 Calculating procedure

A simplified flow chart of the ejector design algorithm to calculate geometry and fluid properties at each cross-section is presented in Fig. 3-12. The calculation begins with the expansion and subsonic acceleration of the secondary fluid from the given stagnation conditions P_6 and T_6, taking into consideration the known flow rate $\dot{m}_s$. Finally, it finishes with deceleration of mixing stream at diffuser. The governing equations account for the conservation of the mass, momentum, and energy are presented below. The details of the calculation procedure for the constant pressure mixing type of ejector by using the conception of polytropic efficiency are also described in the following steps. In each step, inputs, outputs and appropriate equations are introduced.

- Cross-section 7s: To calculate conditions at Cross-section (7s), energy and mass conservation are solved by progressively decreasing the pressure (P) to maximize ($\dot{m}_s$/A). This procedure is repeated until the ratio ($\dot{m}_s$/A) reaches a maximum value. Since the flowrate $\dot{m}_s$ is known, it is then possible to calculate the area A_{7s}. (critical operation)

$$P_j = P_{j-1} - \Delta P_s \tag{3.1}$$

$$\eta_{pol,s} = (h_{j-1} - h_j)/(h_{j-1} - h_{j,is}) \tag{3.2}$$

$$h_{j.is} = h(P_j, s_{j-1}) \tag{3.3}$$

$$h_6 = h_j + 0.5V_j^2 \tag{3.4}$$

$$\dot{m}_s/A_j = V_j/\nu_j \tag{3.5}$$

$$\nu_j = \nu(P_j, h_j) \quad \text{and} \quad s_j = s(P_j, h_j) \tag{3.6}$$

- Cross-section b: By using V_b obtained from CFD, it is possible to determine the gas dynamic and thermodynamic parameters at cross-section (b) as well as the area A_b.

- Cross-section throat: The primary flow is always choked. The same procedure is applied to the expansion of the primary stream in the converging-diverging nozzle and generates the conditions at its throat (th). Since the flowrate $\dot{m}_p$ is fixed the area A_{th} and its diameter D_{th} are both calculated.

- Cross-section 7p: Since $P_{7p} = P_{7s}$ it is possible to continue the procedure in order to determine the conditions of the primary stream at state (7p) and to calculate the area A_{7p} from mass

conservation as well as the corresponding diameter D_{7p}. From $A_7 = A_{7p} + A_{7s}$ it is then possible to calculate the diameter D_7. The isentropic efficiency of the primary stream expansion from (4) to (7p) can then also be determined.

- Cross-section a: To calculate the gas dynamic and thermodynamic parameters at Cross-section (a) as well as the area (A_a), the V_a obtained from CFD is used.

- Cross-section u (before normal shock**):** By applying the equations expressing mass, energy and momentum conservation for the control volume between cross-sections (7) and (u), immediately upstream of the shock.

$$\dot{m}_p + \dot{m}_s = V_u A_u / \upsilon_u \tag{3.7}$$

$$h_4 + \omega h_6 = (1+\omega)(h_u + 0.5V_u^2) \tag{3.8}$$

$$\left(P_{7p}A_{7p} + \dot{m}_p V_{7p}\right) + (P_{7s}A_{7s} + \dot{m}_s V_{7s}) - F_f = P_u A_u + \left(\dot{m}_p + \dot{m}_s\right)V_u \tag{3.9}$$

By simplifying Eq. 9, we have:

$$V_{7p} + \omega V_{7s} = (1+\omega)V_u \tag{3.10}$$

- Cross-section d (after normal shock**):** Since $A_u = A_d$, with the expressions of mass, energy and momentum conservation, we have:

$$\dot{m}_p + \dot{m}_s = V_d A_d / \upsilon_d \tag{3.11}$$

$$h_4 + \omega h_6 = (1+\omega)(h_d + 0.5V_d^2) \tag{3.12}$$

$$(P_d + P_u) = (\dot{m}_p + \dot{m}_s)(V_u - V_d) \tag{3.13}$$

- Cross-section 8 (inlet of the diffuser**):** By using the known back pressure value and expressing mass, energy and momentum conservation for the control volume between cross-sections (8) and (1), the ejector outlet, we have equations 14 to 19. This procedure is repeated until A_j becomes equal to $A_d = A_u$. The corresponding enthalpy, pressure, entropy, and velocity are those of the mixture at cross-section (8). Mixing efficiency also can be calculated using the equations 20.

$$\mathrm{h_j} = \mathrm{h_{j-1}} - \Delta\mathrm{h} \tag{3.14}$$

$$\mathrm{h_{(j-1),is}} = \mathrm{h_j} + (\Delta\mathrm{h}\eta_{\mathrm{pol,D}}) \tag{3.15}$$

$$\mathrm{s_j} = \mathrm{s_{(j-1),is}} = s(\mathrm{p_{j-1}}, \mathrm{h_{(j-1),is}}) \tag{3.16}$$

$$\mathrm{P_j} = P\left(\mathrm{h_j}, \mathrm{s_j}\right) \; and \; \nu_\mathrm{j} = \nu\left(\mathrm{P_j}, \mathrm{h_j}\right) \tag{3.17}$$

$$h_4 + \omega h_6 = (1+\omega)(h_j + 0.5V_j^2) \tag{3.18}$$

$$\mathrm{A_j} = (\dot{m}_p + \dot{m}_s)(\nu_\mathrm{j}/\mathrm{V_j}) \tag{3.19}$$

$$\eta_{mix} = 1 - \frac{F_f}{\dot{m}_p V_{7p} + \dot{m}_s V_{7s}} \quad (3.20)$$

$$F_f = \left(P_{7p}A_{7p} + \dot{m}_p V_{7p}\right) + \left(P_{7s}A_{7s} + \dot{m}_s V_{7s}\right) - P_8 A_8 - \left(\dot{m}_p + \dot{m}_s\right)V_8 \quad (3.21)$$

- Cross-section c (before outlet**):** By using V_c obtained from CFD, it is possible to determine the thermodynamic properties at Cross-section (c) as well as the area A_c.

Finally, all lengths can be calculated based on correlations 22 to 27.

$$L_1 = (D_a - D_{th})/2tan(\theta_1) \quad (3.22)$$

$$L_2 = (D_{7p} - D_{th})/2tan(\theta_2) \quad (3.23)$$

$$L_5 = (D_c - D_8)/2tan(\theta_4) \quad (3.24)$$

$$P_d A_d + \left(\dot{m}_p + \dot{m}_s\right)V_d - F_f = P_8 A_8 + \left(\dot{m}_p + \dot{m}_s\right)V_8 \quad (3.25)$$

$$\Delta P = F_f / A_8 = f\,(L_4/D_8)(\rho V^2/2) \quad \text{(Darcy equation)} \quad (3.26a)$$

$$L_4 = F_f / (f\,(A_8/D_8)(\rho V^2/2)) \quad (3.26b)$$

$$f = \left(\frac{1}{-2log\left(\frac{e}{3.7\,D} + \frac{2.51}{Re\sqrt{f}}\right)}\right)^2 \quad \text{(Colebrook equation)} \quad (3.26c)$$

Absolute wall roughness for commercial new steel (e=0.046 mm) (Re>4000)

$$X = (D_7 - D_u)/2tan(\theta_3) \quad (3.27)$$

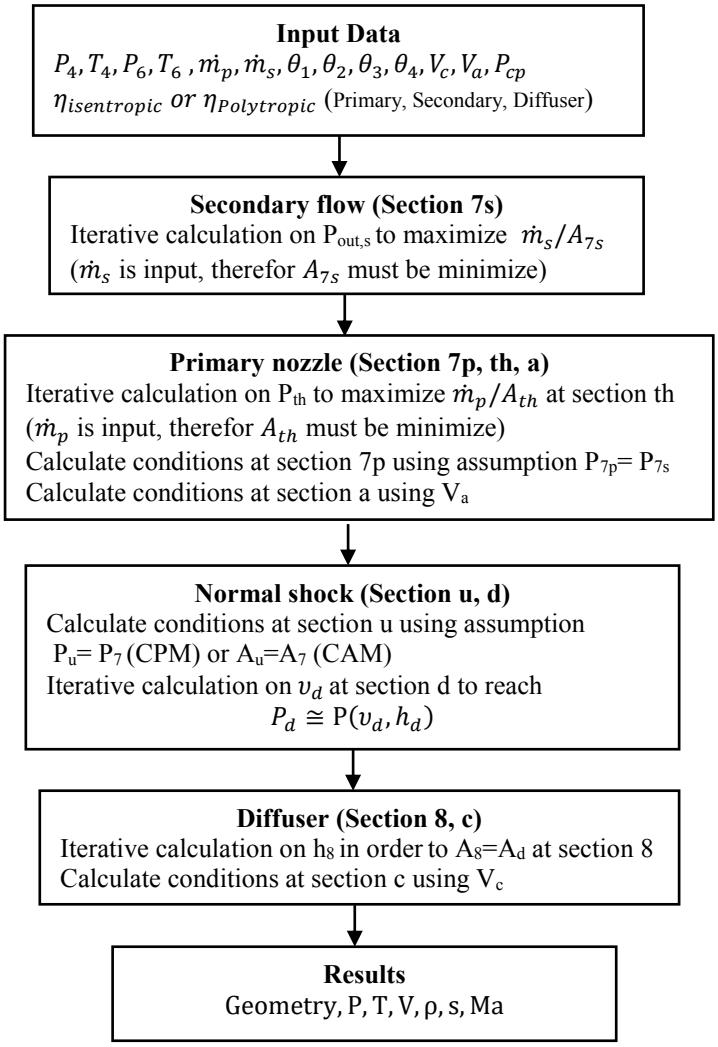

Figure 3.12 Calculation Procedure of ejector dimensions and operating conditions.

3.6 Results of the effect of polytropic efficiencies

The effects of polytropic efficiencies on the ejector dimensions and thermodynamic properties for both CPM and CAM ejectors are analyzed. For validation, a comparison between the dimensions obtained by the 1D model and experimental data is performed. Furthermore, to show the advantages of polytropic efficiencies, a comprehensive comparison between the results obtained based on polytropic and isentropic efficiencies is carried out.

Table 3.6 and 3.7 illustrate the effects of both η_{pol} and η_{is} on ejector dimensions for case 1 and 2 respectively. The results obtained from the 1D model are compared to experimental dimensions (fig. 3-13 & 3-14). The main results can be summarized as follows:

- The results show that the 1D models accurately calculate all of the ejector geometry over the entire range of operation, with average error <2% for both the CPM and CAM ejectors compared to experimental dimensions.

- There is no significant difference in the diameters and lengths calculated based on polytropic and isentropic efficiencies, except for L_4 and L_{tot}.
- The deviation of the constant area duct length (L_4) calculated based on isentropic efficiency from experimental length is 2.83 times that of polytropic efficiency for Case 1. Similarly, 3.01 times for case 2.
- The deviation of the L_{tot} obtained based on isentropic efficiency from experimental length is 3.4 times greater than the one calculated by using a polytropic efficiency for Case 1, while it is 3.97 times for Case 2.
- The obtained dimensions based on polytropic efficiencies are higher than corresponding dimensions based on isentropic efficiencies, except for L_1, L_4, L_5 and L_{tot}.

Table3.6 Effect of polytropic and isentropic efficiencies on ejector dimensions for Case# 1 (CAM) (P_{cp}=190.19)

D, L, X [mm]	Exp.	Therm. (η_{pol})	Error (%) (η_{pol})	Therm. (η_{is})	Error (%) (η_{is})
D_a	32.08	31.76	-0.9975	31.76	-0.9975
D_{th}	14.42	14.3	-0.8321	14.28	-0.9708
D_{7p}	22.47	21.57	-4.0053	21.53	-4.1833
D_7	28.47	27.71	-2.6694	27.67	-2.801
$D_{8, u, d}$	28.47	27.71	-2.6694	27.67	-2.801
D_c	38.10	38.16	0.1574	38.16	0.1574
L_1	100.9	99.77	-1.12	99.88	-1.0109
L_2	46	41.53	-9.7173	41.44	-9.9130
X	7.08	7.041	-0.5508	7.032	-0.6779
L_4	223.77	232.5	3.9013	248.5	11.0515
L_5	46	49.9	8.4783	50.11	8.9348
L_{tot}	416.67	423.7	1.64	439.9	5.575
(L_4/D_8)	7.86	8.39	6.743	8.983	14.2875
$(L_4+X)/D_8$	8.109	8.652	6.696	9.237	13.9105

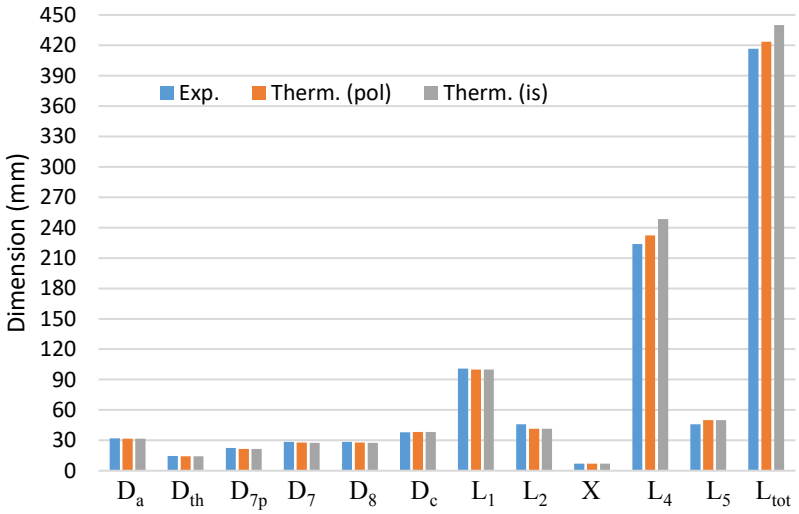

Figure 3.13 Comparisons of dimensions for case# 1 (CAM)

Table 3.7 Effect of polytropic and isentropic efficiencies on ejector dimensions for case# 2 (CPM) (P_{cp}=105.5 kPa)

D, L, X [mm]	Exp.	Therm. (η_{pol})	Error (%) (η_{pol})	Therm. (η_{is})	Error (%) (η_{is})
D_a	8.251	8.029	-2.691	8.029	-2.691
D_{th}	2.810	2.834	0.8541	2.828	0.6406
D_{7p}	6.518	6.577	0.9052	6.548	0.4603
D_7	9.527	9.166	-3.789	9.098	-4.503
$D_{8,\,u,\,d}$	8.794	8.517	-3.15	8.475	-3.627
D_c	25.803	25.76	-0.167	25.76	-0.167
L_1	15.4	14.73	-4.351	14.75	-4.221
L_2	35.4	35.71	0.8757	35.5	0.2825
X	4.2	3.708	-11.71	3.571	-14.98
L_4	146.0	155.1	6.2329	173.4	18.767
L_5	121.6	123.3	1.398	123.6	1.6447
L_{tot}	322.6	328.8	1.9219	347.2	7.6255
(L_4/D_8)	16.6	18.21	9.6988	20.46	23.253
$(L_4+X)/D_8$	17.1	18.64	9.0058	20.88	22.105

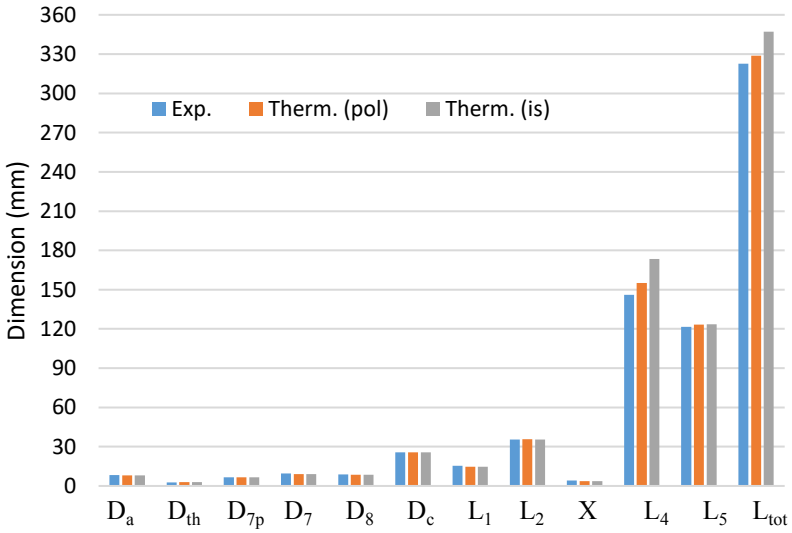

Figure 3.14 Comparisons of dimensions for case# 2 (CPM)

The comparison of flow properties at important sections based on isentropic and polytropic efficiencies against the CFD results are shown in table 3.8 and 3.9.

The polytropic efficiency leads to more accurate results with respect to the isentropic efficiency. The maximum deviation of CFD values takes place at sections “th” and “7s” where the primary and secondary streams are choked. This is due to the thermodynamic assumptions of the choking location in the 1D model for primary and secondary fluids.

Table 3.8 Flow properties at different ejector cross-sections for the critical back pressure point for case 1 (CAM) (P_{cp}=190.19 kPa)

	State	P	T	V	Ma
		[kPa]	[°K]	[m/s]	[-]
Primary Inlet	4	480.6	352.45	0.00	0.0000
Therm. (pol)	a	476.9	352.24	17.21	0.1231
Therm. (is)	a	476.9	352.24	17.21	0.1231
CFD	a	476.89	352.23	17.21	0.1230
Therm. (pol)	th	288.8	338.97	139.6	0.9870
Therm. (is)	th	288.9	338.93	139.9	0.9892
CFD	th	301.98	339.96	134.46	0.9513
Therm. (pol)	7p	59.32	301.78	279.4	2.003
Therm. (is)	7p	59.33	301.59	280.1	2.009
CFD	7p	54.73	299.7	283.75	2.038
Secondary Inlet	6	100.1	303.75	0.00	0.00
Therm. (pol)	b	99.81	303.68	10.05	0.07272
Therm. (is)	b	99.82	303.68	10.05	0. 07272
CFD	b	99.78	303.68	10.05	0.07273
Therm. (pol)	7s	59.32	292	135.1	0.9866
Therm. (is)	7s	59.33	291.95	135.4	0.9891
CFD	7s	66.27	294.4	119.89	0.8736
Therm. (pol)	u	54.63	301.37	243.9	1.748
Therm. (is)	u	54.64	301.21	244.5	1.752
Therm. (pol)	d	170.9	332.88	84.15	0.5863
Therm. (is)	d	172	332.93	83.83	0.5841
Therm. (pol)	8	161.4	332.2	89.15	0.6205
Therm. (is)	8	161.6	332.19	89.29	0.6215
CFD	8	166.45	332.29	82.84	0.5773
Therm. (pol)	c	182	335.86	42	0.2917
Therm. (is)	c	182	335.86	42	0.2917
CFD	c	187.27	335.61	42	0.289
Outlet	1	190.19	336.95	0.00	0.0000

Table 3.9 Flow properties at different ejector cross-sections for the critical back pressure point for case 2 (CPM) (P_{cp}=105.5 kPa)

	State	P	T	V	Ma
		[kPa]	[°K]	[m/s]	[-]
Primary Inlet	4	604.9	373.15	0.00	0.0000
Therm. (pol)	a	603.2	373.04	11.19	0.0738
Therm. (is)	a	603.2	373.04	11.19	0.0738
CFD	a	603.27	373.049	11.19	0.0701
Therm. (pol)	th	363.3	355.43	148.7	0.9655
Therm. (is)	th	363.5	355.35	149.3	0.969
CFD	th	383.46	356.545	145.17	0.9404
Therm. (pol)	7p	23.36	277.25	362.6	2.475
Therm. (is)	7p	23.38	276.4	364.3	2.49
CFD	7p	24.37	277.48	355	2.424
Secondary Inlet	6	39.9	283.45	0.00	0.0000
Therm. (pol)	b	39.77	283.37	10.61	0.0721
Therm. (is)	b	39.78	283.37	10.61	0. 0721
CFD	b	39.85	283.39	10.61	0.0733
Therm. (pol)	7s	23.36	269.44	139.2	0.9638
Therm. (is)	7s	23.38	269.17	141.8	0.9993
CFD	7s	32.61	277.91	86.62	0.593
Therm. (pol)	u	23.36	281.905	302	2.044
Therm. (is)	u	23.38	281.1	303.9	2.06
Therm. (pol)	d	101.7	338.43	81.97	0.5162
Therm. (is)	d	103.4	338.52	81.43	0.513
Therm. (pol)	8	88.32	336.78	94.18	0.5928
Therm. (is)	8	88.08	336.64	95.35	0.6003
CFD	8	91.18	337.4	85.7	0.539
Therm. (pol)	c	105.3	342.52	8.75	0.0548
Therm. (is)	c	105.3	342.52	8.75	0.0548
CFD	c	105.47	342.17	8.75	0.0545
Outlet	1	105.5	342.5	0.00	0.0000

3.7 Parametric study

By applying the improved and validated 1D model, we will be able to size an ejector for different cycles. Based on the strategy shown in fig. 3-4, the most important input parameters for ejector sizing are the primary and secondary inlet pressures (P_4, T_4, P_6, T_6), primary and secondary mass flow rates ($\dot{m}_p, \dot{m}_s$), condenser pressure (P_1) and the polytropic efficiencies ($\eta_{Pol,p}$, $\eta_{Pol,s}$, $\eta_{Pol,D}$). The effects of these input parameters on the ejector dimensions are investigated for a base case (CAM) as shown in table 3.10. All results of the parametric study are summarized in table 3.14.

Table 3.10 Operating conditions

Parameter	**Base case**
Working fluid	R245fa, Real Fluid
P_4, T_4 (Primary Inlet)	480.6 kPa, 352.45 K
P_6, T_6 (Secondary Inlet)	100.1 kPa, 303.75 K
P_1 (Back pressure)	190.19 kPa
$\dot{m}_p, \dot{m}_s$	0.331 kg/s, 0.108 kg/s
$\eta_{Pol,p}, \eta_{Pol,s}, \eta_{Pol,D}$	0.9757, 0.9752, 0.8211

3.7.1 Effect of inlet and outlet pressures on ejector dimensions

Table 3.11 shows the effects of the inlet and outlet pressures on ejector dimensions. It is found that by increasing the back pressure (P_1):

- The value of D_a, D_{th}, D_{7p}, D_7, D_8, L_1 and L_2 stay constant, meaning that these values are independent of the back pressure. In other words, the upstream of the normal shock is not influenced by back pressure.
- The value of D_c and consequently L_5 reduce slightly.

It can be seen that by increasing primary inlet pressure (P_4):

- All diameters and L_1 reduce while L_2 and L_5 increase. L_1 and L_2, as lengths of the converging-diverging primary nozzle, have an inverse relationship to each other based on analytical correlations of perfect gas flow in a fixed mass flowrate.

In the case of L_5, the increase is a direct result of an increase in the difference between changes in D_8 and D_c.

It is found that by increasing secondary inlet pressure (P_6):

- D_a, D_{th} and, therefore L_1 are not influenced by P_6 as expected. However, D_{7p} and D_7 decrease since the P_{7s} increases.
- The diameters D_8 and D_c decrease, however their difference increases simultaneously since the L_5 increases.
- Overall, the effects of P_4 and P_6 on dimensions are the same, except on D_a, D_{th} and consequently L_1 and L_2.

By decreasing P_1 and increasing P_4 and P_6:

- The mixing efficiency decreases considerably based on eq. 20 and 26a due to the increasing pressure difference between cross-sections ‘‘d” and 8 and consequently an increase in friction losses in the constant area duct. Reducing η_{mix} leads to high exergy losses in the constant area duct that should be avoided.
- The length of the constant area duct L_4 significantly increases and consequently the ejector will be longer, which should be avoided. In addition, the effect on the length of the constant area duct L_4 and therefore L_{tot} is more than the effect on other dimensions.

It should be noted that based on the experimental results by Keenan et al. [20] as well as ASHRAE (as reported by Alexis [64]), the value of the ratio $(L_4 + X)/D_8$ should be between 9 and 16 for satisfactory operation of the ejector. In addition, the ratio X/D_8 should be around 1.50 for the best ejector performance [40] [65].

By considering these points, the best operating conditions can be selected. In this case, the pressures P_1=188 kPa or P_4=490 kPa or P_6=105 kPa are recommended based on table 3.11.
The results of the effect of inlet and outlet pressures on ejector dimensions for the base case are in good agreement with the results that have been previously achieved for CPM by Khennich et al. [18].

Table 3.11 Effects of the inlet and outlet pressures on the ejector dimensions

D, L, X	**P_1** [kPa]			**P_4** [kPa]			**P_6** [kPa]		
[mm]	**181**	**188**	**197**	**470**	**480**	**490**	**95**	**105**	**115**
D_a	31.76	31.76	31.76	32.16	31.78	31.41	31.76	31.76	31.76
D_{th}	14.3	14.3	14.3	14.47	14.31	14.16	14.3	14.3	14.3
D_{7p}	21.57	21.57	21.57	21.64	21.57	21.51	21.98	21.2	20.53
D_7	27.71	27.71	27.71	27.76	27.71	27.66	28.32	27.16	26.17
$D_{8,\,u,\,d}$	27.71	27.71	27.71	27.76	27.71	27.66	28.32	27.16	26.17
D_c	39.15	38.39	37.48	38.17	38.16	38.15	39.17	38.16	38.15
L_1	99.77	99.77	99.77	101.1	99.85	98.61	99.77	99.77	99.77
L_2	41.53	41.53	41.53	40.99	41.5	41.99	43.88	39.44	35.61
X	7.247	7.247	7.247	7.229	7.246	7.263	7.485	7.036	6.648
L_4	475.3	293.9	27.99	194.8	230.5	264.3	22.65	381.2	560.7
L_5	54.61	50.99	46.61	49.69	49.89	50.07	46.99	52.48	57.22
L_{tot}	671.2	486.1	215.9	386.5	421.7	454.9	213.3	572.9	753.3
(L_4/D_8)	17.15	10.6	1.01	7.014	8.318	9.553	0.799	14.03	21.43
$(L_4+X)/D_8$	17.41	10.87	1.272	7.275	8.579	9.815	1.064	14.29	21.68
η_{mix}	0.9024	0.931	0.9697	0.9458	0.9405	0.9355	0.9701	0.9153	0.8746

3.7.2 Effect of polytropic efficiency values on ejector dimensions

Table 3.12 displays the effects of polytropic efficiencies on ejector dimensions. It is found that $\eta_{Pol,p}$ has the most impact on L_4, as increasing $\eta_{Pol,p}$ by 6 % leads to more than a fourfold increase in L_4 because the pressure difference between cross-sections ‘‘d” and 8 increases.
According to table 3.12, the third column of each efficiency is recommended due to the desirable value of $(L_4+X)/D_8$.
By increasing polytropic efficiencies, the value of L_4 and therefore L_{tot} increase, while η_{mix} decreases. This can be explained by Eq. 21 and 25, as the properties at cross-section 7 vary little, while the pressure at cross-section 8 decreases considerably and the corresponding velocity increases. As expected, the upstream of the normal shock is not influenced by $\eta_{Pol,D}$. This deduction is reflected in the numerical results in table 3.12. Furthermore, the acceleration/ deceleration processes become isentropic when the polytropic efficiency is equal to 1.

Table 3.12 Effects of the polytropic efficiencies on the ejector dimensions

D, L, X	$\eta_{Pol,p}$			$\eta_{Pol,s}$			$\eta_{Pol,D}$		
[mm]	0.94	0.97	1	0.85	0.9	1	0.75	0.8	0.9
D_a	31.76	31.76	31.76	31.76	31.76	31.76	31.76	31.76	31.76
D_{th}	14.44	14.32	14.21	14.3	14.3	14.3	14.3	14.3	14.3
D_{7p}	21.83	21.61	21.39	21.54	21.55	21.57	21.57	21.57	21.57
D_7	27.92	27.74	27.57	28.09	27.93	27.64	27.71	27.71	27.71
$D_{8,\,u\,d}$	27.92	27.74	27.57	28.09	27.93	27.64	27.71	27.71	27.71
D_c	38.16	38.16	38.16	38.16	38.16	38.16	38.16	38.16	38.16
L_1	98.99	99.65	100.3	99.77	99.77	99.77	99.77	99.77	99.77
L_2	42.24	41.64	41.06	41.36	41.42	41.56	41.53	41.53	41.53
X	7.178	7.236	7.293	7.736	7.53	7.16	7.247	7.247	7.247
L_4	79.84	208.2	331.2	30.3	117.2	266.5	155.8	209.1	320
L_5	48.91	49.74	50.55	48.07	48.84	50.22	49.89	49.89	49.9
L_{tot}	270	399.2	523	219.5	307.2	458	347	400.3	511.2
(L_4/D_8)	2.86	7.505	12.01	1.078	4.196	9.64	5.621	7.545	11.55
$(L_4+X)/D_8$	3.117	7.765	12.27	1.354	4.466	9.899	5.883	7.807	11.81
η_{mix}	0.9628	0.9438	0.9257	0.9623	0.953	0.9364	0.9515	0.9437	0.927

3.7.3 Effect of mass flow rates on ejector dimensions

Table 3.13 shows the effects of the primary and secondary mass flow rates on ejector dimensions. It is found that by increasing $\dot{m}_p$, all of the diameters and lengths increase.

By increasing $\dot{m}_s$, the value of L_4 decreases. It is also shown that $\dot{m}_s$ has an inverse relationship with L_4 and a direct relationship with the mixing efficiency. Furthermore, as expected, the primary nozzle dimensions are independent of $\dot{m}_s$. According to table 3.13, $\dot{m}_p = 0.34$ [kg/s] and $\dot{m}_s = 0.09$ [kg/s] are recommended, due to the desirable value of $(L_4+X)/D_8$.

Table 3.13 Effects of the mass flow rates on the ejector dimensions

D, L, X	$\dot{m}_p$ [kg/s]			$\dot{m}_s$ [kg/s]		
[mm]	0.32	0.33	0.34	0.09	0.11	0.12
D_a	31.23	31.71	32.19	31.76	31.76	31.76
D_{th}	14.06	14.28	14.49	14.3	14.3	14.3
D_{7p}	21.21	21.54	21.86	21.57	21.57	21.57
D_7	27.43	27.68	27.94	26.78	27.81	28.31
$D_{8,\,u,\,d}$	27.43	27.68	27.94	26.78	27.81	28.31
D_c	37.67	38.12	38.57	37.45	38.24	38.63
L_1	98.1	99.62	101.1	99.77	99.77	99.77
L_2	40.83	41.46	42.09	41.53	41.53	41.53
X	7.343	7.256	7.172	6.155	7.366	7.956
L_4	185.2	228.2	463.6	434.6	209.2	90.69
L_5	48.86	49.8	50.73	50.93	49.79	49.25
L_{tot}	373	419.1	463.6	626.8	400.2	281.2
(L_4/D_8)	6.752	8.242	9.652	16.22	7.521	3.203
$(L_4+X)/D_8$	7.019	8.504	9.909	16.45	7.786	3.484
η_{mix}	0.946	0.9407	0.9358	0.9119	0.9433	0.9588

3.7.4 A summary of the results of the parametric study

The parametric analysis results are summarized in table 3.14. The results show that decreasing back pressure and secondary mass flow rate, as well as increasing inlet pressures, primary mass flow rate and polytropic efficiencies, lead to a considerable increase in the constant area duct length while mixing efficiency decreases significantly. In other words, it results in an extremely long ejector and higher exergy losses, which are not desirable. It is further found, by increasing the input parameters, there is an inverse relationship between L_4 and η_{mix}.

Table 3.14 A summary of the results of the parametric study

Parameter	D_a	D_{th}	D_{7p}	D_7	D_8	D_c	L_1	L_2	X	L_4	L_5	L_{tot}	η_{mix}
P_1 (↑)	C	C	C	C	C	↓	C	C	C	↓	↓	↓	↑
P_4 (↑)	↓	↓	↓	↓	↓	↓	↓	↑	↑	↑	↑	↑	↓
P_6 (↑)	C	C	↓	↓	↓	↓	C	↓	↓	↑	↑	↑	↓
$\dot{m}_p$ (↑)	↑	↑	↑	↑	↑	↑	↑	↑	↓	↑	↑	↑	↓
$\dot{m}_s$ (↑)	C	C	C	↑	↑	↑	C	C	↑	↓	↓	↓	↑
$\eta_{Pol,p}$ (↑)	C	↓	↓	↓	↓	C	↑	↓	↑	↑	↑	↑	↓
$\eta_{Pol,s}$ (↑)	C	C	↑	↓	↓	C	C	↑	↓	↑	↑	↑	↓
$\eta_{Pol,D}$ (↑)	C	C	C	C	C	C	C	C	C	↑	C	↑	↓

Increase (↑), Decrease (↓), Constant (C)

3.7.5 Empirical correlations of the ejector component polytropic efficiencies

Empirical correlations for component polytropic efficiencies and mixing efficiency are established according to the additional parametric study results obtained by validated 1D and CFD models. There are many parameters influencing the component efficiencies, however, if these factors are considered to establish the correlations, they are very complex. Empirical correlations proposed by [23] [53] [66] [67] [68] for isentropic efficiencies are functions of ejector geometry, pressure ratio and entrainment ratio. Therefore, by using a multiple nonlinear regression method, empirical correlations are estimated based on four important parameters: (1) the area ratio D_8/D_{th}, (2, 3) the pressure ratios P_4/P_1, P_1/P_6 and (4) the entrainment ratio ω. The empirical correlations for the polytropic efficiencies of the primary, secondary and diffuser ($\eta_{pol,p}$, $\eta_{pol,s}$, $\eta_{pol,D}$) as well as mixing section efficiency (η_{mix}) are showed in table 3.15. The coefficient of determination (R^2) of each correlation is determined in order to show a statistical measure of how close the data are to the fitted regression line. It should be noted that the proposed correlations can be used with refrigerant R245fa under the following operation conditions:

$(2.2 \leq P_4/P_1 \leq 2.8)$, $(1.5 \leq P_1/P_6 \leq 2)$, $(1.7 \leq D_8/D_{th} \leq 2.1)$, $(0.28 \leq \omega \leq 0.38)$

Table 3.15 Ejector polytropic efficiencies regressing equations.

Efficiency	Regressing equation	R^2
$\eta_{Pol,p}$	$= 5.6794 + 1.4884\left(\frac{P_4}{P_1}\right) + 1.8477\left(\frac{P_1}{P_6}\right) - 9.7759\left(\frac{D_8}{D_{th}}\right) + 6.8361\omega - 0.2983\left(\frac{P_4}{P_1}\right)^2 - 0.4862\left(\frac{P_1}{P_6}\right)^2 + 2.5232\left(\frac{D_8}{D_{th}}\right)^2 - 10.1077\omega^2$	0.957
$\eta_{Pol,s}$	$= 6.6184 - 0.0237\left(\frac{P_4}{P_1}\right) + 1.6873\left(\frac{P_1}{P_6}\right) - 9.5562\left(\frac{D_8}{D_{th}}\right) + 12.2939\omega + 0.003\left(\frac{P_4}{P_1}\right)^2 - 0.4405\left(\frac{P_1}{P_6}\right)^2 + 2.4606\left(\frac{D_8}{D_{th}}\right)^2 - 18.3420\omega^2$	0.962
$\eta_{Pol,D}$	$= -86.4666 + 21.575\left(\frac{P_4}{P_1}\right) - 10.52\left(\frac{P_1}{P_6}\right) + 78.6821\left(\frac{D_8}{D_{th}}\right) - 38.489\omega - 4.0977\left(\frac{P_4}{P_1}\right)^2 + 3.0264\left(\frac{P_1}{P_6}\right)^2 - 20.9517\left(\frac{D_8}{D_{th}}\right)^2 + 63.7444\omega^2$	0.941
η_{mix}	$= -0.7477 - 1.6639\left(\frac{P_4}{P_1}\right) - 1.4529\left(\frac{P_1}{P_6}\right) + 5.5129\left(\frac{D_8}{D_{th}}\right) - 2.05652\omega + 0.2661\left(\frac{P_4}{P_1}\right)^2 + 0.3907\left(\frac{P_1}{P_6}\right)^2 - 1.2646\left(\frac{D_8}{D_{th}}\right)^2 + 2.6217\omega^2$	0.986

3.8 Conclusion

A thermodynamic model applicable for two types of ejectors, constant area mixing (CAM) ejectors and constant pressure mixing (CPM) ejectors, is developed and validated against experimental data. The model is based on the application of the polytropic efficiency concept. The reference values of polytropic efficiencies are extracted from CFD models of two ejector types. Unlike previous models, the developed model allows calculating the length of the constant area duct, a parameter essential for ejectors sizing. Compared to experimental data, the model accurately predicts the ejector's dimensions over the entire range of operation with an average error less than 2%.

The results show that the best agreement with experimental data for both types of ejectors (CPM and CAM) is achieved by polytropic efficiencies. It is illustrated that $\eta_{Pol,p}$ has the most impact on the constant area duct length. The parametric analysis completed through the application of the model shows that an increase in P_1 and $\dot{m}_s$ lead to the decrease of a constant area duct length, the main factor responsible for the ejector's size.

3.9 Acknowledgements

The authors wish to thank Hydro-Québec laboratory Shawinigan for their valuable contribution during this research study. This project is a part of the Collaborative Research and Development (CRD) Grants Program at 'Université de Sherbrooke'. The authors also acknowledge the

support of the Natural Sciences and Engineering Research Council of Canada, Rio Tinto Alcan and CanmetENERGY Research Center of Natural Resources Canada.

CHAPTER 4 : The impact of internal ejector working characteristics and geometry on the performance of a refrigeration cycle

AVANT-PROPOS

Auteurs et affiliation:

- Payam Haghparast: étudiant au doctorat, Université de Sherbrooke, Faculté de génie, Département de génie mécanique.
- Mikhail Sorin: professeur, Université de Sherbrooke, Faculté de génie, Département de génie mécanique.
- Hakim Nesreddine: Institut de recherche d'Hydro-Québec (IREQ), 600 Rue de la montagne, Shawinigan, QC, G9N 7N5, Canada

Date d'acceptation: 7 August 2018

État de l'acceptation: version finale publiée.

Revue: Energy

Référence: [69]

Titre français: L'impact des caractéristiques de fonctionnement et de la géométrie de l'éjecteur interne sur les performances d'un cycle de réfrigération

Contribution au document: Cet article présente une comparaison entre quatre cas expérimentaux différents afin de déterminer les effets des caractéristiques internes de fonctionnement de l'éjecteur sur le cycle. Les résultats aident à mieux concevoir les éjecteurs supersoniques pour différentes applications.

This article contributes the thesis by comparison of four different experimental cases to find out the effects of internal ejector working characteristics on the cycle. The results help to better design of supersonic ejectors for different applications.

Résumé français:

L'amélioration des performances du cycle de réfrigération et la conception appropriée des éjecteurs pour la récupération d'énergie de compression nécessitent une analyse détaillée des caractéristiques de fonctionnement et de la géométrie de l'éjecteur interne. À cette fin, une étude expérimentale et numérique d'un système de réfrigération à éjecteur (ERS) est menée afin de déterminer l'effet des dimensions les plus importantes de l'éjecteur et des principales conditions de fonctionnement sur les caractéristiques de fonctionnement et la performance du cycle de l'éjecteur. Les résultats expérimentaux montrent que les meilleures performances de l'éjecteur et, par conséquent, du cycle de réfrigération ont été atteintes pour le rapport de pression

maximal au point critique de la température du condenseur. Ainsi, selon les études numériques effectuées, les pertes d'exergie interne de l'éjecteur sont minimes. En outre, il a été constaté que le diamètre de la buse primaire était le facteur le plus déterminant pour l'amélioration des performances de l'éjecteur et l'amélioration du rapport de pression. Les résultats montrent qu'une augmentation du diamètre primaire conduit à une double amélioration du rendement global de l'éjecteur. De plus, il a été constaté que la plupart des pertes d'exergie à l'intérieur de l'éjecteur sont localisées dans trois régions, soient, respectivement: la section de mélange à surface constante, la chambre de mélange et la buse primaire.

4.1 Abstract

Improvement of the refrigeration cycle performance and the proper design of ejectors for compression energy recovery require a detailed analysis on the internal ejector working characteristics and geometry. To this aim, an experimental and numerical investigation of an ejector refrigeration system (ERS) is conducted to determine the effect of the most important ejector dimensions and main operating conditions on ejector working characteristics and cycle performance. Experimental results show that the best performance of the ejector and consequently the refrigeration cycle were achieved for the maximum pressure ratio at the critical condenser temperature point. At this condition, ejector internal exergy losses are minimal according to the carried out numerical studies. Furthermore, it has been found that the primary nozzle diameter is the most influential factor for ejector performance and pressure ratio improvement. Results show that an increase in the primary diameter leads to the double improvement of the overall ejector efficiency. In addition, it has been found that most of the exergy losses inside the ejector are located in three regions, respectively: the constant area mixing section, the mixing chamber and the primary nozzle.

Keywords: *Ejector Refrigeration cycle; Pressure ratio; Experimental study; Numerical simulation; Internal exergy losses*

Nomenclature

A	Cross section area (mm^2)	exe	Exergy
D	Diameter (mm)	exp	Experimental
F	Force (N)	g	Generator
f	Friction coefficient (-)	in	Inlet
h	Specific enthalpy ($kJ.kg^{-1}$)	is	Isentropic
L	Length (m)	m	Constant area mixing duct inlet
$\dot{m}$	Mass flow rate ($kg.s^{-1}$)	mix	Mixing
Ma	Mach number	out	Outlet
P	Pressure (kPa)	pol	Polytropic
PR	Pressure Ratio=P_1/P_6 (-)	pr	Primary nozzle
s	Specific entropy ($kJ.kg^{-1}\ K^{-1}$)	p	Pump
T	Temperature (K)	sat	Saturation
V	Velocity ($m.s^{-1}$)	sec	Secondary nozzle
v	Specific volume ($m^3.kg^{-1}$)	th	Ejector throat
ΔE	Exergy destruction (kW)	tot	Total
		1	Exit of ejector
Greek symbols		4	Primary inlet
η	Efficiency (%)	6	Secondary inlet
ξ	Exergy destruction index (-)	7	Nozzle exit
ω	Entrainment ratio (-)	8	Inlet of diffuser
ρ	Density ($kg.m^{-3}$)		
		Acronyms	
Subscripts		CFD	Computational Fluid Dynamics
c	Condenser	COP	Coefficient of performance
d	Diffuser	HRN	High Reynolds Number
eje	Ejector	NXP	Nozzle Exit Position
e	Evaporator		

4.2 Introduction

Ejector refrigeration systems (ERS) are a promising alternative to the traditional compressor-based refrigeration technologies for energy consumption reduction. They are a cost-effective, low-maintenance refrigeration option which do not require a compressor. Many works have been carried out to explore the ERS capacity to operate using low-grade heat sources, such as: solar energy, biomass, geothermal resources and industrial waste heats.

Previous works by [52], [29], [70], [71] present detailed literature reviews on the application of ejectors in refrigeration cycles. The most important issues include 1D modeling of the supersonic ejector and other cycle components [72] [73], optimizing the cycle performance [74], experimental studies [75], CFD modeling [76] [77] [78], the effect of the ejector geometry on the cycle performance [79] [80], comparison of results from different simulation models [81] [82], cycle exergy analysis [83] [84] and the performance of novel ERS configurations [85].

Proper design of ejectors for compression energy recovery requires a detailed analysis using both an experimental and a numerical approach. The literature on experimental and numerical simulation of ejector refrigeration cycles is extensive. Experimental studies allow to validate results of numerical models using global operation parameters. Zhu et al. [65] have carried out comparisons of experimental and 1D results. It is shown that the shock circle model can better predict the ejector performance. Eames et al. [86] conducted a combined experimental and CFD study of an advanced jet-pump refrigerator operating with R245fa. It is observed that NXP has strong influence on system entrainment ratio and coefficient of performance. Different ejector dimensions, such as the sizing of the motive nozzle and the diffuser have been studied experimentally in [50] [27]. Nakagawa et al. [28] performed an experimental analysis of the effect of the mixing length on the ejector performance. The ejector with the shortest mixing section led to the lowest COP and efficient pressure recovery. Using much longer mixing section had negative impact on ejector's performance.

Nonetheless, experimental studies are often limited to the relationship between the cycle operating conditions and ejector global performance due to the difficulties for quantitative flow measurements inside the device. Therefore, numerical methods are an essential and valuable tool to have better insight into the flow and thermal fields inside the ejector. The two main approaches for this purpose are thermodynamic and CFD models.

A thermodynamic model is a suitable tool to analyze and validate ejector performance [55]. In combination with an exergy analysis, it allows to determine the possibilities for enhancing system

performance. The losses in the ejector are one of the main reasons for a low ERS performance, which raises the need for knowledge of ejector internal processes, especially the characteristics of internal irreversibilities [23]. It has been found that, for a two-phase steam-water ejector, irreversibilities arise from friction, spontaneous condensation, steam-water droplet mixture flow and shock-waves, with the largest losses occurring in the two-phase region and the steam nozzle [87]. Arbel et al. [88] have also shown that pure mixing, high kinetic energy and normal shock-waves are important sources of irreversibility within the ejector.

Nevertheless, in the ejector refrigeration system, the knowledge concerning ejector internal irreversibilities is still limited. Identifying these losses through the ejector is of great importance for improving its design and evaluating its performance. Within this context, CFD is a valuable tool that allows to represent the complex flow features within the device. Banasiak et al. [25] examined, numerically and experimentally, different ejector configurations in order to achieve an optimum ejector geometry. They assessed various mixing duct lengths and diameters as well as various angles of divergence for the diffuser. Varga et al. [34] and Zhang et al. [54] extracted component isentropic efficiencies using CFD modeling. Different turbulence modeling approaches for supersonic ejectors and their successful CFD implementations are reported in [89] [60]. As a result, they found that the k-ω SST model shows better performance in terms of global and local flow phenomena predictions for the different ejector geometries and operating conditions. Empirical correlations based on CFD results have been proposed by Besagni et al. [66] for determining the isentropic efficiencies as functions of ejector geometry, pressure ratio and entrainment ratio.

Furthermore, researchers have shown that there is a direct relationship between the cycle performance and internal ejector working characteristics. Chen et al. [23] studied the relationship between internal and external ejector parameters and cycle performance. It has been found out that the ejector component efficiencies have dramatic effects on the system COP and ejector behavior. Croquer et al. [59] performed an internal exergy analysis at various characteristic sections of the ejector based on different turbulence models. They showed that fifteen percent of the ejector (starting at the exit of the primary nozzle) is responsible for up to 84% of the total losses. Losses in the inlet region are negligible. Khennich et al. [90] evaluated the thermodynamic performance and the transformations of different sources of exergy linked to intensive thermodynamic properties through an ERS. Nevertheless, none of the aforementioned works includes a detailed investigation on the interactions and relationships between cycle parameters, ejector geometry and internal ejector working conditions.

In this study, experimental results concerning an ejector within a refrigeration system are presented under various operating conditions. These data is useful as a reference for validating the developed numerical models. The main objective of this study is to provide deep insight into the interactions and relationships existing between various ejector working conditions, ejector geometry and main operating parameters of the refrigeration system. This research paper has the following novelty and originality items:

(1) An experimental investigation is carried out in order to study the performance of an ejector refrigeration system (ERS) under different operational conditions for both single-choking and double-choking regimes.

(2) A 1D thermodynamic model of the ejector is developed in order to investigate the effects of ejector dimensions on the ejector compression ratio. In addition, a geometrical optimization of the ejector for increasing the pressure ratio and ejector performance is carried out.

(3) The interactions and relationships between refrigeration cycle performance, ejector performance and the main operating conditions of the cycle with the internal ejector working characteristics are investigated in detail using a CFD model.

(4) A parametric study of the ejector geometry is performed to improve the ejector performance by using the validated 1D model.

4.3 Description of the ejector refrigeration test bench

In order to investigate the ejector performance, the ejector refrigeration system (ERS) designed and operated by Hamzaoui et al. [91] was used in the present work with different ejector geometry. Figure 4-1 represents a schematic diagram of the experimental set up which consists of an ERS and three auxiliary utility circuits: a heating loop, a cooling loop and a thermal load loop. The process of the ejector refrigeration system (ERS) is characterized by a pressure-enthalpy diagram in fig. 4-2. In addition, two photographs of the complete experimental set-up and its components are depicted in fig. 4-3.

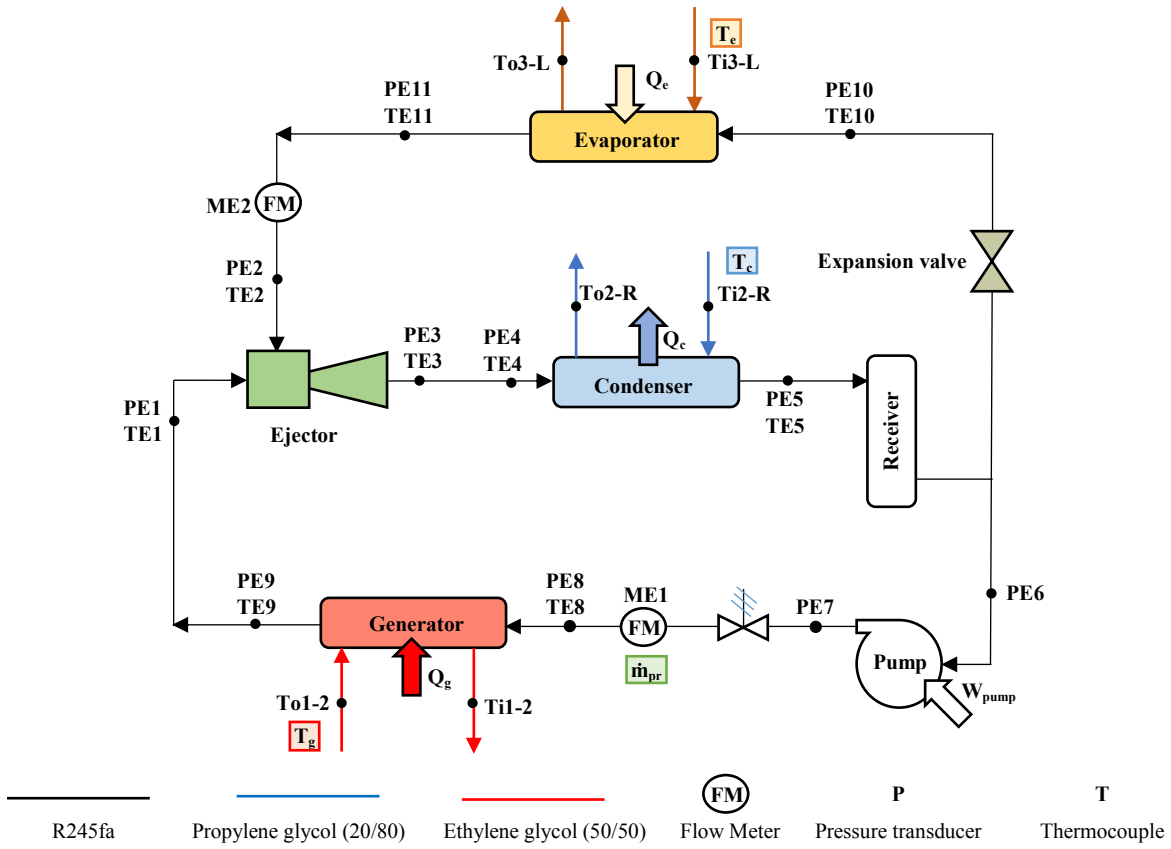

Figure 4.1 Schematic diagram of the ejector refrigeration system (ERS).

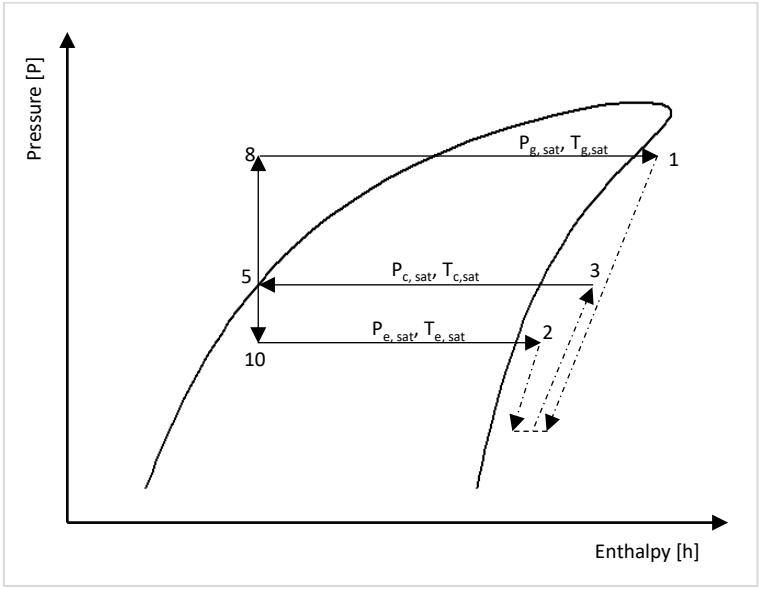

Figure 4.2 P-h diagram of the ejector refrigeration system (ERS).

R245fa is the working fluid. Previous studies [92] have found that it is suitable for ejector applications. It meets the performance criteria as well as the requirements of safety and

environmental protection. R245fa is mostly used with low temperature heat sources (T<150 ºC). Many aspects have been taken into account for its selection among the other potential candidates.

- The high critical temperature point (154 °C), making it convenient for heat recovery.
- Its operating pressure levels are low. This characteristic allows access to a variety of pumps and mechanical seals selection at very competitive costs.
- It has a positive slope (i.e. ds/dT > 0) which indicates a dry working fluid. As a dry refrigerant, no superheating is needed in the generator to prevent condensation during its expansion inside the ejector. The presence of liquid droplets seems to deteriorate the system performances.
- It is particularly safe because of non-flammability and low toxicity.
- Its lifetime in the atmosphere is relatively short: 7.2 years.
- Its ODP (Ozon depletion potential) value is 0 proving that it has a negligible impact on the environment, while its GWP (Global warming potential) value is 950 which can be acceptable.
- The liquid mass densities of R245fa are significantly high due to its high molar mass [93].

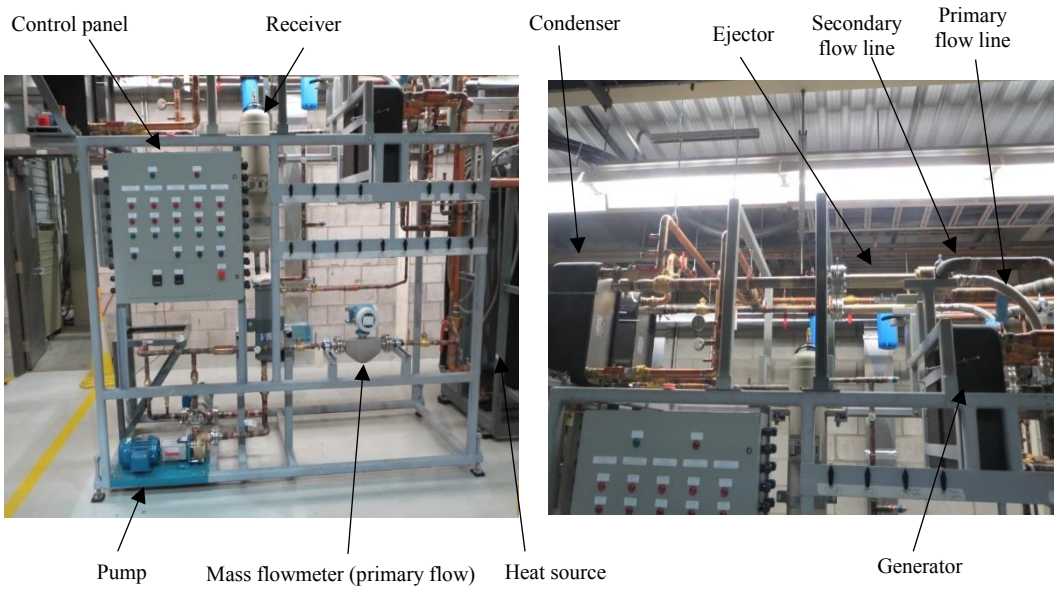

Figure 4.3 Experimental set up of the ejector refrigeration system (ERS).

4.3.1 Ejector

As mentioned above, the ejector analyzed in this work (figure 4-4) has different geometry characteristics than that investigated by Hamzaoui et al. [91]. It has been designed to enhance the system's performances. The corresponding geometric characteristics are summarized in figure 4-4.

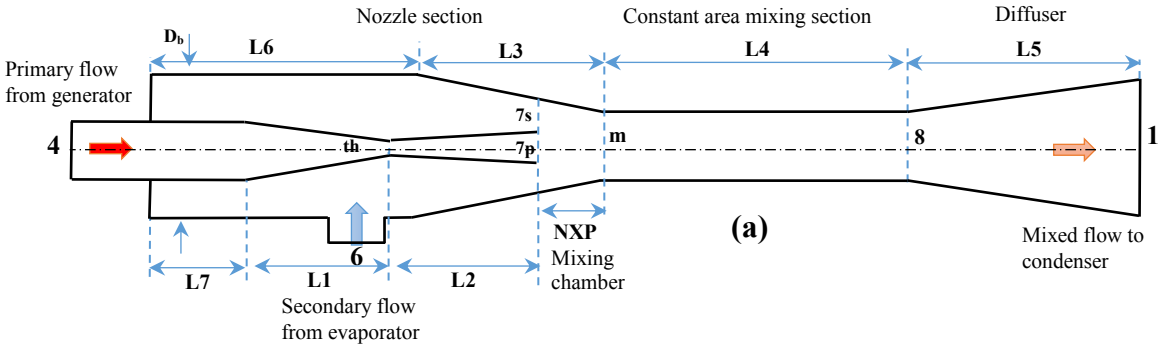

L_1	L_2	L_3	L_4	L_5	L_6	L_7	L_{tot}
89.05	116.99	170.85	80	28.12	100.9	46	429.87
D_4	D_{th}	D_{7p}	D_b	D_8	D_6	D_1	D_7
32.08	14.42	22.47	57.15	28.47	50	38.1	36.072

*All dimensions are in millimeter

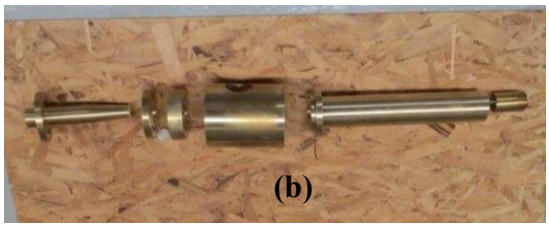

Figure 4.4 (a) Ejector geometry, parts and main cross-sections (b) the general view of the tested ejector

4.3.2 Heat exchangers, feed pump and instruments

The cycle consists of three main heat exchangers. To achieve a higher thermodynamic performance, counter-flow copper brazed plate heat exchangers were used as the condenser (300 kW), the vapor generator (250 kW) and the evaporator (35 kW).

The generator consists of two 125 kW compact plate heat exchangers being warmed by a propylene glycol secondary loop. Vapor flows from the generator towards the ejector. The heat source is a boiler that heated by a 250 kW electrical element.

The secondary flow into the ejector exits from the accumulator and passes through an electronic expansion valve (2500 steps) before entering the evaporator. The prescribed superheat is regulated using a controller that senses temperature and pressure at the outlet of the evaporator and reacts accordingly [91].

The evaporator consists of a 35 kW plate heat exchanger heated with an ethylene-glycol (50% - 50%) mixture. The temperature of the ethylene-glycol mixture is measured immediately before entering and after exiting the evaporator. The refrigerant in vapor phase leaves the ejector and passes through a condenser before entering the accumulator. The condenser consists of two 150 kW plate heat exchangers that are cooled using a propylene glycol (20% - 80%) mixture. The condensing loop is maintained at a constant temperature with a cooling tower with a capacity in excess of 400 kW. Its flow rate is measured with a flow meter and is controlled with a variable speed pump.

The pump feeding the generator with R245fa is based on a regenerative turbine impeller technology and driven by a 3 horsepower motor. This type of rotary pump is well suited for applications where volatile fluids are involved and transient cavitation conditions are likely to occur. The flow rate delivered to the generator inlet is controlled by a variable frequency drive which varies the pump rotational speed [91].

The monitoring points of the prototype are presented in figure 4-1. Temperature measurements were made using T- type thermocouples in direct contact with the corresponding fluid (accuracy ±0.5°C after calibration). Pressure measurements are performed using pressure transducers for display and monitoring, which have an accuracy of ±0.25% of reading. R245fa primary and secondary mass flow rates were acquired using Coriolis mass flowmeters with an accuracy of ±0.05% of the reading value. Electric measurements were carried out using AC watt transducers (accuracies: ±0.2% reading) to monitor the electric consumption of the feed pump, the boiler and the thermal load heater.

4.3.3 Measurement procedure

Table 4.1 shows some operating conditions of a reference case once the steady state is reached. All experimental data including temperature, pressure, heating power and flow rate should be stable for at least 100 minutes before starting the data logging at an acquisition interval of 5 seconds. Steady state conditions were validated by plotting the temperature time evolution at selected points.

Table 4.1 steady state operating conditions of a reference case ($T_g = 80\ °C$, $T_c = 24\ °C$ $T_e = 30\ °C$, $\dot{m}_{pr} = 0.33\ kg/s$)

Parameter	TE1 [°C]	PE1 [kPa]	TE2 [°C]	PE2 [kPa]	TE3 [°C]	PE3 [kPa]	$\dot{m}_{sec}$ [kg/s]	TE5 [°C]	PE5 [kPa]	PE6 [kPa]	PE7 [kPa]	TE10 [°C]	PE10 [kPa]
	78.8	485.5	28.3	110.8	62.8	202.4	0.133	30.54	196.5	195.5	499.8	24.5	112.8

To investigate the relationship between the cycle operating conditions and the ejector working characteristics, four different cases are considered. The tested conditions include the effects of the inlet boiler temperatures (in glycol side) ranging from 70 to 90 °C, inlet condenser temperatures (in glycol side) ranging from 18 to 30 °C, and inlet evaporator temperatures (in glycol side) of 16 to 24 °C. Primary mass flow rates also vary between 0.34 kg/s and 0.38 kg/s. It should be noted that table 4.2 shows the glycol inlet temperatures in the different heat exchangers (generator, condenser and evaporator) which are controlled parameters. On the other hand, table 4.3 indicates the corresponding uncontrolled variables represented by the evaporating, condensing, boiling temperatures of the working fluid.

Table 4.2 Operating conditions (glycol inlet temperatures in heat exchangers and ejector primary mass flow rate)

Parameter	Case# 1	Case# 2	Case# 3	Case# 4
T_g [°C]	70, 75, 80, 85, 90	80	90	85
T_c [°C]	20	18, 19, 20, 21, 22, 23, 24, 25, 26, 27, 30	20	22
$\dot{m}_{pr}$ [kg/s]	0.33	0.33	0.34, 0.35, 0.36, 0.37, 0.38	0.33
T_e [°C]	20	30	20	16, 18, 20, 22, 24

Table 4.3 Operating conditions (evaporating, condensing, boiling temperatures and ejector primary mass flow rate)

Parameter	Case# 1	Case# 2	Case# 3	Case# 4
$T_{g,\,sat}$ [°C]	61.3, 61.5, 61.6, 61.8, 62	61.5	63, 64, 65, 66, 67	62
$T_{c,\,sat}$ [°C]	30	28, 29 30, 31, 32, 33, 34, 35, 36, 37, 40	30	32
$\dot{m}_{pr}$ [kg/s]	0.33	0.33	0.34, 0.35, 0.36, 0.37, 0.38	0.33
$T_{e,\,sat}$ [°C]	10	17, 17, 17, 17, 17, 17, 17, 19, 20, 21, 24	10	8, 10, 12, 14, 16

4.4 System performance analysis

The ejector capacity is evaluated using the entrainment ratio (ω), which is defined as the ratio between the secondary mass flow rate and the primary mass flow rate, and the pressure ratio, which is the ratio of the outlet to secondary inlet pressure:

$$\omega = \frac{\dot{m}_{sec}}{\dot{m}_{pr}} \tag{4.1}$$

$$PR = \frac{P_{out}}{P_{sec}} \tag{4.2}$$

The energy efficiency of a refrigeration system is usually expressed in terms of the Coefficient of Performance (COP) which is the ratio of the heat extraction rate to the rate of energy use:

$$Q_e = \dot{m}_{sec}(\mathrm{h_{e,out}} - \mathrm{h_{e,in}}) \tag{4.3}$$

$$Q_g = \dot{m}_{pr}(\mathrm{h_{g,out}} - \mathrm{h_{g,in}}) \tag{4.4}$$

$$W_p = (\dot{m}_{pr} + \dot{m}_{sec})(\mathrm{h_{p,in}} - \mathrm{h_{p,out}}) \tag{4.5}$$

$$COP = \frac{Q_e}{(Q_g + W_p)} \approx \omega\,\frac{\Delta h_e}{\Delta h_g} \tag{4.6}$$

Definitions of the four component efficiencies of the ejector (primary nozzle, secondary inlet, mixer and diffuser) are presented in equations 7 to 11:

The mixing efficiency (η_{mix}) is calculated by applying momentum conservation between cross sections 7p, 7s and 8 [39]. The mixing efficiency accounts for exergy losses due to the mixing process, friction and oblique shocks in the mixing chamber and constant area section.

$$\eta_{pr} = \frac{\mathrm{h}_4 - \mathrm{h}_{7p}}{\mathrm{h}_4 - \mathrm{h}_{is,7p}} \tag{4.7}$$

$$\eta_{sec} = \frac{\mathrm{h}_6 - \mathrm{h}_{7s}}{\mathrm{h}_6 - \mathrm{h}_{is,7s}} \tag{4.8}$$

$$\eta_{\mathrm{mix}} = 1 - \frac{F_f}{\dot{m}_{pr}V_{7p} + \dot{m}_{sec}V_{7s}} \tag{4.9}$$

$$F_f = \left(P_{7p}A_{7p} + \dot{m}_{pr}V_{7p}\right) + \left(P_{7s}A_{7s} + \dot{m}_{sec}V_{7s}\right) - P_8A_8 - \left(\dot{m}_{pr} + \dot{m}_{sec}\right)V_8 \tag{4.10}$$

$$\eta_d = \frac{\mathrm{h}_{is,1} - \mathrm{h}_8}{\mathrm{h}_1 - \mathrm{h}_8} \tag{4.11}$$

where the superscript '*is*' refers to the temperature at the given location for an isentropic process.

The frictional and mixing losses in the nozzle, diffuser and mixing section of the ejector are taken into account using the total efficiency, η_{eje}. Due to difficulties in determining the efficiencies of the ejector components from experimental data, a definition of the ejector performance as a function of entrainment ratio was obtained using equation 12. There are many ways to define the ejector efficiency, η_{eje}. The efficiency used by Elbel [94] is defined as the ratio between the isentropic recovered compression energy in the secondary flow and the available theoretical energy in the isentropic expansion of the motive stream. This efficiency definition has been also used by other researchers [28], [95]:

$$\eta_{eje} = \frac{\dot{m}_{sec}}{\dot{m}_{pr}} \frac{h\left(P_{d,out}, S_{sec,in}\right) - h_{sec,in}}{h_{pr,in} - h\left(P_{d,out}, S_{pr,in}\right)} = \omega \frac{h(P_1, S_6) - h_6}{h_4 - h(P_1, S_4)} \tag{4.12}$$

The exergy analysis permits to compare the energy performance of a device or thermodynamic system in terms of energy quality rather than energy amount. Through the ejector process, heat and work transfer with the surroundings is negligible. Hence, the exergy analysis becomes important to understand the occurring losses [59]. Exergy represents the maximum amount of work theoretically available between any specific state and a reference dead state, typically environmental conditions. The exergy of a thermodynamic state "i" and exergy loss of a stream can be computed, respectively, from equations 13 and 14 [23] [96].

$$\mathrm{E}_i = \dot{\mathrm{m}}[(\mathrm{h}_i - \mathrm{h}_0) - \mathrm{T}_0(\mathrm{h}_i - \mathrm{h}_0)] \tag{4.13}$$

$$\Delta\mathrm{E} = \mathrm{E}_{in} - \mathrm{E}_{out} \tag{4.14}$$

$$\Delta\mathrm{E}_{eje} = (\mathrm{E}_4 + \mathrm{E}_6) - \mathrm{E}_1 \tag{4.15}$$

$$\Delta\mathrm{E}_{pr} = \mathrm{E}_4 - \mathrm{E}_{7p} = \dot{m}_{pr}[\left(\mathrm{h}_4 - \mathrm{h}_{7p}\right) - \mathrm{T}_0\left(\mathrm{s}_4 - \mathrm{s}_{7p}\right)] \tag{4.16}$$

$$\Delta E_{sec} = E_6 - E_{7s} = \dot{m}_{sec}[(h_6 - h_{7s}) - T_0(s_6 - s_{7s})] \quad (4.17)$$

$$\Delta E_{mix} = (E_7 - E_m) + (E_m - E_8) = (\dot{m}_{pr} + \dot{m}_{sec})[(h_{7p,7s} - h_8) - T_0(s_{7p,7s} - s_8)] \quad (4.18)$$

$$\Delta E_d = E_8 - E_1 = (\dot{m}_{pr} + \dot{m}_{sec})[(h_8 - h_1) - T_0(s_8 - s_1)] \quad (4.19)$$

$$\eta_{exe} = \frac{E_{out}}{E_{in}} = \frac{E_1}{E_4 + E_6} \quad (4.20)$$

where $\dot{m}$ is the mass flow rate (kg/s), "h" the specific enthalpy (kJ/kg) and "s" the specific entropy (kJ/kg/K). The subscript "0" refers to dead state conditions. The dead state in this study corresponds to T_0 = 20 °C and P_0 = 101 kPa.

The exergy (E_i) can be used to pinpoint the losses in energy quality across a specific process. This is readily done using the exergy destruction index ξ defined by Banasiak et al. [97]: where the subscripts "j" and "eje" represent the exergy destruction rate respectively between the entrance and the j-section, and for the total ejector [98]:

$$\xi = \frac{\Delta E_j}{\Delta E_{eje}} \quad (4.21)$$

4.5 CFD model

A RANS-CFD model has been carried out to study the fluid flow within the ejector. The model computational domain and boundary conditions are based on the experimental data. The CFD model results will be used to calculate some important parameters such as the component efficiencies, entrainment ratio and exergy losses inside the ejector.

4.5.1 Numerical setup

In this work, the commercial package Ansys Fluent 17.0 was used to model the flow within the ejector, following successful implementations reported in the literature [60] [59]. Turbulence effects have been modeled using the k-ω SST turbulence model. A second order accurate discretization scheme coupled with a pressure-based implicit solver was chosen for numerical resolution. With this approach, the energy equation is solved in a secondary step and the density (as well as other fluid properties) is computed using the REFPROP v9.1 equation database. The conservation equations governing the fluid flow in the ejector are solved under the assumption of a compressible, steady state and axisymmetric flow. The boundary conditions at the walls

are represented by the non-slip and adiabatic conditions for velocity and temperature respectively. Pressure boundary conditions are applied at the inlet and outlet of the ejector. Table 4.4 summarizes the main numerical settings used in this study:

Table 4.4 CFD Settings

Working fluid	R245fa, Real fluid
Turbulence Model	k-w SST(HRN)
Solver Numerical schemes	Pressure based Coupled, Pressure: PRESTO! Momentum, Turbulence, Energy: 2nd order Upwind
Convergence criteria	Residuals RMS<1×10^{-5} Mass imbalances<1%

4.5.2 Details of the geometry meshing

In order to test the independence of the numerical results with respect to mesh density, several mesh sizes were examined. The results of four sets of grids were compared. The results reveal that the mesh density has a strong influence on convergence and stability. The Mach number along the ejector is used to detect the influence of the cell number (Fig. 4-5). A final mesh with 5.94×10^5 quadrilateral cells was considered sufficiently fine to give satisfactory results in terms of the entrainment ratio (Fig. 4-6). This mesh is refined from the primary nozzle lips along the shear layer and also in the vicinity of walls, with an average value for the wall coordinate ($30\leq y^+\leq100$), adequate for the application of a High-Reynolds approach [61]. A standard wall function was applied to the flow in the near-wall region and the cells close to the walls were further refined to capture the complex supersonic flow.

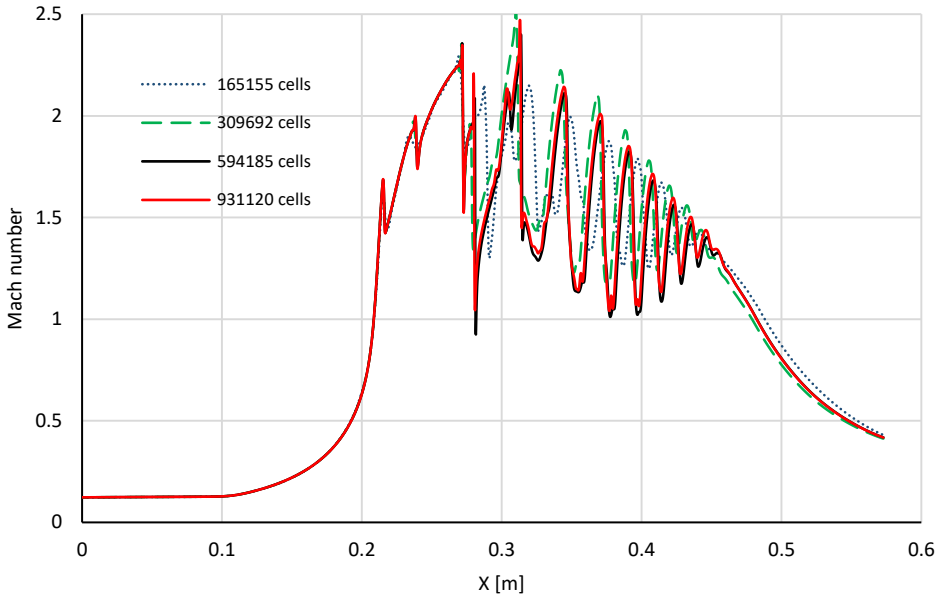

Figure 4.5 Variation of the axial Mach number with different grid levels

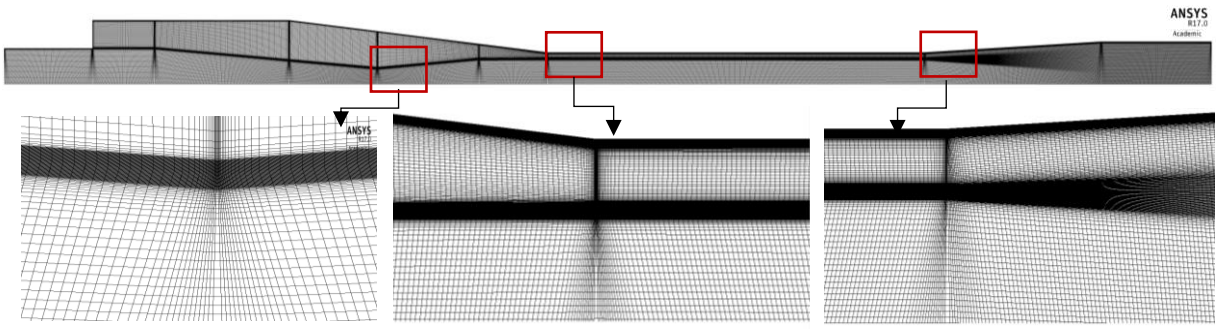

Figure 4.6 Details of the mesh grid used in the CFD calculations

4.5.3 Validation of the CFD simulation

The CFD predictions were validated against the ejector experimental data. Fig. 4-7 displays a comparison between the entrainment ratio as predicted by the present CFD model and the experimental data. The simulations offer an acceptable prediction in the double-choking regime. The average deviation between the estimated and the measured entrainment ratio is around 5.92% in the double-choking regime and about 18.2% for the single-choking regime. It should be noted that the constant entrainment ratio is caused by the choking of the secondary flow before mixing with the primary flow. Basically, the ejector performance can be divided into three operational modes according to the back pressures: (1) double-choking or critical mode (2) single-choking or subcritical mode and (3) back-flow or malfunction mode [99].

At the subcritical mode, the deviation of the CFD calculated entrainment ratio values from experimental data is greater than at the critical mode (Fig. 4-7). One reason for this difference

can be the shocking phenomenon that causes a very complex flow at the single-choking flow region, probably leading to unexpected experimental results. Another reason can be the difficulties in calibrating the absolute pressure transducers. Because the entrainment ratio in the single-choking region is very sensitive to the changes in downstream pressure, a slight change in this value causes more effect to the entrainment ratio than what can happen in the double-choke region. Therefore, a small error in calibrating the absolute pressure transducer may result in an important error in reading the entrainment ratio [100].

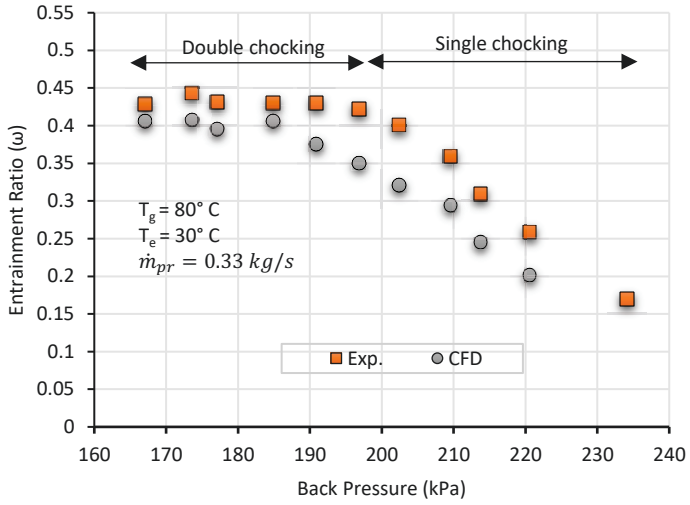

Figure 4.7 Ejector operational moods (Performance Curves) ($T_g = 80\ °C$, $T_e = 30\ °C$, $\dot{m}_{pr} = 0.33\ kg/s$)

4.6 Performance analysis under various operating conditions

The relationship between the refrigeration cycle parameters and the ejector component efficiencies, entrainment ratio, pressure ratio and ejector exergy losses inside the ejector are analyzed. Furthermore, a comparison between the results obtained by the CFD model and the experimental data is performed. All efficiencies and exergy losses are estimated using CFD numerical results with boundary conditions at inlets and outlet obtained from experimental data.

4.6.1 Effect of generator temperature

The entrainment ratio ω and the COP generally increase with a rise in T_g. In fact, the pressure and enthalpy of the primary flow increase with the T_g, and a higher T_g causes a better entrainment effect at a given T_c and T_e. Therefore, as more secondary flow is entrained into the ejector, a higher ω is observed (table 4.5). It should be noted that for given condenser and

evaporator temperatures, every ejector in a particular configuration has an optimum generator temperature at which the maximum COP could be obtained [101].

According to the results, an increment in T_g leads to a rise in all exergy losses inside the ejector and consequently the total exergy losses ΔE_{eje} augment. Moreover, the value of PR, η_{pr} , η_{sec}, η_{mix} and η_d decrease (fig. 4-8).

Results also show that there is a good agreement between numerical results and experimental data with an average error of -7.06 %. Note that the negative sign indicates that the CFD model under-predicts the experimental results.

The exergy calculations have been performed using temperature and pressure mean values extracted from the CFD model using a surface integrals method across the main sections. Exergy losses are then calculated in EES (Engineering Equation Solver), which includes relations for the fluid properties [63].

Fig. 4-9 shows that the highest exergy losses occur during mixing between cross-sections (7-m) and across the normal shock between cross-sections (m-8). They represent in average about 81.14% of the total exergy losses.

The contributions to exergy losses for the primary nozzle, the suction chamber and the diffuser account for 12.93, 1.14 and 4.78 % of the total exergy losses respectively. These losses are mainly due to the large velocity and pressure gradients within the ejector. An appropriate redesign of the regions with large exergy losses may contribute to potential enhancements. Unlike the entrainment ratio (the traditional criteria measuring the performance of ejectors), the exergy efficiency is firmly based on both the first and second laws of thermodynamics [102]. For the present experiments and under the operating conditions considered, the average exergy efficiency is 51. 65% for case 1.

It is further found that T_g has the most significant impact on ΔE_d. Indeed, increasing T_g by 22.23 % leads to an increase in ΔE_d by 74.59%, since an increase in the T_g will force the oblique shocks to pass through the diffuser section and move towards the exit, which rises the irreversibilities generated in the diffuser.

Table 4.5 Effects of generator temperature (T_g) on ejector working characteristics at fixed operating conditions ($\boldsymbol{T_c = 20\,°C, T_e = 20\,°C, \dot{m}_{pr} = 0.33\,kg/s}$)

T_g [°C]	Experimental						CFD									
	ω_{exp} [-]	PR [-]	COP [-]	ΔE_{eje} [kW]	η_{eje} [%]	η_{exe} [%]	ω_{CFD} [-]	dif_{ω} [%]	η_{pr}	η_{sec}	η_{mix}	η_d	ΔE_{pr} [kW]	ΔE_{sec} [kW]	ΔE_{mix} [kW]	ΔE_d [kW]
70	0.3065	2.14	0.2495	4.442	22.17	52.02	0.2893	-5.6	0.9832	0.9873	0.9292	0.7312	0.6048	0.054	3.9557	0.0902
75	0.3112	2.13	0.2511	4.559	21.63	52.01	0.2897	-6.9	0.9827	0.9868	0.9251	0.7155	0.6089	0.055	4.0364	0.1499
80	0.3142	2.12	0.2526	4.643	21.19	51.9	0.2920	-7.01	0.9826	0.9861	0.9114	0.6572	0.6477	0.056	4.0485	0.268
85	0.3287	2.05	0.2581	4.726	20.66	51.34	0.3066	-6.7	0.9823	0.9858	0.9053	0.5837	0.6645	0.059	4.0528	0.3426
90	0.3543	1.99	0.2673	4.844	20.57	51.01	0.3224	-9.01	0.982	0.9849	0.8992	0.5665	0.6889	0.062	4.0637	0.3552

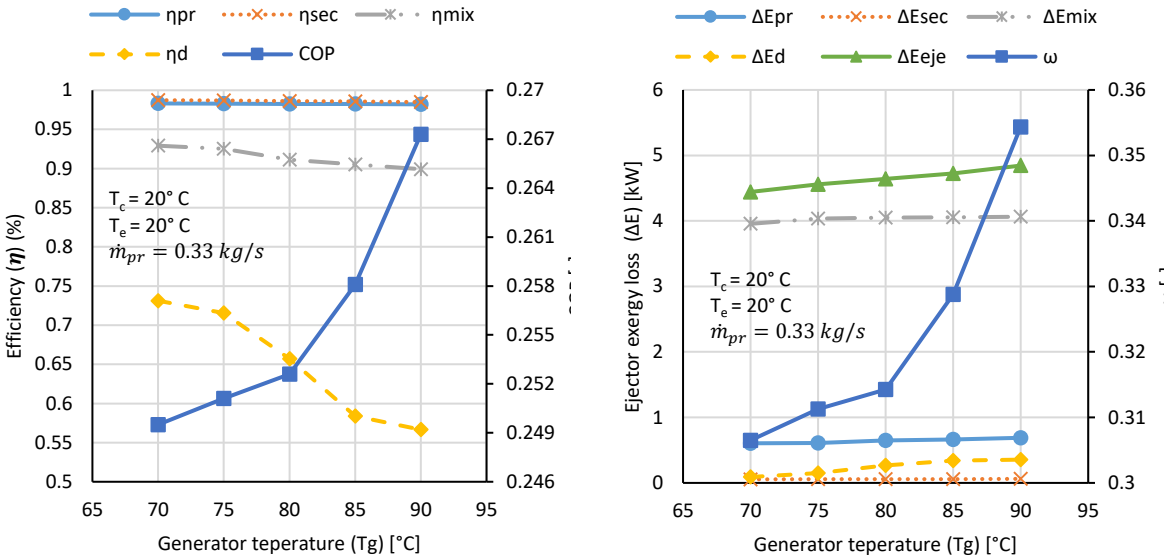

Figure 4.8 Effects of generator temperature (T_g) ***(a)*** *on the coefficient of performance (COP) and component ejector efficiencies* ***(b)*** *on the entrainment ratio and ejector exergy losses at fixed operating conditions ($T_c = 20\,°C, T_e = 20\,°C, \dot{m}_{pr} = 0.33\,kg/s$)*

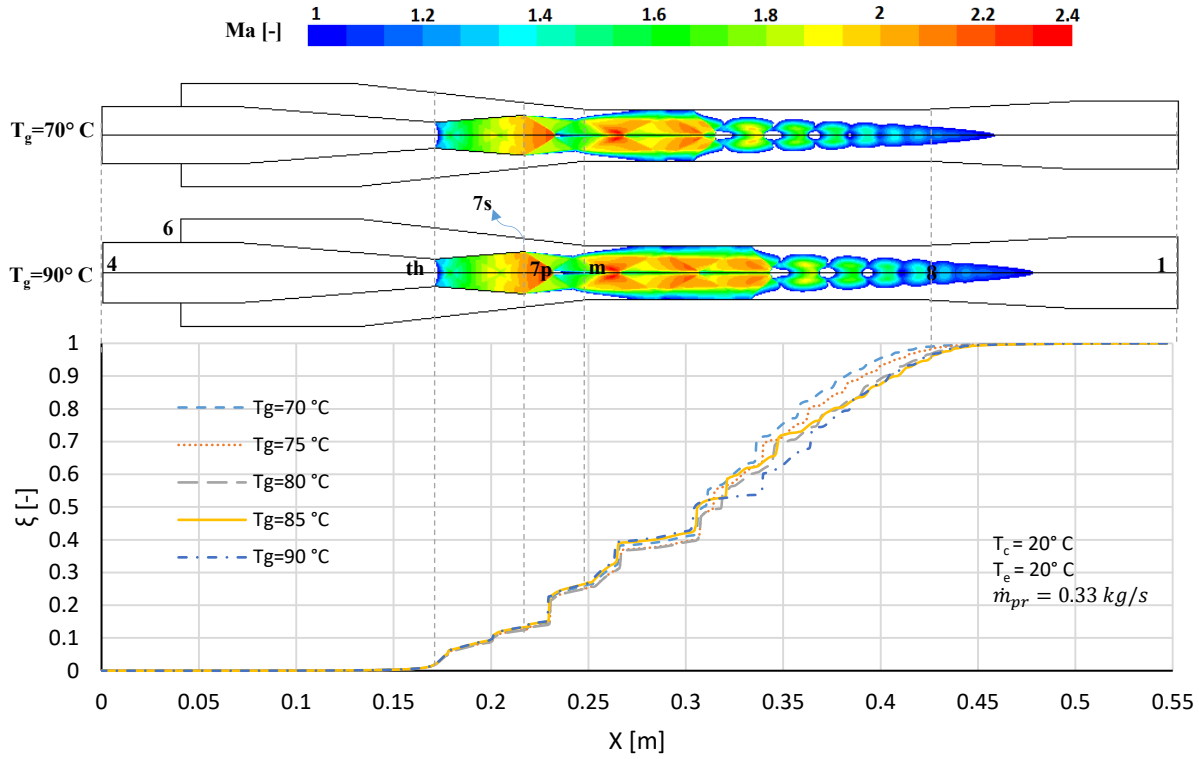

Figure 4.9 Comparisons between the different generator temperatures (T_g) for exergy destruction index ξ and Mach number contour within the ejector for case# 1.

4.6.2 Effect of condenser temperature

Table 4.6 shows the effects of condenser temperature (T_c) on ejector's performance. The following effects were observed when increasing the condenser temperature:

In the double-choking regime:

- The value of η_{pr} , η_{sec} ΔE_{pr}, ΔE_{sec} and ω stay constant, meaning that these values are independent of the condenser temperature T_c when it is lower than the critical condenser temperature point T_c^*. In other words, the upstream of the normal shock is not influenced by condenser temperature. A slightly further increase of T_c beyond T_c^* will cause the COP, ω and exergy losses in mixing and diffuser to drop sharply. It should be noted that critical condenser temperature point T_c^* predicted by CFD model is about $T^*_{c,(\,CFD)} = 22°C$ while experimental study shows that it is about $T^*_{c,(\,exp)} = 24°C$. In other words, the CFD model predicts an earlier start of the single-choking mode relative to the experimental data. In addition, the maximum pressure ratio was observed at the critical condenser temperature point T_c^*.

In the single-choking regime:

- An increase in T_c leads to a gradual decrease in ω, η_{pr}, ΔE_{sec} and PR while η_{sec}, ΔE_{pr} and ΔE_{eje}increase. This is because less secondary flow can be entrained into the ejector if the backpressure increases. Another reason might be that an increase in the P_c will force the shock to pass through the mixing section and move towards the nozzle exit, which limits the entrainment effect. [103]

It should be noted that the increase in ΔE_{eje} is not significant and can be neglected.

In both double-choking and single-choking regimes:

Fig. 4-12 shows that the highest exergy losses occur during mixing between cross-sections (7-m) and across the normal shock between cross-sections (m-8). They represent in average 72.02% of the total exergy losses.

There is a direct relationship between the pressure ratio (PR) and the ejector performance in the double choking regime. The contributions of exergy losses in the primary nozzle, the suction chamber and the diffuser account for 23.57, 1.26 and 3.13 % of the total exergy losses respectively. Under the assessed operating conditions, the average exergy efficiency is 60. 25%. At these conditions, the value of the ΔE_{mix} and ΔE_d diminish and consequently η_{mix} and η_d increase. The system COP continuously decreases with any increase in T_c. Fig. 4-11 illustrates the effects of ejector back pressure (P_1) on the pressure ratio (PR) and on the entrainment ratio (ω) at fixed operating conditions.

Table 4.6 Effects of condenser temperature (T_c) on ejector working characteristics at fixed operating conditions ($\boldsymbol{T_g = 80\ °C}$, $\boldsymbol{T_e = 30\ °C}$, $\boldsymbol{\dot{m}_{pr} = 0.33\ kg/s}$)

T_c [°C]	Experimental						CFD									
	ω_{exp} [-]	PR [-]	COP [-]	ΔE_{eje} [kW]	η_{eje} [%]	η_{exe} [%]	ω_{CFD} [-]	dif_ω [%]	η_{pr}	η_{sec}	η_{mix}	η_d	ΔE_{pr} [kW]	ΔE_{sec} [kW]	ΔE_{mix} [kW]	ΔE_d [kW]
18	0.4279	1.59	0.3711	5.042	17.51	50.723	0.4061	-5.1	0.9891	0.9901	0.8902	0.5967	0.6913	0.097	3.7752	0.7705
19	0.4428	1.61	0.369	4.781	19.22	53.72	0.4076	-7.9	0.9883	0.9904	0.9241	0.6632	0.6848	0.098	3.7539	0.4753
20	0.4313	1.7	0.3619	4.521	21.52	55.648	0.3958	-8.2	0.9884	0.9903	0.9421	0.6963	0.6801	0.098	3.7434	0.2635
21	0.4299	1.76	0.3575	4.236	23.65	58.634	0.4061	-5.5	0.9826	0.9903	0.9662	0.757	0.6775	0.095	3.6598	0.0497
22	0.4301	1.78	0.3567	4.064	24.73	60.756	0.3758	-12.6	0.9821	0.9904	0.9685	0.809	0.6765	0.082	3.5182	0.0354
23	0.4211	1.78	0.349	3.91	24.97	62.448	0.3497	-16.9	0.9794	0.9911	0.9693	0.8211	0.6775	0.071	3.4766	0.0239
24	0.4009	1.83	0.3322	3.766	25.65	64.49	0.3208	-19.9	0.9778	0.9919	0.9708	0.8345	0.875	0.035	3.1505	0.0225
25	0.3589	1.79	0.2974	3.726	23.06	64.487	0.2936	-18.1	0.9706	0.9922	0.9728	0.8592	0.9733	0.023	3.0043	0.0215
26	0.3088	1.75	0.2558	3.801	19.58	64.045	0.2458	-20.4	0.9656	0.9923	0.9761	0.8596	1.304	0.014	2.5279	0.0201
27	0.2581	1.71	0.2141	3.827	16.19	64.066	0.2017	-21.8	0.9075	0.9989	0.9784	0.8599	1.4814	0.012	2.2938	0.0198
30	0.1693	1.66	0.1388	3.862	10.56	64.275	0.1335	-21.1	0.7264	0.9997	0.9802	0.8602	2.0696	0.009	1.7747	0.0187

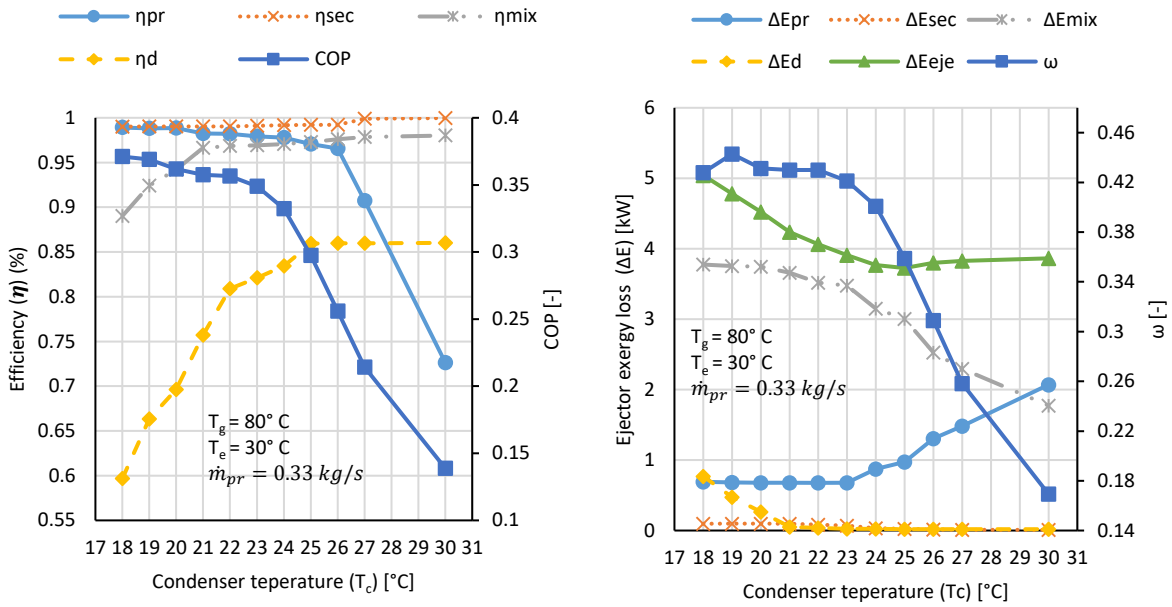

Figure 4.10 Effects of condenser temperature (T_c) ***(a)*** *on the coefficient of performance (COP) and component ejector efficiencies* ***(b)*** *on the entrainment ratio and ejector exergy losses at the fixed operating conditions ($T_g = 80\ °C$, $T_e = 30\ °C$, $\dot{m}_{pr} = 0.33\ kg/s$)*

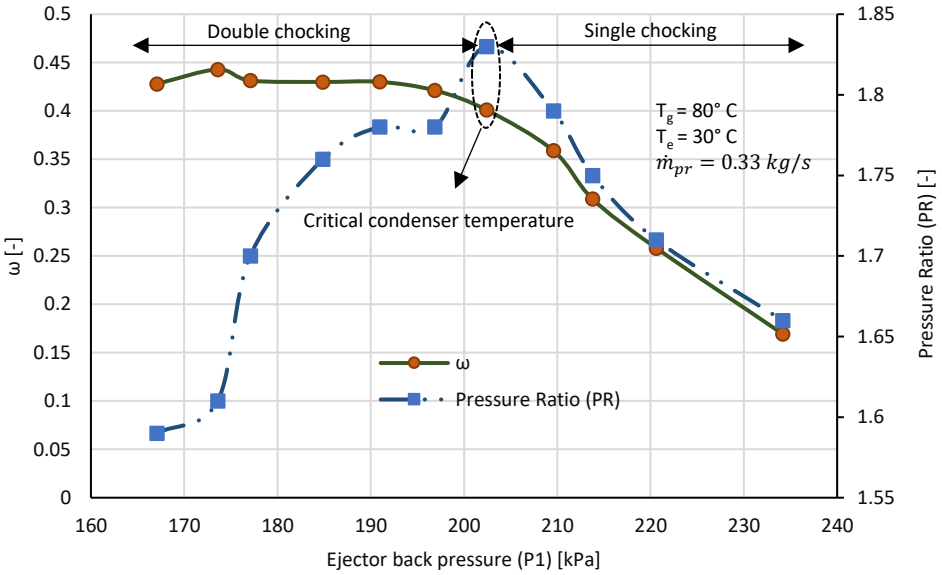

Figure 4.11 Effects of ejector back pressure (P_1) on the pressure ratio (PR) and on the entrainment ratio (ω) at the fixed operating conditions ($T_g = 80\ °C$, $T_e = 30\ °C$, $\dot{m}_{pr} = 0.33\ kg/s$)

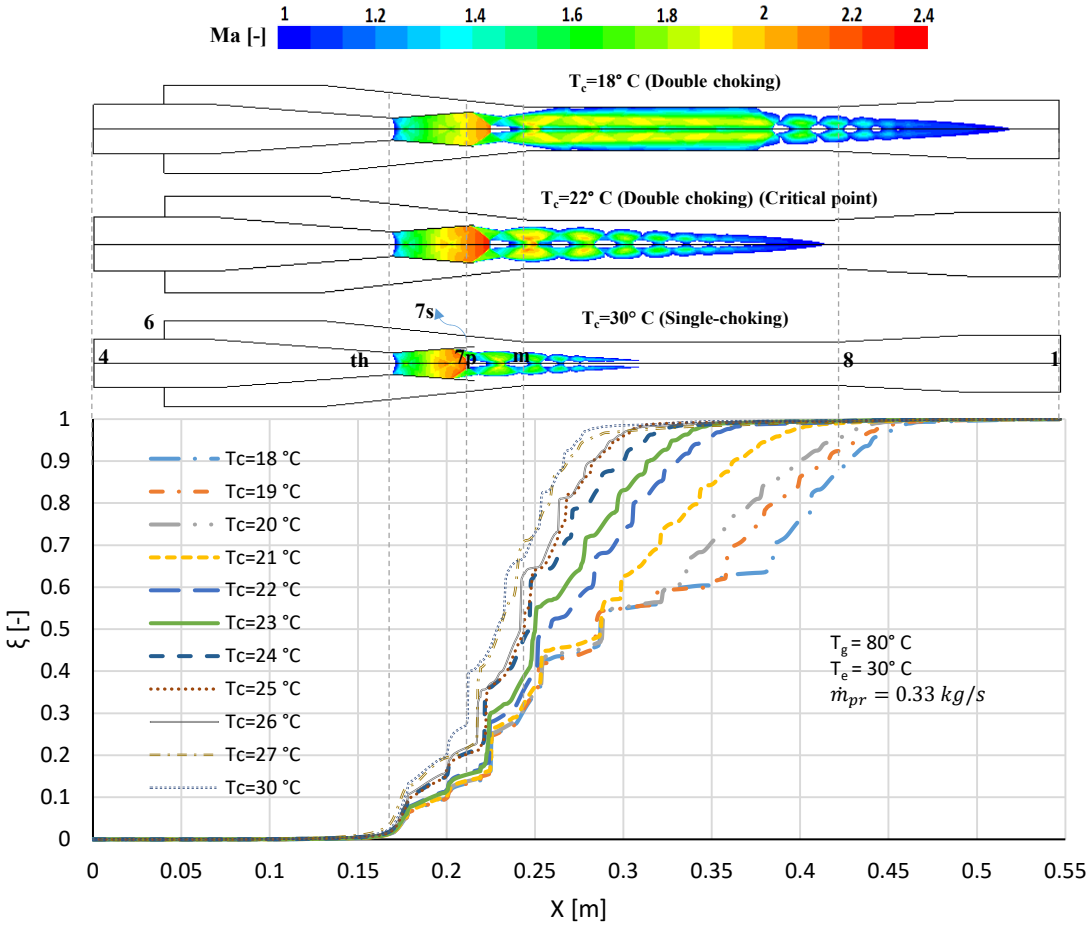

Figure 4.12 Comparisons between the different condenser temperatures (T_c) for exergy destruction index ξ and Mach number contour within the ejector for case# 2.

4.6.3 Effect of primary mass flow rate

Table 4.7 shows the effects of the primary mass flow rate $\dot{m}_{pr}$ on ejector's performance and refrigeration cycle. It has been found that by increasing $\dot{m}_{pr}$, all of the component efficiencies decrease. As expected, the entrainment ratio ω and the COP generally decrease with a rise in $\dot{m}_{pr}$. Results also show that PR is independent of $\dot{m}_{pr}$.

Fig. 4-13 depicts the effect of $\dot{m}_{pr}$ on the efficiency of components, system COP, exergy losses and entrainment ratio. A direct relationship between $\dot{m}_{pr}$ and exergy exergy losses inside the ejector, and consequently total exergy losses ΔE_{eje} , is observed.

Furthermore, Fig. 4-14 shows that the highest exergy losses occur during mixing, between cross-sections (7-m), and across the normal shock, between cross-sections (m-8). These represent in average 70.06% of the total exergy losses.

The contributions of exergy losses generated in the primary nozzle, the suction chamber and the diffuser account respectively for 11.86, 0.95 and 17.12 % of the total exergy loss. Under the operating conditions considered, the average exergy efficiency is 51. 74%.

Table 4.7 Effects of primary mass flow rate ($\dot{m}_{pr}$) on ejector working characteristics at fixed operating conditions ($T_g = 90\ °C, T_c = 20\ °C, T_e = 20\ °C$)

$\dot{m}_{pr}$ [kg/s]	Experimental						CFD									
	ω_{exp} [-]	PR [-]	COP [-]	ΔE_{eje} [kW]	η_{eje} [%]	η_{exe} [%]	ω_{CFD} [-]	dif_{ω} [%]	η_{pr}	η_{sec}	η_{mix}	η_d	ΔE_{pr} [kW]	ΔE_{sec} [kW]	ΔE_{mix} [kW]	ΔE_d [kW]
0.34	0.3303	2.14	0.2503	5.215	19.11	52.847	0.3061	-7.3	0.9926	0.9831	0.8866	0.6134	0.6595	0.056	4.1747	0.6049
0.35	0.2907	2.14	0.2243	5.441	18.24	52.248	0.2909	0.09	0.9816	0.9819	0.87	0.6116	0.6661	0.056	4.1812	0.7757
0.36	0.2826	2.14	0.2183	5.767	17.39	51.707	0.2804	-0.78	0.9814	0.9713	0.8527	0.5713	0.7235	0.056	4.1865	1.039
0.37	0.2757	2.13	0.2134	6.055	16.71	51.168	0.2697	-2.1	0.9812	0.9455	0.8432	0.5492	0.7528	0.059	4.242	1.2073
0.38	0.2704	2.13	0.2095	6.329	16.12	50.75	0.2621	-3.1	0.9812	0.9417	0.8354	0.5425	0.7779	0.061	4.2687	1.6444

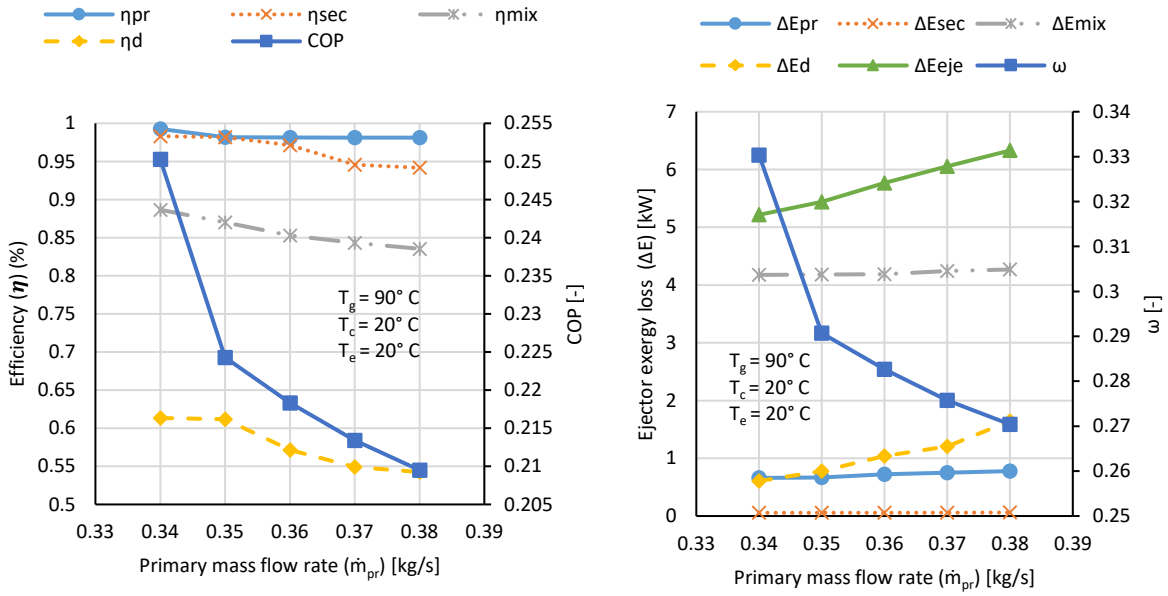

*Figure 4.13 Effects of primary mass flow rate ($\dot{m}_{pr}$) **(a)** on the coefficient of performance (COP) and component ejector efficiencies **(b)** on the entrainment ratio and ejector exergy losses at fixed operating conditions ($T_g = 90\ °C, T_c = 20\ °C, T_e = 20\ °C$)*

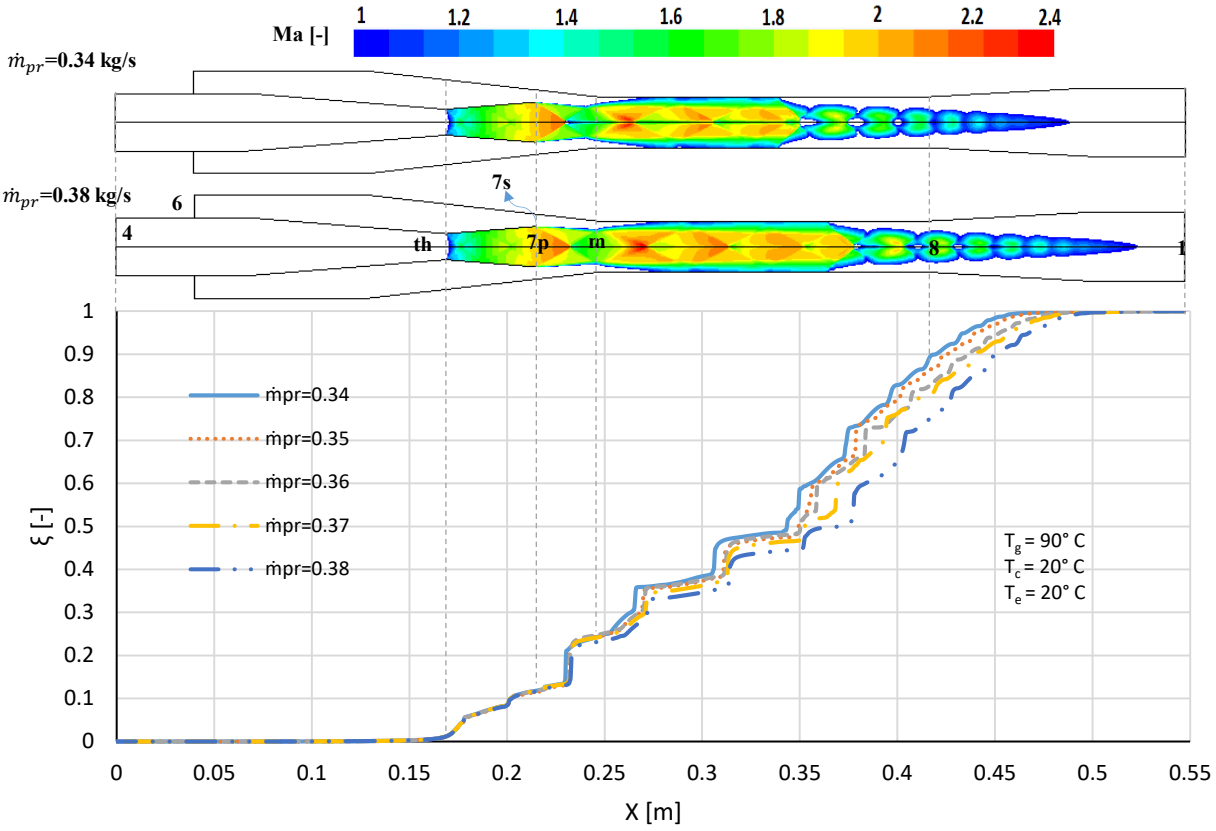

Figure 4.14 Comparisons between the different primary mass flow rates ($\dot{m}_{pr}$) for exergy destruction index ξ and Mach number contour within the ejector for case# 3.

4.6.4 Effect of evaporator temperature

Table 4.8 shows the effects of evaporator temperature (T_e) on ejector's performance. It is found that by increasing the evaporator temperature, both ω and COP increase. The impact on the total exergy losses is very little as illustrated in table 4.8. Fig. 4-16 shows that the highest exergy losses occur during mixing, between cross-sections (7-m), and across the normal shock, between cross-sections (m-8). They represent in average 82.78% of the total exergy losses.

The contributions of exergy losses generated in the primary nozzle, the suction chamber and the diffuser account, respectively, for 15.88, 0.74 and 0.58 % of the total exergy losses. Under the operating conditions considered, the average exergy efficiency is 57. 36%.

Table 4.8 Effects of evaporator temperature (T_e) on ejector working characteristics at fixed operating conditions ($\boldsymbol{T_g = 85\,°C, T_c = 22\,°C, \dot{m}_{pr} = 0.33\,kg/s}$)

T_e [°C]	Experimental						CFD									
	ω_{exp} [-]	PR [-]	COP [-]	ΔE_{eje} [kW]	η_{eje} [%]	η_{exe} [%]	ω_{CFD} [-]	dif_{ω} [%]	η_{pr}	η_{sec}	η_{mix}	η_{d}	ΔE_{pr} [kW]	ΔE_{sec} [kW]	ΔE_{mix} [kW]	ΔE_{d} [kW]
16	0.2619	2.49	0.2026	4.409	22.04	56.067	0.2031	-22.4	0.9814	0.9992	0.9748	0.8471	0.8619	0.014	3.9925	0.0245
18	0.2902	2.29	0.2261	4.385	22.24	56.786	0.2473	-14.7	0.9827	0.9989	0.9756	0.8464	0.747	0.025	3.9595	0.0254
20	0.3223	2.12	0.2528	4.352	22.57	57.555	0.2771	-14	0.9845	0.9984	0.9792	0.8384	0.707	0.038	3.8440	0.0279

22	0.3276	2.09	0.2586	4.331	22.68	57.796	0.2945	-10.1	0.9849	0.9981	0.9811	0.8384	0.7051	0.041	3.8359	0.0287
24	0.3575	1.98	0.2839	4.294	23.02	58.643	0.3191	-10.7	0.9865	0.9976	0.9839	0.8383	0.7024	0.055	3.7458	0.0308

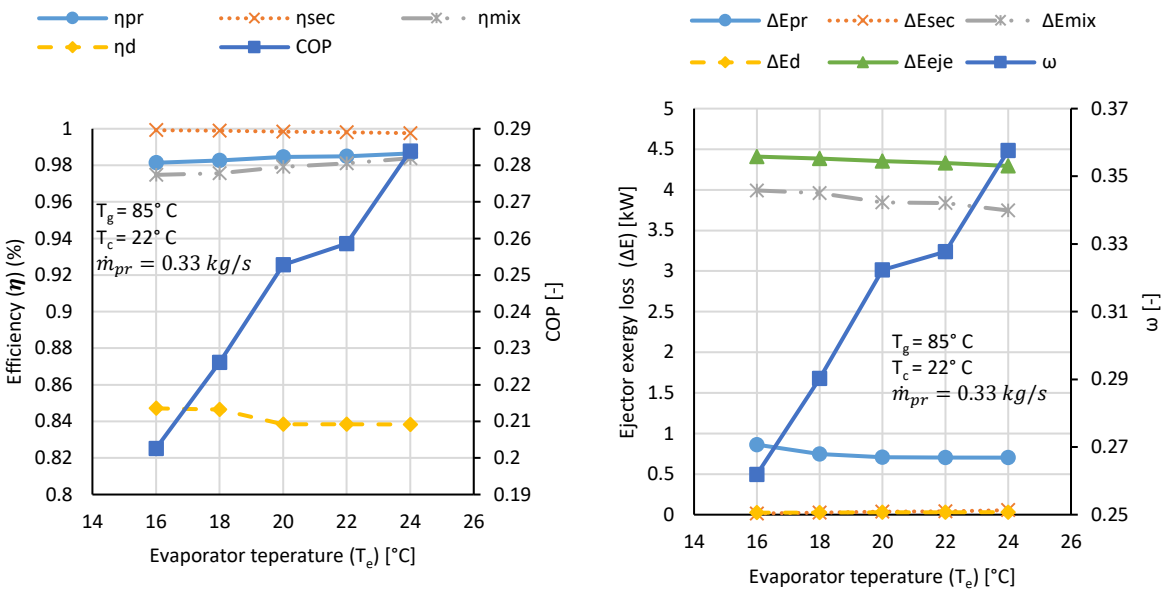

*Figure 4.15 Effects of evaporator temperature (T_e) **(a)** on the coefficient of performance (COP) and component ejector efficiencies **(b)** on the entrainment ratio and ejector exergy losses at fixed operating conditions ($T_g = 85\ °C$, $T_c = 22\ °C$, $\dot{m}_{pr} = 0.33\ kg/s$)*

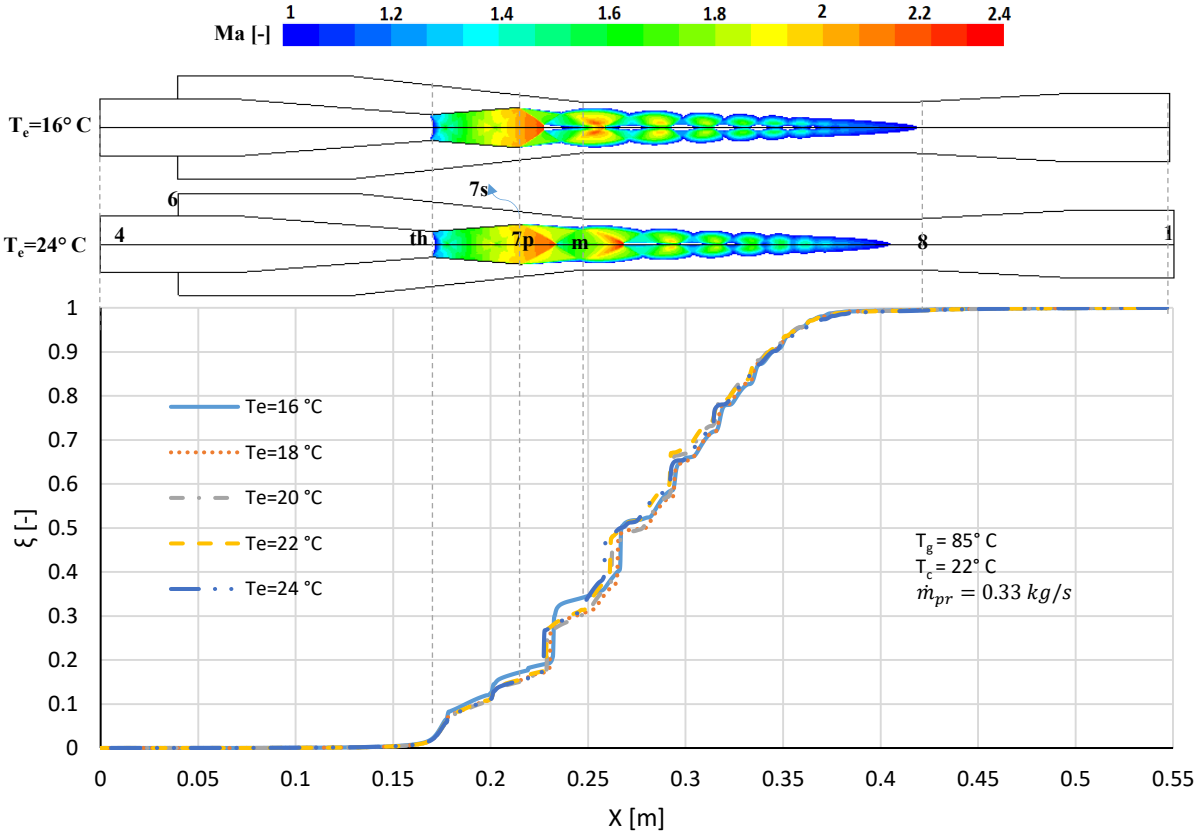

Figure 4.16 Comparisons between the different evaporator temperatures (T_e) for exergy destruction index ξ and Mach number contour within the ejector for case# 4.

4.6.5 A summary of the obtained results of four cases

A summary of the relationships between the assessed variables is presented in table 4.9. The system performance in terms of COP and ejector entrainment ratio ω, as well as the ejector efficiency, strongly depends on the operating temperatures. The main observations can be summarized as follows:

- It has been demonstrated that both system COP and ejector ω augment with an increase in the generator temperature T_g and the evaporator temperature T_e, however, these parameters decrease when the condenser temperature T_c or $\dot{m}_{pr}$ raise. The results show that evaporator temperature T_e is the most influential factor on system COP, PR and ω.

- Exergy losses inside the ejector and total ejector irreversibility are extremely dependent on cycle operating conditions. According to the results, an increase in T_g and $\dot{m}_{pr}$lead to greater exergy losses inside the ejector and consequently higher total exergy losses ΔE_{eje}.

- Results show that the most significant impact of increasing any of the four main operating parameters of the refrigeration cycle is on the efficiency and exergy losses in the diffuser.

- There is a direct relationship between the variations of COP and ω and increasing the refrigeration cycle parameters, as revealed by the percentage of variation in the COP and ω which is approximately similar. In other words, the coefficient of performance (COP) is extremely dependent on the entrainment ratio ω.

- Most of the exergy losses inside the ejector are located in three regions: the constant area duct (m-8), the mixing chamber (7-m) and the primary nozzle (th-7p). Irreversibilities in the mixing region are generated by two processes: firstly the contact and mixing of both fluids, and secondly the motive stream's mild shocks and its continuing expansion into the mixing area. At region (m-8), the sudden drop in Mach number reveals the presence of the second shock train. This abrupt change in the fluid regime leads to a sudden increase in losses over a short length.

- The results reveal that in the double-choking regime, the variation in condenser temperature T_c has the greatest impact on the overall ejector efficiency η_{eje}, the ejector exergy efficiency η_{exe}, mixing and diffuser exergy losses ($\Delta E_{mix}, \Delta E_d$) and corresponding efficiencies (η_{mix}, η_d). Moreover, the variation in the primary mass flow rate $\dot{m}_{pr}$ has the greatest impact on the total exergy losses ΔE_{eje}, primary and secondary exergy losses ($\Delta E_{pr}, \Delta E_{sec}$) and corresponding efficiencies (η_{pr}, η_{sec}).

Table 4.9 A summary of the relationship between refrigeration cycle parameters and the ejector working characteristics

Parameter	ω_{exp}	PR_{exp}	COP	ΔE_{eje}	η_{eje}	η_{exe}	η_{pr}	η_{sec}	η_{mix}	η_d	ΔE_{pr}	ΔE_{sec}	ΔE_{mix}	ΔE_d
T_g (↑)	↑	↓	↑	↑	↓	↓	↓	↓	↓	↓	↑	↑	↑	↑
T_c (↑)	C↓	↑↓	↓	↓↑	↑↓	↑↓	C↓	C↑	↑	↑	C↑	C↓	↓	↓
$\dot{m}_{pr}$ (↑)	↓	C	↓	↑	↓	↓	↓	↓	↓	↓	↑	↑	↑	↑
T_e (↑)	↑	↓	↑	↓	↑	↑	↑	↓	↑	↓	↓	↑	↓	↑

Increase (↑), Decrease (↓), Constant (C)

Fig. 4-17 shows the total ejector exergy losses as a function of the mixing efficiency for the four cases analyzed in Section 5. It shows that the total ejector exergy losses ΔE_{eje} decrease when η_{mix} increases in the double-choking regime. In other words, there is a direct relationship between ΔE_{eje} and η_{mix}. By increasing T_g, $\dot{m}_{pr}$ and decreasing T_c and T_e, the value of ΔE_{eje} increases while η_{mix} decreases. As previously mentioned, most of the exergy losses inside the ejector are located in the mixing area (7-8), since ΔE_{eje} is very sensitive to exergy losses incurred in this part.

This relationship between ΔE_{eje} which is calculated for the entire ejector and η_{mix} which only depends on the properties at cross-sections 7 and 8 is a remarkable feature for ejector analysis. It suggests that the mixing efficiency should not be assumed constant, opposite to the conclusions of Liu and Groll [68].

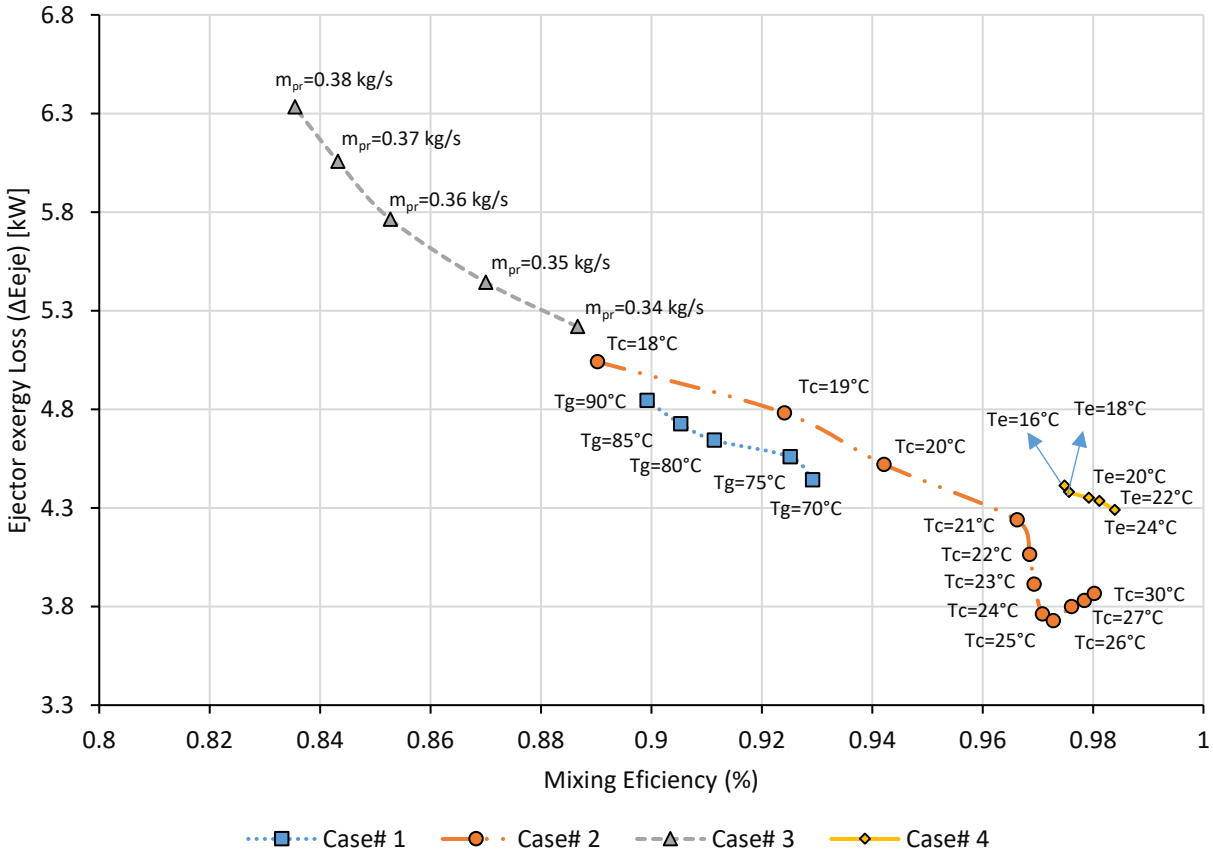

Figure 4.17 Total exergy destruction versus mixing efficiency.

Fig. 4-18 presents the variation of overall ejector efficiency versus COP for the four cases. For the experimental data presented, ejector efficiencies between 10.56% and 25.65% were achieved. These values were associated with experimental uncertainties of ±0.006. The highest overall ejector efficiency and ejector exergy efficiency were achieved for the critical condenser temperature point T_c^* in case 2. This indicates that the internal losses in the ejector minimize at this point as previously calculated. These results also shown that the ejector exergy efficiency is constant in the single-choking regime while COP increase (Fig. 4-19).

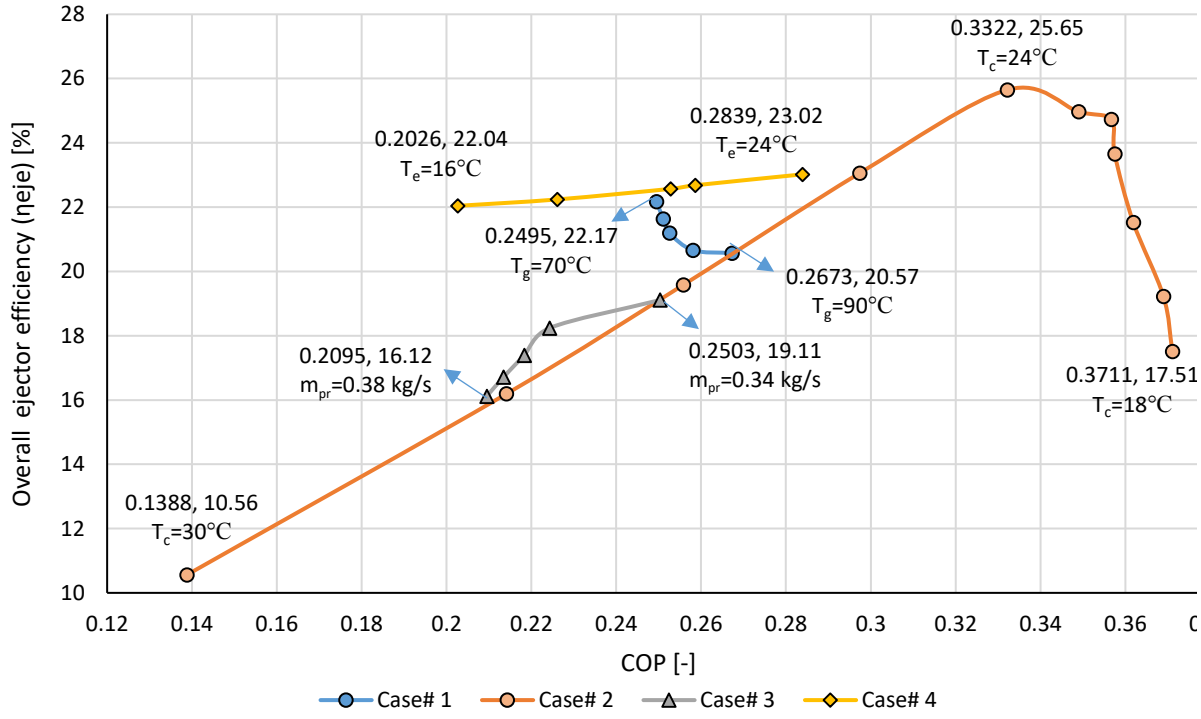

Figure 4.18 Overall ejector efficiency versus COP

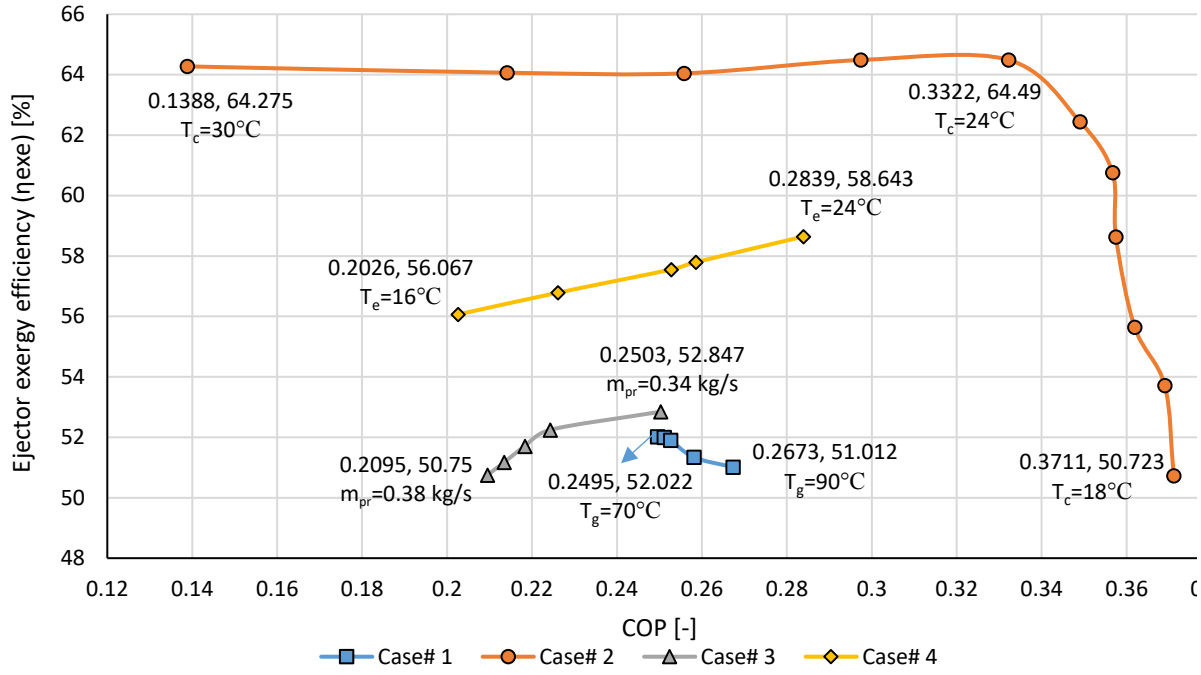

Figure 4.19 Ejector exergy efficiency versus COP

4.7 Geometrical improvement of the ejector for increasing the pressure ratio

The experimental and numerical results presented in section 5 show that the best performance of the ejector and the refrigeration cycle occur when the ejector offers the maximum pressure ratio for the critical condenser temperature (T_c^*=24°C). Thus, it is desirable to enhance the ejector performance by modifying its dimensions. In this section, the effect of the main ejector geometrical parameters on the pressure ratio is investigated in order to improve the performance of the present ejector refrigeration cycle at the optimum operating condition (T_c^*=24°C). To this end, a 1D thermodynamic model is developed in order to increase the pressure ratio (PR) at the fixed entrainment ratio and the optimum operating condition.

In this study, the operating conditions based on the critical condenser temperature (which resulted in the best performance among 26 experimental runs) are considered as the base case (table 4.10).

Table 4.10 Optimum operating conditions at the critical condenser temperature (T_c^*=24°C)

Parameter	Base case
Working fluid	R245fa, Real Fluid
T_g,T_c,T_e	80°C, 24°C, 30°C
P_4, T_4 (Primary inlet)	485.46 kPa, 78.81°C
$\eta_{Pol,pr}, \eta_{Pol,sec}, \eta_{Pol,d}$	0.968, 0.9821, 0.8845
$\dot{m}_p, \dot{m}_s, \omega$	0.33 kg/s, 0.13 kg/s, 0.4
Geometry	Fig. 4-4

4.7.1 Thermodynamic Model

A 1D thermodynamic model has been developed based on the approach presented by Haghparast et al. [104] and Khennich et al.[39]. This model is applicable to design a single-phase ejector in double-choking regime using the polytropic efficiency concept that was first proposed for ejectors evaluation by Galanis and Sorin [36]. This model is programmed in EES (Engineering Equation Solver), which includes relations for the fluid properties [63]. The main procedure is the same as in the precedent model, however, some changes have been carried out:

- All ejector dimensions are considered as inputs of the model. In fact, the approach in terms of required inputs and outputs is reversed in comparison with the previous model.
- Some important thermodynamic parameters such as P_1, P_6 and PR are deemed key outputs.
- Component polytropic efficiencies for the base case are calculated using the CFD model results. The polytropic efficiencies are used extensively in the design and analysis of compressors and turbines, but has only recently been applied to the study of ejectors. Polytropic efficiencies access more precisely the effects of the pressure ratio variation on the irreversibilities of the acceleration and deceleration processes. The polytropic efficiency is defined as the isentropic efficiency of an elemental process [104].
- The entrained secondary flow is choked at a hypothetical throat somewhere in the constant area duct, which requires the area of this section to be calculated accurately. The exact position of the hypothetical throat depends on the geometrical design, which is mainly affected by the distance between the nozzle exit and the entrance of the constant area duct [65].

4.7.2 Effects of the ejector dimensions on the ejector performance

The effects of ejector dimensions on its working characteristics, particularly the pressure ratio (PR), are analyzed. By considering the optimum input parameters, the results from the 1D model for different geometries are calculated. In each case, one of the dimensions is changed while others are fixed. Table 4.11 and 4.12 illustrate these effects on the baseline ejector

performance. It should be noted that the ejector works in the double-choking regime for all the assessed cases.

The results reveal that the pressure ratio (PR) and consequently the ejector performance are significantly affected by changing ejector dimensions due to variations in the internal exergy losses related to different parts of the ejector.

Increasing the nozzle exit diameter (D_{7p}) and the diffuser exit diameter (D_1) lead to improving the pressure ratio and the ejector performance. Results show that the primary nozzle diameter (D_{7p}) is the most influential geometrical parameter affecting the pressure ratio and the ejector performance. By increasing the value of D_{7p} from 18 to 23 mm (about 21%), the overall ejector efficiency, the ejector exergy efficiency and pressure ratio are increased by 67%, 29% and 37% respectively.

By decreasing the primary throat diameter (D_{th}), the value of the pressure ratio (PR) significantly increases and consequently the ejector performance raises. Decreasing the constant area duct length and diameter (L_4 and D_8) lead to improving the ejector performance and pressure ratio, since exergy losses related to the oblique shock waves in this part are reduced.

Increasing the mixing section diameter (D_8) will result in a greater flow area for the secondary stream in the hypothetical throat section. Since the entrainment ratio and compression work available from the primary flow are constant, increasing D_8 beyond certain point has a negative result as the ejector is no longer capable of compressing to higher discharge pressures.

The constant area section length (L_4) has a very small impact on the pressure ratio. However, it can be concluded that smaller mixers cause a higher exergy and energy efficiency because of the reduction of effects of wall friction and train shock waves. In addition, it has been previously shown that the constant area duct length, in general, has no influence on the entrainment ratio [42].

Table 4.11 Effects of the ejector dimensions on the pressure ratio at the fixed entrainment ratio for the optimum operating condition.

	D_{th} [mm]			D_{7p} [mm]		
	12	**14.42***	**19**	**18**	**20**	**23**
PR	2.392	2.146	1.682	1.35	1.878	2.147
η_{eje}	0.3759	0.327	0.1889	0.1073	0.2425	0.328
ΔE_{eje}	3.2	3.69	5.256	5.89	4.629	3.68
η_{exe}	0.6738	0.6321	0.4858	0.4512	0.5416	0.6323
η_{mix}	0.9764	0.9795	0.9797	0.7221	0.8932	0.9796
ω	0.4009	0.4009	0.4009	0.4009	0.4009	0.4009
	$D_{u\,d,\,8}$ [mm]			D_1 [mm]		
	28	**29**	**30**	**30**	**35**	**45**
PR	2.204	2.188	2.097	1.961	2.104	2.193
η_{eje}	0.3257	0.3177	0.293	0.2631	0.3121	0.3442
ΔE_{eje}	3.524	3.949	4.479	4.545	3.877	3.485
η_{exe}	0.6524	0.5991	0.5336	0.5469	0.6134	0.6526
η_{mix}	0.985	0.972	0.9562	0.9795	0.9795	0.9795
ω	0.4009	0.4009	0.4009	0.4009	0.4009	0.4009
	D_7 [mm]			L_4 [mm]		
	30.2	**43.8**	**56.9**	**40**	**110**	**150**
PR	2.013	2.387	2.905	2.162	2.136	2.119
η_{eje}	0.2801	0.3646	0.4215	0.3328	0.3233	0.3172
ΔE_{eje}	3.978	3.558	3.431	3.629	3.73	3.796
η_{exe}	0.6045	0.6337	0.6423	0.6382	0.6281	0.6216
η_{mix}	0.9851	0.964	0.8308	0.9854	0.9756	0.9694
ω	0.4009	0.4009	0.4009	0.4009	0.4009	0.4009

* 1D model results for the base case (the maximum ejector pressure ratio at the critical condenser temperature (T_c^*=24°C) that is the best experimental performance of the ejector)

Table 4.12 A summary of the relationship between ejector dimensions and the ejector working characteristics

Parameter [mm]	**PR** [-]	η_{eje} [%]	ΔE_{mix} [kW]	η_{exe} [%]	η_{mix} [%]
D_{th} (↑)	↓	↓	↑	↓	↓
D_{7p} (↑)	↑	↑	↓	↑	↑
D_8 (↑)	↓	↓	↑	↓	↓
D_1 (↑)	↑	↑	↓	↑	**C**
D_7 (↑)	↑	↑	↓	↑	↓
L_4 (↑)	↓	↓	↑	↓	↓

Increase (↑), Decrease (↓), Constant (C)

4.8 Conclusions

This paper studies the relationship between the ejector refrigeration cycle performance and the working characteristics of the ejector including pressure ratio, overall ejector efficiency, component efficiencies, entrainment ratio, ejector exergy efficiency and internal irreversibilities in each part (nozzle, mixing zone and diffuser) as well as ejector geometry. It aims to get a better understanding of the effects of the external and internal parameters on the ejector behavior in order to improve ejector design and cycle performance. The following conclusions can be extracted:

- The best performance of the refrigeration cycle using R245fa refrigerant is achieved at the maximum pressure ratio (PR) for the critical condenser temperature point (T_c^*), these conditions correspond to the minimum of the internal exergy losses generated in the ejector.
- The primary nozzle diameter (D_{7p}) is the geometrical parameter with the greatest effect on the pressure ratio and ejector performance. By increasing the value of the D_{7p} from 18 to 23 mm (about 21%), the overall ejector efficiency is increased by about 67%.
- Results show that the pressure ratio and the ejector performance enhance when decreasing the constant area duct diameter and length (D_8 and L_4) due to lesser exergy losses related to the oblique shock waves in this part.
- A higher generator temperature and primary mass flow rate always leads to a decrease in ejector component efficiencies. In addition, the results show that most of the exergy losses inside the ejector are located in three regions, namely: the constant area mixing section (m-8), the mixing chamber (7-m) and the primary nozzle (th-7p).
- the system COP and ω increase with an increase in generator temperature T_g and evaporator temperature T_e, but decrease with increasing condenser temperature T_c and $\dot{m}_{pr}$.
- The evaporator temperature is the operating parameter with the greatest impact on system COP, PR and ω.
- An increase in T_g and $\dot{m}_{pr}$ leads to a rise in all exergy losses inside the ejector and consequently in the total exergy losses, ΔE_{eje}.
- A rise in the generator temperature and the primary mass flow rate always leads to a reduced ejector component efficiencies.

4.9 Acknowledgements

The authors wish to thank Hydro-Québec laboratory in Shawinigan for their valuable contribution during this research study. This project is a part of the Collaborative Research and Development (CRD) Grants Program at 'Université de Sherbrooke'. The authors also acknowledge the support of the Natural Sciences and Engineering Research Council of Canada, Rio Tinto Alcan and CanmetENERGY Research Center of Natural Resources Canada.

CHAPTER 5 : Effect of assumptions of normal shock location on the design of supersonic ejectors for refrigeration

AVANT-PROPOS

Auteurs et affiliation:

- Payam Haghparast: étudiant au doctorat, Université de Sherbrooke, Faculté de génie, Département de génie mécanique.
- Mikhail Sorin: professeur, Université de Sherbrooke, Faculté de génie, Département de génie mécanique.
- Hakim Nesreddine: Institut de recherche d'Hydro-Québec (IREQ), 600 Rue de la montagne, Shawinigan, QC, G9N 7N5, Canada

Date d'acceptation: 20 March 2018

État de l'acceptation: version finale publiée.

Revue: Mechanical and Mechatronics Engineering

Référence: [105]

Titre français: Effet des hypothèses de localisation d'un choc normal sur la conception des éjecteurs supersoniques pour la réfrigération

Contribution au document: Cet article contribue à la thèse en comparant les hypothèses de choc normales pour trouver la meilleure solution pour une modélisation thermodynamique plus précise. Les résultats aident à mieux concevoir les éjecteurs supersoniques pour différentes applications.

This article contributes the thesis by comparison of normal shock assumptions to find out the best one for a more accurate thermodynamic modeling. The results help to better design of supersonic ejectors for different applications.

Résumé français:

Le phénomène complexe de choc oblique peut simplement découler d'un choc normal au niveau de la section à surface constante pour simuler une forte augmentation de la pression et une diminution de la vitesse dans les modèles thermodynamiques 1-D. L'emplacement présumé des chocs normaux est l'une des plus grandes sources d'erreur dans les modèles thermodynamiques des éjecteurs. La plupart des chercheurs considèrent un endroit arbitraire sans le justifier. Notre étude compare l'effet de la place d'un choc normal sur les dimensions de l'éjecteur dans les modèles 1D. Dans ce but, deux bancs d'essai expérimentaux d'éjecteurs différents, un éjecteur à mélange de surface constant (CAM) et un mélangeur à pression

constante (CPM), sont envisagés, avec des géométries, des conditions de fonctionnement et des fluides de travail différents (R245fa, R141b). Lors de la première étape, afin d'évaluer la valeur réelle de l'efficacité des différentes parties de l'éjecteur et de la contre-pression critique, un modèle CFD a été construit et validé par des données expérimentales pour deux types d'éjecteurs. Ces données de référence sont ensuite utilisées comme entrée dans le modèle 1D pour calculer les longueurs et les diamètres des éjecteurs. Ensuite, la géométrie de sortie de conception calculée par le modèle 1D est comparée directement à la géométrie expérimentale correspondante. Il a été constaté qu'il existe une bonne concordance entre, d'une part les dimensions de l'éjecteur obtenues par le modèle 1D, à la fois pour le CAM et le CPM, et, d'autre part, les données expérimentales sur l'éjecteur. De plus, il a été démontré que l'emplacement normal du choc n'affecte que la longueur de la zone, car il est prouvé que l'hypothèse de choc normal à l'entrée donne une longueur plus précise. En prenant en compte les modèles 1D précédents, les résultats suggèrent l'utilisation de l'emplacement supposé de choc normal à l'entrée du conduit à zone constante pour concevoir les éjecteurs supersoniques.

5.1 Abstract

The complex oblique shock phenomenon can be simply assumed as a normal shock at the constant area section to simulate a sharp pressure increase and velocity decrease in 1-D thermodynamic models. The assumed normal shock location is one of the greatest sources of error in ejector thermodynamic models. Most researchers consider an arbitrary location without justifying it. Our study compares the effect of normal shock place on ejector dimensions in 1-D models. To this aim, two different ejector experimental test benches, a constant area-mixing ejector (CAM) and a constant pressure-mixing (CPM) are considered, with different known geometries, operating conditions and working fluids (R245fa, R141b). In the first step, in order to evaluate the real value of the efficiencies in the different ejector parts and critical back pressure, a CFD model was built and validated by experimental data for two types of ejectors. These reference data are then used as input to the 1D model to calculate the lengths and the diameters of the ejectors. Afterwards, the design output geometry calculated by the 1D model is compared directly with the corresponding experimental geometry. It was found that there is a good agreement between the ejector dimensions obtained by the 1D model, for both CAM and CPM, with experimental ejector data. Furthermore, it is shown that normal shock place affects only the constant area length as it is proven that the inlet normal shock assumption results in more accurate length. Taking into account previous 1D models, the results suggest the use of the assumed normal shock location at the inlet of the constant area duct to design the supersonic ejectors.

Keywords : *1D model, constant area-mixing, constant pressure-mixing, normal shock location, ejector dimensions.*

Nomenclature

A	Cross section area, mm^2
D	Diameter, mm
h	Specific enthalpy, $kJ.kg^{-1}$
L	Length, m
$\dot{m}$	Mass flow rate, $kg.s^{-1}$
M	Mach number
p	Pressure, kPa
PR	Pressure ratio (pressure lift)
s	Specific entropy, $kJ.kg^{-1}\ K^{-1}$
T	Temperature, K
u	Velocity, $m.s^{-1}$
v	Specific volume, $m^3.kg^{-1}$
X	Position of nozzle exit, mm

Greek symbols

η	Efficiency
φ	Half-angle, deg
ω	Entrainment ratio = $\dot{m}_s.\dot{m}_p^{-1}$ (-)
ρ	Density, $kg.m^{-3}$

Subscripts

d	Downstream of shock
diff	Diffuser
e	Exit
ejec	Ejector
is	Isentropic
mix	Mixing
out	Outlet
pol	Polytropic
pr	Primary nozzle
sec	Secondary nozzle
Th	Thermodynamic
th	Ejector's throat
tot	Total
u	Upstream of shock

Acronyms

CAM	Constant area mixing
CPM	Constant pressure mixing
NI	Normal shock at the inlet of the constant area duct
NO	Normal shock at the outlet of the constant area duct

5.2 Introduction

An ejector is an apparatus which creates vacuum by accelerating a gas, vapour or liquid in a nozzle. It can therefore be used to entrain a secondary or suction fluid. Ejectors are widely used in refrigeration systems. Ejector refrigeration systems usually have low maintenance cost because they operate without a compressor. Fig. 5-2 illustrates a typical ejector construction including ejector geometry, parts and main cross-sections. Convergent–divergent nozzle, suction chamber attached to a constant area duct and diffuser are the most important parts of an ejector. Many theoretical and experimental studies have been carried out to enhance the performance of ejectors in recent years. Among these studies, the effect of the lengths and diameters on the ejector performance and the selection of an appropriate refrigerant proportional to the ejector application are considerably investigated.

Some researchers have investigated the effect of ejector geometry on its performance, such as nozzle exit location, mixing chamber/nozzle area ratio, and nozzle design. Cizungu et al. [26] optimized the ejector geometry to achieve maximum values for either the entrainment ratio or the pressure ratio. Vereda et al. [50] and Elbel and Hrnjak [27] experimentally studied different ejector dimensions, such as the sizing of the motive nozzle and the diffuser.

Banasiak et al. [25] examined different ejector configurations in order to achieve optimum ejector geometry. They used various lengths and diameters of the mixing duct and various angles of divergence for the diffuser. Nakagawa et al. [28] experimentally analyzed the effect of the mixing length on ejector system performance. Chen et al. [6] and Gil and Kasperski [24] studied the effect of different refrigerants on the ejector efficiency in the refrigeration systems. A Review of recent developments in advanced ejector technology can be found in [29].

Researchers always make assumptions for theoretical analyses of the ejectors. One of the most important assumptions in 1-D thermodynamic models is to consider a normal shock in constant area duct to justify the complex oblique shock phenomenon. The Mach number of the working fluid is larger than 1 before this shock, whereas smaller than 1 after the shock. This process is irreversible and cannot be treated as isentropic. [106]

Referring to the assumptions proposed by different researchers, three different places of the constant area duct have been usually considered. Some researchers consider a normal shock at the end of the constant area section for thermodynamic modeling, without justification [10, 11, 12]. Some researchers assume a place at the inlet of the constant area section [39]. Some consider a place

inside the constant area section [106]. Therefore, determination of the appropriate place of the normal shock can help in achieving a more accurate simulation.

The objective of the present study is to develop a more accurate 1D model to design the supersonic ejectors. The effects of the normal shock assumption on the ejector dimensions and mixing efficiency are evaluated. All ejector geometries are calculated by a developed thermodynamic model. This model is applicable for both types of the ejectors, CPM and CAM. The obtained dimensions by 1D model based on different normal shock location are compared to experimental data in order to determine more accurate assumption.

5.3 Ejector analysis procedure

Fig. 5-1 shows the analysis procedure used in the present research to determine the more accurate assumption of the normal shock location. Depending on where the normal shock takes place, at the inlet or outlet of the constant area duct, the geometries and properties are calculated and compared with experimental data. To determine dimensions by 1D models, it is first necessary to extract some important data from CFD and experimental models. The critical back pressure, efficiencies and boundary conditions are the most important data obtained from corresponding models.

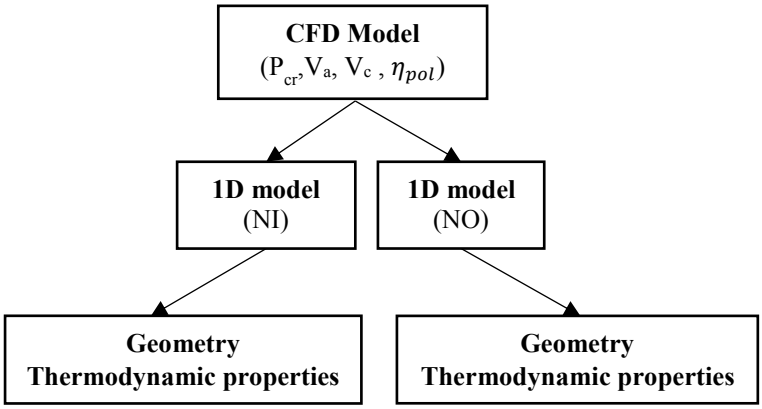

Figure 5.1 Procedure for the optimization of calculating ejector parameters based on normal shock assumptions

5.4 Ejector operation and geometry

Fig. 5-2 illustrates the geometry, parts and main cross-sections of ejectors under investigation. Two different types of the ejector test benches according to the position of the nozzle exit are considered, constant-area mixing (CAM) and constant-pressure mixing (CPM). For case 1 (CAM), available experimental ejector data were used from the Hydro-Québec laboratory in Shawinigan. For case 2 (CAM), the experimental data of Huang et al. [40] were used.

As shown in fig. 5-2, the ejector design can be classified into two categories according to the position of the nozzle. For the nozzle with its exit located within the constant-area section of an ejector, the mixing of the primary and the entrained flows occurs inside the constant-area section and the ejector is known as “constant-area mixing ejector”. For the nozzle with its exit located within the suction chamber which is in front of the constant-area section, the ejector is referred as “constant-pressure mixing ejector”. For this kind of ejector, it was assumed that the mixing of the primary and the entrained streams occurs in the suction chamber with a uniform or constant pressure [40] . It is known that the constant-pressure ejector has a better performance than the constant-area ejector and is thus widely used [15, 16].

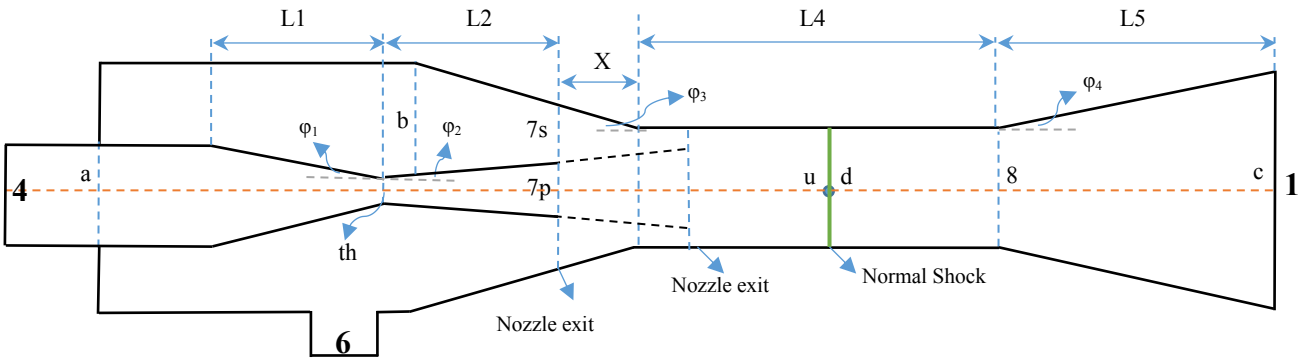

Figure 5.2 Ejector geometry, parts and main cross-sections

Operating conditions, as well as the geometry of the ejectors, are illustrated in tables 5.1 and 5.2. Further, a flowchart of the main inputs and outputs of the models are introduced in Fig. 5-3.

Table 5.1 Operating condition

Parameter	Case# 1 (CAM)	Case# 2 (CPM)
Working fluid	R245fa, **Real Fluid**	R141b, **Real Fluid**
P4, T4 (Primary Inlet)	480.6 kPa, 352.45 K	604 kPa, 368.15 K
P6, T6 (Secondary Inlet)	100.1 kPa, 303.75 K	40 kPa, 283.45 K

Table 5.2 Geometry of the ejectors (Case# 1 & 2)

D [mm]	**Case# 1**	**Case# 2**	**L, X [mm]**	**Case# 1**	**Case# 2**	**φ [deg]**	**Case# 1**	**Case# 2**
Da	32.08	8.251	L_1	100.9	15.4	φ_1	5	10
D_{th}	14.42	2.810	L_2	46	35.4	φ_2	5	3
D_{7p}	22.47	6.518	X	7.08	4.2	φ_3	6.99	5
D_7	28.47	9.527	L_4	223.77	146.0	φ_4	5.98	4
D_8= D_u=D_d	28.47	8.794	L_5	46	121.6	φ_5	22.96	
Dc	38.10	25.803	L_{tot}	416.67	322.6			

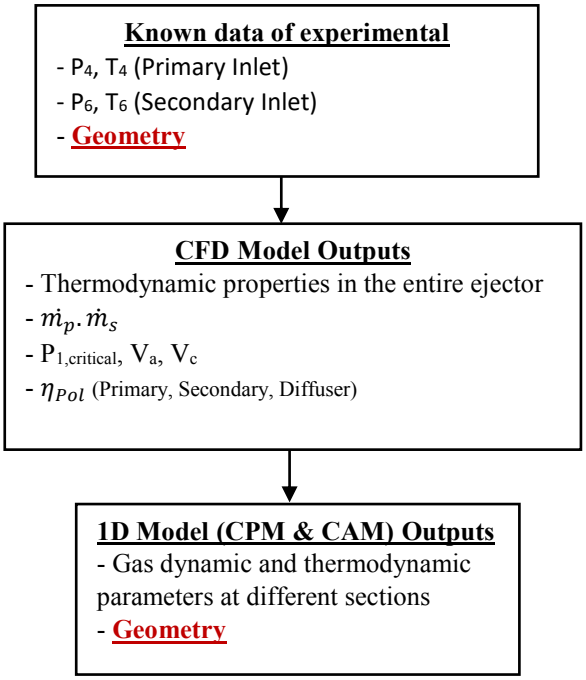

Figure 5.3 Overall procedure for calculating the inputs and outputs

5.5 CFD model

Numerical simulations have been carried out to determine some important values such as critical back pressure (point c) and polytropic efficiencies, velocity value at section a and c (V_a and V_c) for two test benches. The numerical value of the calculated dimensions by 1D models are extremely dependent on these CFD reference values.

- CFD Setting

A numerical investigation has been carried out by means of ANSYS Workbench V17 for mesh generation and ANSYS Fluent V17 to solve the governing equations by control volume method. Based on successful implementations reported in the literature [59], turbulence effects in the ejector have been modeled using the k-ω SST turbulence model. Second order accurate discretization scheme coupled with a pressure-based implicit solver is used. The energy equation is solved in a second step and density is computed through the REFPROP v 9.1 database equation [110]. The conservation equations governing the fluid flow in the ejector are of the compressible, steady state, axisymmetric form and all the walls are assumed adiabatic. In conclusion, the main features of the numerical scheme can be summarized in table 5.3:

Table 5.3 CFD Settings (Case# 1 & 2)

Working fluid	R245fa, Real fluid (Case# 1) R141b, Real fluid (Case# 2)
Turbulence Model	k-w SST(HRN)
Solver Numerical schemes	Pressure based Coupled, Pressure: PRESTO! Momentum, Turbulence, Energy: 2nd order Upwind
Convergence criteria	Residuals RMS<1×10^{-5} Mass imbalances<1%

- Details of the mesh grid used in the CFD calculations

Before proceeding the main calculation, a grid convergence study was performed to ensure overall mesh-independent results. Finally, 5.66×105 quadrilateral cells for Case# 1 and 6.81×105 quadrilateral cells for Case# 2 was considered sufficient to give satisfactory results in terms of entrainment ratio (Fig. 5-4 & 5-5). This mesh is refined from the primary nozzle lips along the shear layer and also close to walls in order to achieve an average value for the wall coordinate (y+), adequate for the application of a High-Reynolds approach [61].

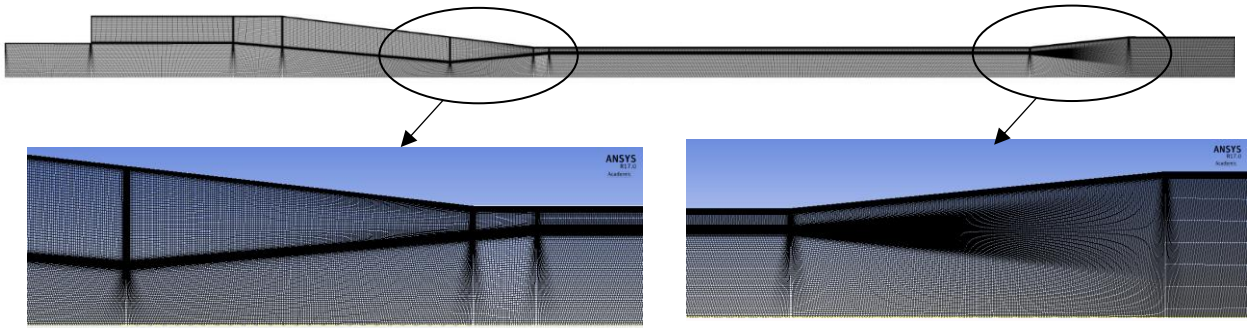

Figure 5.4 Details of the mesh grid used in the CFD calculations for Case# 1 (CAM)

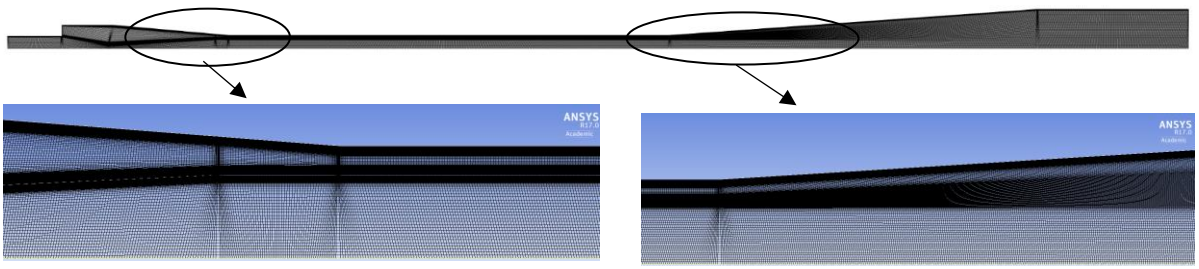

Figure 5.5 Details of the mesh grid used in the CFD calculations for Case# 2 (CPM)

- Mach contours of various back pressures

After accelerating the secondary stream to sonic velocity and mixes with the primary stream in the constant area duct, the region of supersonic flow is terminated by a normal shock wave further down the duct or in the diffuser. Across the shock, pressure increases but Mach number (velocity) reduces to a subsonic value. The mixture of primary and secondary flows then passes through the subsonic diffuser where it converts kinetic energy into pressure energy by a recompression process to reach the back-pressure (condenser pressure) at near zero velocity. Fig. 5- 6 shows Mach number contour plots of the different flow fields along the ejector and into the constant area duct.

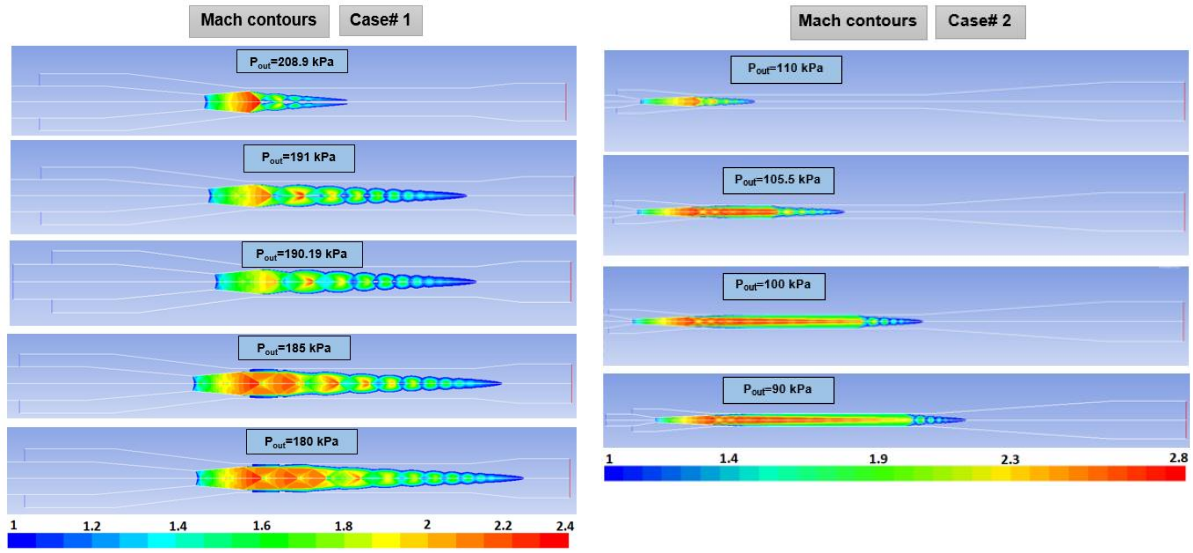

Figure 5.6 Mach number plots of the ejectors at various back pressures for case# 1 and case# 2

According to the performance curves of the ejectors, the critical back pressure for case 1 is equal to 190.19 kPa and for case 2 is equal to 105.5 kPa. Table 5.4 present the calculated efficiencies for critical back pressures at fixed inlet conditions for two cases by CFD models.

Table 5.4 Efficiencies according to the CFD models for critical back pressure point for case 1 and 2.

	P_{out} (KPa)	PR	Polytropic (CFD)			Mixing (CFD)
	P1	**P1/P6**	**Primary**	**Secondary**	**Diffuser**	**Mixing**
Case 1	**190.19**	1.9	0.9757	0.9752	0.8211	0.9681
Case 2	**105.5**	2.644	0.9373	0.9352	0.9436	0.9137

5.6 Thermodynamic model

Among the different models, the model proposed by Galanis and Sorin [36] is able to calculate all ejector dimensions and fluid properties. In this study, a new model is developed which has the ability to simulate both types of ejectors, CPM and CAM for two assumed normal shock locations. A thermodynamic model is programmed in EES (Engineering Equation Solver)

which includes relations for the fluid properties [63]. To simplify the analysis, some assumptions are considered [39]. Flow is one dimensional, compressible and steady state throughout the ejector. The primary and secondary fluids are identical vapors, with real fluid properties. Pressure, temperature and mass flow are known from experimental data for both the primary and secondary inlets. All fluid properties are uniform across their respective cross-sectional areas. Both primary and secondary fluids are choked (critical operation). The details of the calculation procedure for the constant pressure mixing type of ejector by using the conception of polytropic efficiency are described in the following steps. In each step, inputs, outputs and appropriate equations are introduced.

The calculation begins with the expansion and subsonic acceleration of the secondary fluid from the given stagnation conditions P_6 and T_6, taking into consideration the known flow rate $\dot{m}_s$. Finally, it finishes with deceleration of mixing stream at diffuser. The governing equations account for the conservation of the mass, momentum, and energy are presented below.

- Cross-section 7s: To calculate conditions at Cross-section (7s), energy and mass conservation are solved by progressively decreasing the pressure (P) to maximize ($\dot{m}_s$/A). This procedure is repeated until the ratio ($\dot{m}_s$/A) reaches a maximum value. Since the flowrate $\dot{m}_s$ is known it is then possible to calculate the area A_{7s}. (Critical operation)

$$P_j = P_{j-1} - \Delta P_s \quad (5.1)$$

$$\eta_{pol,s} = (h_{j-1} - h_j)/(h_{j-1} - h_{j,is}) \quad (5.2)$$

$$h_{j.is} = h(P_j, s_{j-1}) \quad (5.3)$$

$$h_6 = h_j + 0.5V_j^2 \quad (5.4)$$

$$\dot{m}_s/A_j = V_j/\nu_j \quad (5.5)$$

$$\nu_j = \nu(P_j, h_j) \quad \text{and} \quad s_j = s(P_j, h_j) \quad (5.6)$$

- Cross-section b: By using V_b obtained from CFD, it is possible to determine the gas dynamic and thermodynamic parameters at cross-section (b) as well as the area A_b.

- Cross-section throat: The primary flow is always choked. The same procedure is applied to the expansion of the primary stream in the converging-diverging nozzle and generates the conditions at its throat (th). Since the flowrate $\dot{m}_p$ is fixed the area A_{th} and its diameter D_{th} are both calculated.

- Cross-section 7p: Since $P_{7p} = P_{7s}$ it is possible to continue the procedure in order to determine the conditions of the primary stream at state (7p) and to calculate the area A_{7p} from mass conservation as well as the corresponding diameter D_{7p}. From $A_7 = A_{7p} + A_{7s}$ it is then possible

to calculate the diameter D_7. The isentropic efficiency of the primary stream expansion from (4) to (7p) can then also be determined.

- Cross-section a: To calculate the gas dynamic and thermodynamic parameters at Cross-section (a) as well as the area (A_a), the V_a obtained from CFD is used.

- Cross-section u (before normal shock**):** By applying the equations expressing mass, energy and momentum conservation for the control volume between cross-sections (7) and (u), immediately upstream of the shock.

$$\dot{m}_p + \dot{m}_s = V_u A_u / \upsilon_u \tag{5.7}$$

$$h_4 + \omega h_6 = (1+\omega)(h_u + 0.5V_u^2) \tag{5.8}$$

$$\left(P_{7p}A_{7p} + \dot{m}_p V_{7p}\right) + \left(P_{7s}A_{7s} + \dot{m}_s V_{7s}\right) - F_f = P_u A_u + \left(\dot{m}_p + \dot{m}_s\right)V_u \tag{5.9}$$

By simplifying Eq. 9, we have:

$$V_{7p} + \omega V_{7s} = (1+\omega)V_u \tag{5.10}$$

- Cross-section d (after normal shock**):** Since $A_u = A_d$, with the expressions of mass, energy and momentum conservation.

$$\dot{m}_p + \dot{m}_s = V_d A_d / \upsilon_d \tag{5.11}$$

$$h_4 + \omega h_6 = (1+\omega)(h_d + 0.5V_d^2) \tag{5.12}$$

$$(P_d + P_u) = (\dot{m}_p + \dot{m}_s)(V_u - V_d) \tag{5.13}$$

- Cross-section 8 (inlet of the diffuser**):** By using the known back pressure value and expressing mass, energy and momentum conservation for the control volume between cross-sections (8) and (1), the ejector outlet, we have equations 14 to 19. This procedure is repeated until A_j becomes equal to $A_d = A_u$. The corresponding enthalpy, pressure, entropy, and velocity are those of the mixture at cross-section (8). Mixing efficiency also can be calculated using the equations 20.

$$\mathrm{h_j} = \mathrm{h_{j-1}} - \Delta\mathrm{h} \tag{5.14}$$

$$\mathrm{h_{(j-1),is}} = \mathrm{h_j} + (\Delta\mathrm{h}\eta_{\mathrm{pol,D}}) \tag{5.15}$$

$$\mathrm{s_j} = \mathrm{s_{(j-1),is}} = s(\mathrm{p_{j-1}}, \mathrm{h_{(j-1),is}}) \tag{5.16}$$

$$\mathrm{P_j} = P\left(\mathrm{h_j}, \mathrm{s_j}\right) \; and \; \nu_\mathrm{j} = \nu\left(\mathrm{P_j}, \mathrm{h_j}\right) \tag{5.17}$$

$$h_4 + \omega h_6 = (1+\omega)(h_j + 0.5V_j^2) \tag{5.18}$$

$$\mathrm{A_j} = (\dot{m}_p + \dot{m}_s)(\nu_\mathrm{j}/\mathrm{V_j}) \tag{5.19}$$

$$\eta_{\mathrm{mix}} = 1 - \frac{F_f}{\dot{m}_p V_{7p} + \dot{m}_s V_{7s}} \tag{5.20}$$

$$F_f = \left(P_{7p}A_{7p} + \dot{m}_p V_{7p}\right) + \left(P_{7s}A_{7s} + \dot{m}_s V_{7s}\right) - P_8 A_8 - \left(\dot{m}_p + \dot{m}_s\right)V_8 \quad (5.21)$$

- Cross-section c (before outlet**):** By using V_c obtained from CFD, it is possible to determine the thermodynamic properties at cross-section (c) as well as the area A_c.

All lengths can be calculated based on correlations 22 to 29.

$$L_1 = (D_a - D_{th})/2tan(\varphi_1) \quad (5.22)$$

$$L_2 = (D_{7p} - D_{th})/2tan(\varphi_2) \quad (5.23)$$

$$L_5 = (D_c - D_8)/2tan(\varphi_4) \quad (5.24)$$

$$P_d A_d + \left(\dot{m}_p + \dot{m}_s\right)V_d - F_f = P_8 A_8 + \left(\dot{m}_p + \dot{m}_s\right)V_8 \quad \text{(NI)}$$
$$P_u A_u + \left(\dot{m}_p + \dot{m}_s\right)V_u + F_f = P_7 A_7 + \left(\dot{m}_p + \dot{m}_s\right)V_7 \quad \text{(NO)} \quad (5.25)$$

$$\Delta P = F_f/\mathrm{A_8} = \mathrm{f\,(L_4/}D_8)(\rho V^2/2) \quad \text{(Darcy equation)}$$
$$\mathrm{L_4} = F_f/(\mathrm{f\,(A_8/}D_8)(\rho V^2/2)) \quad (5.26)$$

$$f = \left(\frac{1}{-2log\left(\frac{e}{3.7\,D} + \frac{2.51}{Re\sqrt{f}}\right)}\right)^2 \quad \text{(Colebrook equation)} \quad (5.27)$$

Absolute wall roughness for commercial new steel (e=0.046 mm) (Re>4000)

Calculation of nozzle exit position is as follows:

$$X = (D_7 - D_u)/2tan(\varphi_5) \quad \text{(CPM)} \quad (5.28)$$

$$X = (D_{7s})/2tan(\varphi_3) \quad \text{(CAM)} \quad (5.29)$$

5.7 Results and discussion

The effect of assuming that the normal shock location is within the constant area duct can be evaluated with the help of Tables 5.5 to 5.8. The conclusion that can be drawn from these results is that the choice of the location of the normal shock only affects the constant area length (L_4) and the flow properties at sections u and d.

The absolute deviation of the L_4 from experimental dimension based on normal shock at the inlet is 3.9% for case 1 while it is 34.94% for normal shock at the outlet (Table 5.5 and 5.6). Similarly, it is observed 6.24 % and 66.84% deviation for case 2 compared to experimental length for inlet and outlet normal shock assumption respectively (Table 5.7 and 5.8).

Table 5.5 Effect of the assumed normal shock location on ejector dimensions for case 1 (CAM) ($P_{out,\ critical}$=190.19 kPa)

D, L, X [mm]	Experimental test bench	Normal Shock (inlet)	Error (%)	Normal Shock (outlet)	Error (%)
D_{th}	14.42	14.3	-0.8321	14.3	-0.8321
D_{7p}	22.47	21.57	-4.0053	21.57	-4.0053
D_7	28.47	27.71	-2.6694	27.71	-2.6694
D_8= D_u=D_d	28.47	27.71	-2.6694	27.71	-2.6694
D_c	38.10	38.16	0.1574	38.16	0.1574
L_1	100.9	99.77	-1.12	99.77	-1.12
L_2	46	41.53	-9.7173	41.53	-9.7173
L_4	223.77	232.5	3.9	145.6	34.94
L_5	46	49.9	8.4783	49.9	8.4783
L_{tot}	416.67	423.7	1.69	336.8	19.17

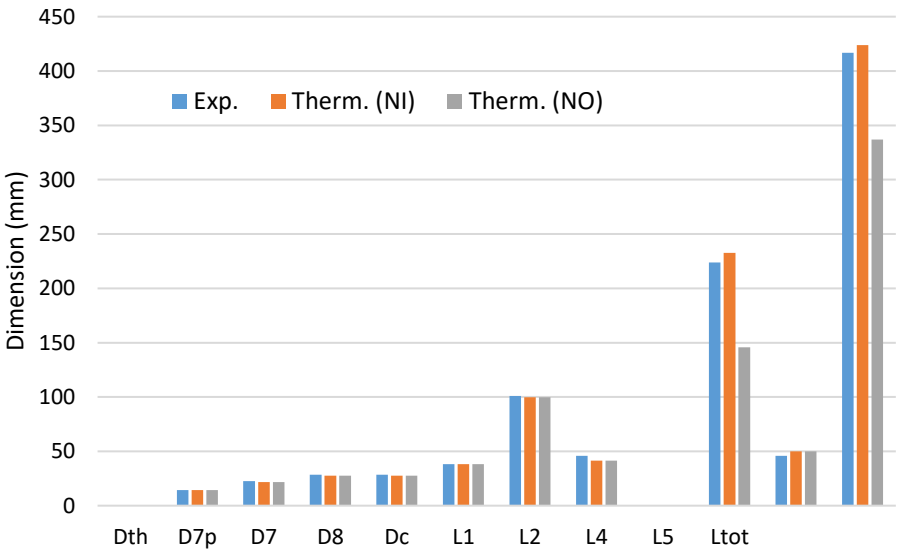

Figure 5.7 Comparisons of dimensions for case 1 (CAM)

Table 5.6 Effect of the assumed normal shock location on flow properties at sections u and d for case 1 (CAM) ($P_{out,\ critical}$=190.19 kPa)

	States	P [kPa]	T [°K]	V [m/s]	M [-]
1D model (NI)	u	54.63	301.37	243.9	1.748
1D model (NI)	d	170.9	332.88	84.15	0.5863
1D model (NO)	u	58.49	305.06	230.5	1.642
1D model (NO)	d	161.4	332.2	89.15	0.6205

Table 5.7 Effect of the assumed normal shock location on ejector dimensions for case 2 (CPM) ($P_{out,\ critical}$=105.05 kPa)

D, L, X [mm]	Experimental test bench	Normal Shock (inlet)	Error (%)	Normal Shock (outlet)	Error (%)
D_{th}	2.810	2.834	0.8541	2.834	0.8541
D_{7p}	6.518	6.577	0.9052	6.577	0.9052
D_7	9.527	9.166	-3.789	9.166	-3.789
D_8	8.794	8.517	-3.15	8.517	-3.15
D_c	25.803	25.76	-0.167	25.76	-0.167
L_1	15.4	14.73	-4.351	14.73	-4.351
L_2	35.4	35.71	0.8757	35.71	0.8757
L_4	146	155.1	6.24	48.42	66.84
L_5	121.6	123.3	1.398	123.3	1.398
L_{tot}	322.6	328.8	1.92	225.9	29.97

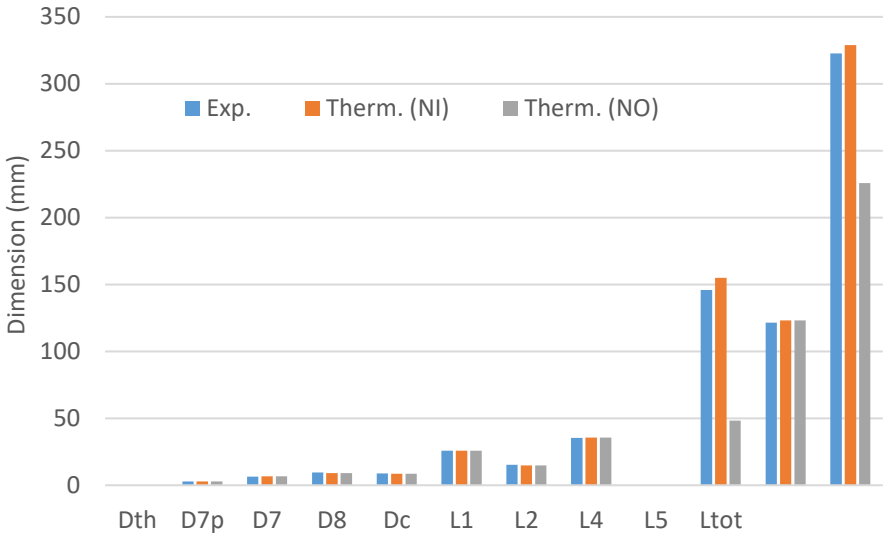

Figure 5.8 Comparisons of dimensions for case 2 (CPM)

Table 5.8 Effect of the assumed normal shock location on flow Properties at sections u and d for case 2 (CPM) ($P_{out,\ critical}$=105.05 kPa)

	States	P [kPa]	T [°K]	V [m/s]	M [-]
1D model (NI)	u	23.36	281.9	302	2.044
1D model (NI)	d	101.7	338.43	81.97	0.5162
1D model (NO)	u	28.19	296.79	263.2	1.739
1D model (NO)	d	88.32	336.81	94.18	0.5928

5.8 Conclusion

In the present study, the effect of the normal shock location on the design of a one-phase supersonic ejector was investigated. CFD technique first was used to evaluate the exact value of the efficiencies, critical back pressure and also more detailed information about the flow, density and temperature distributions in the ejector. Afterwards, data obtained from the CFD simulations were applied in the 1D thermodynamic models to calculate all ejector dimensions. To this aim, two test benches, a constant area-mixing ejector (CAM) and a constant pressure-mixing (CPM) were considered with different geometries, working fluids and operating conditions.

It is shown that the present thermodynamic model is able to calculate precisely all ejector dimensions for both types of the ejectors compared to experimental dimensions over the entire range of operation. It is further found that the effect of normal shock place is only on constant area length (L_4) and flow properties at sections u and d. The value of the L_4 based on normal shock at the inlet is more accurate than normal shock at the outlet against the experimental one. In conclusion, the research findings will be meaningful for researchers to have a better understanding of the normal shock assumption. The results show that when the normal shock

assumed at the inlet of constant area duct, obtained dimensions by the 1D model are more accurate for both types of ejectors (CPM and CAM) Compared to experimental dimensions.

5.9 Acknowledgements

The authors wish to thank Hydro-Québec laboratory Shawinigan for their valuable contribution during the ejector design used in the present paper. This project is a part of the Collaborative Research and Development (CRD) Grants Program at 'Université de Sherbrooke'. The authors also acknowledge the support of the Natural Sciences and Engineering Research Council of Canada, Rio Tinto Alcan and CanmetENERGY Research Center of Natural Resources Canada.

CHAPTER 6 : Analysis and design optimization of an ejector integrated into an organic Rankine cycle

AVANT-PROPOS

Auteurs et affiliation:

- Payam Haghparast: étudiant au doctorat, Université de Sherbrooke, Faculté de génie, Département de génie mécanique.
- Mikhail Sorin: professeur, Université de Sherbrooke, Faculté de génie, Département de génie mécanique.
- Marc A. Richard : Institut de recherche d'Hydro-Québec (IREQ), 600 Rue de la montagne, Shawinigan, QC, G9N 7N5, Canada
- Hakim Nesreddine: Institut de recherche d'Hydro-Québec (IREQ), 600 Rue de la montagne, Shawinigan, QC, G9N 7N5, Canada

Date de soumission: December, 2018

État de l'acceptation: article en cours de préparation.

Revue: Applied thermal engineering

Référence: [-]

Titre français: Optimisation de l'analyse et de la conception d'un éjecteur intégré dans un cycle de Rankine organique

Contribution au document: Cet article contribue à la thèse en améliorant la production d'énergie du système EORC.

Résumé français:

Le cycle organique de Rankine (ORC) est une technologie prometteuse pour convertir la chaleur de basse qualité en énergie électrique. Au cours de cette décennie, l'amélioration de la performance de la CCO attire davantage l'attention. Il a été fait dans de précédentes études d'intégrer un éjecteur dans un cycle organique de Rankine pour augmenter la capacité de production d'énergie. Dans cette étude, l'impact de la géométrie de l'éjecteur et des caractéristiques de fonctionnement sur le cycle de performance, en particulier la capacité de puissance, est étudié. L'éjecteur fonctionne dans le régime de double suffocation. À cette fin, une étude de sensibilité des paramètres est réalisée à l'aide d'indicateurs importants. Les résultats montrent que la puissance de sortie nette augmente avec l'augmentation du rapport de la surface d'éjection ou du débit massique secondaire; il diminue avec l'augmentation du diamètre de la gorge, de la pression d'entrée primaire ou de la température d'entrée primaire. La

zone constante est l'un des paramètres géométriques les plus importants qui influent sur la production d'énergie et les performances du cycle. La capacité de puissance de sortie est indépendante lorsque l'éjecteur fonctionne dans la région à double étranglement. Le document présente et discute également divers paramètres d'énergie et d'exergie.

6.1 Abstract

The organic Rankine cycle (ORC) is a promising technology to convert low-grade heat to electric power. In this decade, the improvement of the ORC performance is attracting more attention. It has been proven in previous studies that integrating an ejector into an organic Rankine cycle increases the power output capacity. In this study, the impact of both ejector geometry and working characteristics on cycle performance, in particular, the power output capacity is investigated. The ejector functions in the double-choking regime. To this aim, a parameter sensibility study is conducted using some important indicators. Results show that the net power output rises with increasing ejector area ratio or secondary mass flow rate; it falls with increasing throat diameter, primary inlet pressure, or primary inlet temperature. The constant area duct diameter is one of the most important geometrical parameters influencing the power generation and the cycle performance. Power output capacity is found to be independent of the ejector outlet parameters when the ejector operates in the double-choking region. The paper also presents and discusses various energy and exergy metrics as a means of evaluating the cycle performance.

Keywords: *Parametric study; Organic Rankine Cycle; Ejector; Thermodynamic modeling; Power generation*

Nomenclature			
AR	Ejector area ratio to (-)	ev	Evaporator
D	Diameter (mm)	exe	Exergy
e	Specific exergy (kJ.kg^{-1})	Ex	Experimental
ER	Entrainment ratio (-)	exp	Expander
h	Specific enthalpy (kJ.kg^{-1})	G	Generator
L	Length (m)	h	heat
ṁ	Mass flow rate (kg.s^{-1})	in	Inlet
P	Pressure (kPa)	is	Isentropic
PR	Pressure Ratio=P_1/P_6 (-)	i	Thermodynamic state
Q	Heat transfer (kW)	mix	Mixing
S	Specific entropy (kJ.kg^{-1} K^{-1})	oc	Environment
T	Temperature (K)	out	Outlet
v	Specific volume (m^3.kg^{-1})	pol	Polytropic
ΔE	Exergy destruction (kW)	pr	Primary nozzle
W	Work (kW)	p	Pump
E	Energy transfer rate (kW)	s	System
Therm	Thermodynamic	sec	Secondary nozzle
Sim	Simulation	th	Ejector's throat
Greek symbols		tot	Total
η	Efficiency (%)	wf	Working fluid
ρ	Density (kg.m^{-3})	4	Primary inlet
θ	half-angle (°)	6	Secondary inlet (Expander back pressure)
Subscripts		8	Constant area duct exit
c	Condenser	1	Inlet of diffuser
com	Components	**Acronyms**	
d	Diffuser	LGHS	Low-grade heat source
eje	Ejector	NXP	Nozzle Exit Position

6.2 Introduction

The interest in low-grade heat recovery has increased significantly over the past decades. A large number of new solutions have been suggested for producing electricity from low-temperature heat sources such as biological waste heat, geothermal heat, solar thermal power, engine exhaust gases, domestic boilers, etc.

Among the proposed solutions, the organic Rankine cycle (ORC) system is the most widely applied. Two main advantages of ORC systems are the simplicity and the availability of its components. In such systems, the working fluid is an organic component, better adapted than water to low heat source temperatures. Unlike traditional power cycles, local and small-scale power generation is made possible by this technology [3].

On the other hand, the low performance of the organic Rankine cycle (ORC) with a low-grade heat source (LGHS) has limited its use in the industry. In order to enhance the power output capacity and performance of the ORC, a new structure known as the organic Rankine cycle combined with ejector (EORC) has been presented and investigated in few papers [111] [16] [112].

Scientific literature covering only the organic Rankine cycles is abundant, unlike the EORC system. The research on ORC is mainly focused on the selection of working fluids, analysis of thermal performance, and cycle optimization [1] [2].

Figure 6.1 (a) and (b) illustrate the principle of the organic Rankine cycle with and without ejector and corresponding T-S diagrams. The vapor from the second-stage evaporator works as the primary fluid for the ejector, inducing the exhaust from the expander into the ejector secondary port. This decreases the expander backpressure and increases the pressure difference through the expander, resulting in an increase in the cycle power output capacity [15].

Ejectors are simple devices in which the energy of a flow is used to entrain and enhance the pressure of a secondary stream by direct mixing. They are used due to their simple operation, low maintenance requirements and the absence of moving parts [52] [113].

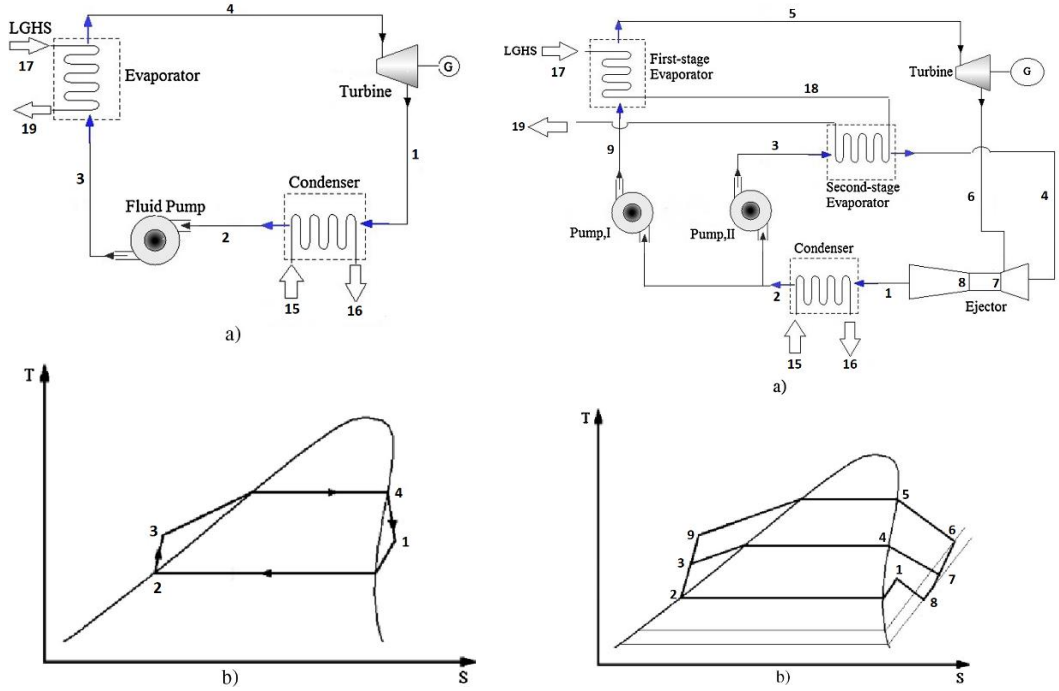

Figure 6.1 (a) the principle of the organic Rankine cycle with and without ejector and (b) corresponding T-s diagrams

Since 1858, ejectors have been intensively studied for a large number of very diverse applications. For example, they have been widely used in different cycles for refrigeration purposes. In recent decades, they are also used in cascade power cycles.

Although many studies on ORCs have been conducted, only a few papers have presented an experimental, numerical or optimization study of an organic Rankine cycle integrated with ejector [111] [16] [112]. It should be mentioned that the number of investigations on the cascade organic Rankine cycles is abundant, unlike EORC system [3].

Li et al. proposed a combined ORC with ejector for the first time in 2012. In this new configuration, an ejector and a second-stage evaporator were added to the ORC [15]. The ejector in the EORC caused the expander outlet pressure to decrease by 0.32 bar compared to the ORC system, which meant that the output power was increased by approximately 35%. Li et al. also proposed a Kalina cycle integrated with ejector. The Kalina cycle and the organic Rankine cycle (ORC) are potentially feasible to recover energy from low-grade heat sources (LGHS) for power generation. The Kalina cycle is similar to an ORC, but uses a mixture of water and ammonia with a variable composition as working fluid. Their results show that the net power output of the Kalina cycle with ejector is higher than that of the Kalina cycle [17].

Kheiri et al. [112] presented four new ORC configurations, each with an ejector integrated into the system. It was found that the power production of the cycles increased, as compared with that of the basic ORC. In addition, they showed that R245fa is the best working fluid among four refrigerants applied.

A supercritical or transcritical Rankine cycle with ejector (ESRC, ETRC) based on the basic supercritical or transcritical Rankine cycle (SRC, TRC) in order to generate electricity from low-grade heat sources is introduced by Li et al. [18]. The authors increased the net power output of the cycle by increasing the pressure difference in the expander. Carbon dioxide was chosen as the working fluid for the cycles. Water was chosen as the fluid for the low-grade heat. Results showed that the net power output of the cycles could be ranked from highest to lowest: ESRC > ETRC > SRC > TRC [18].

In the aforementioned studies, there is no detailed analysis on effects of ejector geometry and working characteristics on the EORC performance. The number of papers dedicated to the analysis of the ORC systems or ejectors separately is considerable. Investigation on the effects of the ejector parameters as well as some cycle operating parameters is important for optimizing the design of an EROC system. In this research, a comprehensive study is carried out in order to enhance the power generation capacity of the EORC. This research paper has some novelty and originality items for EORC systems, as follows:

(1) The performance of the EORC system is evaluated and a thermodynamic model of combined ORC with ejector is developed and validated against available experimental data.
(2) A supersonic ejector that will work in the double-choking regime is designed for an available ORC test bench.
(3) For the EORC, the impact of both ejector geometry and working characteristics is investigated in order to maximize the expander power.

(4) Energy and exergy efficiencies of the EORC are calculated and compared with the expander power trend.

6.3 Thermodynamic modeling and analysis

In this section, a thermodynamic model developed to characterize the performance of the organic Rankine cycle with ejector. The computer code for the thermodynamic performance calculation is written in the EES programming environment, which includes relations for the fluid properties [63]. By considering all equations related to energy and exergy analysis of the EORC system, a global methodology is developed.

In the first step, a thermodynamic model of the ORC system and a 1D model of the ejector are prepared separately, and then validated against available experimental data. Afterwards, the global model is built by interconnecting the ORC and ejector models.

6.3.1 ORC modeling

The steady-state thermodynamic models of the different components of the ORC system are described in this section (2.1): condenser, evaporator, expander, and pump. For evaluation of the ORC system performance, a sufficient number of thermodynamic parameters must be set, such as the inlet temperatures and mass flow rates of the heat source and sink, pressure drop, and the pinch temperature difference.

Neglecting the changes in kinetic and potential energy, as well as the heat losses to the environment, the control volume energy balance for a system component can be expressed as:

$$\dot{Q} - \dot{W} = \sum_{in} \dot{m}_{in} h_{in} - \sum_{out} \dot{m}_{out} h_{out} \tag{6.1}$$

Numerical correlations are used to calculate the heat transfer coefficients in the heat exchangers using a distributed parameter model, based on the model suggested by Wang et al. [114].

The pressure drop in each heat exchanger is the condition of convergence in the calculation of the heat transfer area, and is designated as 30 kPa. In the condenser model, it is assumed that the state of working fluid at the condenser outlet is saturated. The condenser is divided into two different regions: a two-phase condensation region and single-phase superheated region. The evaporator is also divided into three different regions: a single-phase sub-cooled region, a two-phase evaporation region, and a single-phase superheated region.

The heat balance equations in the condenser and evaporator between the hot and cold side are also explained in detail by Wang et al. [114]. The power output of the twin screw expander, cycle net power output, and total input heat are obtained by the following equations:

$$W_{exp,EORC} = \dot{m}_{sec}(h_5 - h_{6,is})\eta_{is,exp} \quad (6.2)$$

$$W_{exp,ORC} = \dot{m}_{wf}(h_4 - h_{1,is})\eta_{is,exp} \quad (6.3)$$

$$W_{net} = W_{exp} - W_p \quad (6.4)$$

$$Q_{tot,EORC} = \dot{m}_{h,source}(h_{17} - h_{19}) \quad (6.5)$$

$$Q_{tot,ORC} = \dot{m}_{h,source}(h_{17} - h_{19}) \quad (6.6)$$

The energy efficiency of an EORC system is usually expressed in terms of the net output power and total input heat:

$$\eta_s = \frac{\text{Net output capacity}}{\text{Total input heat}} = \frac{W_{net}}{Q_{tot}} \quad (6.7)$$

6.3.2 Ejector modeling

The ejector simulation is based on the approach presented by Haghparast et al. [104]. This model is applicable to the design a single-phase ejector in double-choking regime using the polytropic efficiency concept that was first proposed for ejector evaluation by Galanis and Sorin [36]. This method is used for sizing an ejector for available ORC system at Hydro-Quebec. In the global model, the main simulation procedure of the ejector is the same as the precedent model, however, some changes have been carried out:

- Some ejector dimensions (D_{th}, D_{7p}, D_8) are considered as inputs of the model. In fact, the approach in terms of required inputs and outputs is somewhat reversed in comparison with the previous model.
- Some important thermodynamic parameters such as primary mass flow rate, P_6, and PR are deemed key outputs.
- Component polytropic efficiencies for the present case are calculated using the empirical equations presented by Haghparast et al. [104]. Polytropic efficiencies are used extensively in the design and analysis of compressors and turbines but have only recently been applied to the study of ejectors. Polytropic efficiencies access more precisely the effects of the pressure ratio variation on the irreversibilities of the acceleration and deceleration processes. The polytropic efficiency is defined as the isentropic efficiency of an elemental process [39].
- The entrained secondary flow is choked at a hypothetical throat somewhere in the constant area duct, which requires the area of this section to be calculated accurately. The exact position

of the hypothetical throat depends on the geometrical design, which is mainly affected by the distance between the nozzle exit and the entrance of the constant area duct [65]. Fig. 6.2 illustrates the geometry, parts and main cross-sections of the ejector.

In order to evaluate the ejector performance, two important parameters are considered: the entrainment ratio (ER), which is defined as the ratio between the secondary mass flow rate and the primary mass flow rate, and the pressure ratio (PR), which is the ratio of the diffuser outlet pressure to secondary inlet pressure:

$$ER = \frac{\dot{m}_{sec}}{\dot{m}_{pr}} \tag{6.8}$$

$$PR = \frac{P_{out}}{P_{sec}} = \frac{P_1}{P_6} \tag{6.9}$$

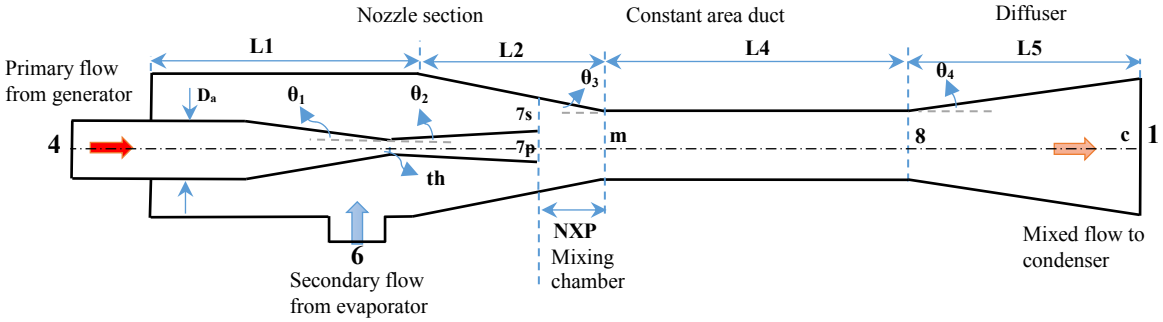

Figure 6.2 Ejector geometry, parts, and main cross-sections

6.3.3 Exergy analysis

Exergy is a measure of energy quality, stating the maximum work that can be extracted from a system only interacting with its environment. It could theoretically be obtained from any state of the system relative to the given environment [16]. The specific exergy (work production capacity per unit mass) of a thermodynamic state "i" is calculated from the following expression:

$$e_i = (h_i - h_{oc}) - T_{oc}(S_i - S_{oc}) \tag{6.10}$$

Moreover, the exergy destroyed in each component of the EORC system is determined by considering all corresponding entering and leaving streams. Therefore, the exergy loss in the heat exchangers is equal to the exergy loss in the working fluid plus the exergy loss in the heat or sink source. The exergy loss in the ejector also calculates with the entropy increase from the inlets to the diffuser in the ejection process by the working fluid.

$$\Delta E_{ev1} = \dot{m}_{sec}(e_9 - e_5) + \dot{m}_{h,source}(e_{17} - e_{18}) \tag{6.11}$$

$$\Delta E_{ev2} = \dot{m}_{pr}(e_3 - e_4) + \dot{m}_{h,source}(e_{18} - e_{19}) \quad (6.12)$$

$$\Delta E_{ev,\mathrm{tot}} = \Delta E_{ev1} + \Delta E_{ev2} \quad (6.13)$$

$$\Delta E_c = (\dot{m}_{pr} + \dot{m}_{sec})(e_1 - e_2) + \dot{m}_{h,sink}(e_{15} - e_{16}) \quad (6.14)$$

$$\Delta E_{exp} = \dot{m}_{sec}(e_5 - e_6) - W_{exp} \quad (6.15)$$

$$\Delta E_p = \dot{m}_{sec}(e_2 - e_9) + \dot{m}_{pr}(e_2 - e_3) + W_p \quad (6.16)$$

$$\Delta E_{eje} = \Big(\dot{m}_{sec}(e_6) + \dot{m}_{pr}(e_4)\Big) - \Big((\dot{m}_{pr} + \dot{m}_{sec})(e_1)\Big) \quad (6.17)$$

Exergy efficiency provides a deeper understanding of performance than energy efficiency, and it is a significant indicator for system level analysis [115]. System efficiency is not able to quantify the energy quality. Therefore, it is necessary to consider exergy efficiency. The exergy efficiency of the EORC system is the ratio of outlet exergy to total available exergy [16] [116]. It should be noted that the exergy of the heat source fluid leaving the system (state 19 in fig. 6.1) is considered as a loss.

$$\eta_{exe} = \frac{E_{h,source,in} - \Delta E_{tot,com} - E_{h,source,out}}{E_{h,source,in} + W_p} \quad (6.18)$$

$$E_{h,source,in} = \dot{m}_{h,source}(e_{17}) = \dot{m}_{h,source}\big((h_{17} - h_{oc}) - T_{\mathrm{oc}}(S_{17} - S_{\mathrm{oc}})\big) \quad (6.19)$$

$$E_{h,source,out} = \dot{m}_{h,source}(e_{19}) = \dot{m}_{h,source}\big((h_{19} - h_{oc}) - T_{\mathrm{oc}}(S_{19} - S_{\mathrm{oc}})\big) \quad (6.20)$$

$$\Delta E_{tot,com} = \Delta E_{ev} + \Delta E_c + \Delta E_{exp} + \Delta E_{eje} + \Delta E_p \quad (6.21)$$

$$\Delta E_{tot} = \Delta E_{ev} + \Delta E_c + \Delta E_{exp} + \Delta E_{eje} + \Delta E_p + E_{h,source,out} \quad (6.22)$$

6.4 Validation of thermodynamic models

For validation of the ORC system and the ejector thermodynamic model, two different test benches located at Hydro-Québec laboratory Shawinigan are considered. Available experimental data from a small-scale beta-prototype 50 kW ORC machine and an ejector refrigeration test bench are used. In both cases, the working fluid is refrigerant R245fa.

6.4.1 Validation of the ORC model

In order to validate the ORC thermodynamic model, a comparison between the results obtained from the thermodynamic model and the experimental data is carried out. Table 6.1 compares four different cases, where the thermodynamic results are noted as “Sim.”, and the experimental results from Minea et al. [13] are noted as “Ex.” The small-scale beta prototype 50 kW ORC system converts low-grade waste heat, with an inlet temperature ranging between 85 ºC and

116 ºC, into electricity. The cooling fluid temperature varies from 15 ºC to 30 ºC. The prototype includes a single-stage twin-screw expander, a stainless steel condenser, a pre-heater/evaporator heat exchanger assembly, a liquid receiver, and a working fluid variable speed circulation pump. The machine is connected to a 700 kW electrical boiler that simulates the waste heat source, to an air-cooled liquid cooler, and to the Hydro-Québec electrical grid [13]. The system is comprehensively instrumented with thermocouples, power and pressure transducers, flow meters for the working fluid and for the ancillary fluids in the source and sink circuits. A data acquisition system and associated analysis software are set up to monitor system operation.

The flow of R245fa is produced by the variable speed pump, which maintains the superheating after the evaporator at a value around 5 °C. When the heat source is at a high temperature and the pump is at maximum speed, the superheat can go higher than 5 °C. The speed of the double screw expander is fixed [13].

Results reveal that there is a good agreement between experimental and simulation data for the four cases, as shown in table 6.1. As a result, the deviation of the net power output and cycle efficiency for all cases are lower than 8%.

The results also confirm that both net power output and energy conversion efficiency depend on the value of the superheat at the evaporator exit. It can be seen in table 6.1 that the net power output increases from 35.66 to 40.6 when the inlet temperature increases from 100 ºC to 115 ºC. After comparing and validating the obtained results from ORC simulation, it is now possible to link this thermodynamic model with the ejector 1D model, shown in the next section.

Table 6.1 Comparison between ORC simulation and experimental data for different cases

Parameter	**Unit**	**Case #1**			**Case #2**			**Case #3**			**Case #4**		
Outlet temperature of evaporator	°C	91.06			113.9			79			82.5		
Superheat	°C	4.3			25.5			4.6			3.5		
Mass flow rate of working fluid	kg/s	2.38			2.439			2.004			2.193		
Mass flow rate of heat source	kg/s	11.2			11.2			11.2			11.78		
Mass flow rate of heat sink	kg/s	14.53			11.35			14.8			10.25		
Inlet temperature of heat source	°C	100.8			115.3			85.9			90		
Inlet temperature of heat sink	°C	24.6			13.5			24.7			36.1		
Parameter	**Unit**	Sim.	Ex.	Diff.	Sim.	Ex.	Diff.	Sim.	Ex.	Diff.	Sim.	Ex.	Diff.
Net power output (W_{net})	kW	35.66	33	8.06	44.2	40.6	8.87	21.1	19.3	8.53	12.08	11	8.94
System efficiency (η_s)	%	6.454	6	7.57	6.8	7	2.9	4.86	4.9	0.81	2.74	2.7	1.48

6.4.2 Validation of the ejector model

For validation of the ejector model, a comparison between the dimensions obtained by the 1D model and experimental data is performed. To this aim, the available experimental data of test bench located at the Hydro-Québec laboratory in Shawinigan are used [69].

The results obtained from the 1D model are compared to experimental dimensions. The results show that the 1D model accurately calculates all of the ejector geometry over the entire range of operation, with an average error <2% compared to experimental dimensions. From table 6.2 and figure 6.3 it can be inferred that there is good agreement between the results obtained from the present model and experimental geometry.

Table 6.2 Comparison between dimensions calculated by thermodynamic model and experimental data

D, L, X [mm]	Ex.	Therm.	Error (%)
D_a	32.08	31.76	-0.99
D_{th}	14.42	14.3	-0.83
D_{7p}	22.47	21.57	-4.01
D_7	36.072	35.41	-1.83
D_8	28.47	27.71	-2.67
D_c	38.1	38.16	0.157
L_1	100.9	99.8	-1.09
L_2	170.85	166.3	-2.66
L_4	80	88.2	10.25
L_5	28.12	30.81	9.57
L_{tot}	379.87	385.11	1.38

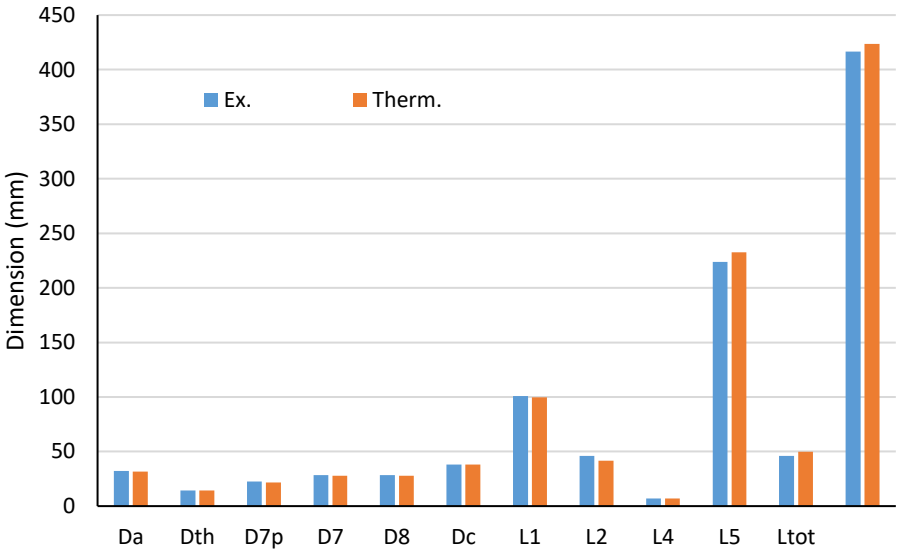

Figure 6.3 Comparisons of calculated dimensions with experimental geometry

6.5 Sizing an ejector for available ORC test bench

In this section, a constant pressure mixing ejector working in double-choking regime is designed for the 50 kW ORC test bench discussed in section 6.3.1. Thermodynamic properties of the ORC system, Case# 1 in table 6.1, are considered as a base case for designing the ejector. All dimensions of the ejector appropriately designed for this ORC system are shown in table 6.2. This ejector works in the double-choking regime. It should be mentioned that some

researchers previously have shown that the constant-pressure mixing ejector has better performance than that of the constant area [40] [44].

For optimal design of an ejector that will be integrated into an ORC system, some important condition should be considered: the allowable operating conditions of the ORC system; the effect of ejector geometry and working characteristics (parametric study in section 6.7); the mixing type of the ejector, including constant area mixing and constant pressure mixing; the ejector flow regime, where the best performance is in double-choking mode. It should be noted that based on the experimental results by Keenan et al. [56] as well as ASHRAE (as reported by Alexis [64]), the value of the ratio $(L_4 + NXP)/D_8$ should be between 9 and 16 for satisfactory operation of the ejector.

Table 6.3 The geometry of the designed ejector for ORC base case

D [mm]	Base case	L [mm]	Base case	θ [deg]	Base case
D_a	125	L_1	178.9	θ_1	10
D_{th}	61.96	L_2	113.2	θ_2	3
D_{7p}	73.83	NXP	12.01	θ_3	5
D_7	95.5	L_4	1454	θ_4	4
D_8	93.4	L_5	302		
D_c	135.6	L_{tot}	2048		
		$(L_4+NXP)/D_8$	15.69		

6.6 Evaluation of EORC system for a fixed ejector performance

Simulation results of the EORC system are compared with those obtained from the ORC system of the experimental base case. For both ORC and EORC systems, calculations are carried out in the condition of the same outlet point from the first-stage evaporator (Fig. 6.1). Based on the presented ORC base case 1, the heat source and sink are selected as temperatures of 100.8 °C and 24.6 °C, heating and cooling flow rates of 11.2 and 14.53 kg/s. R245fa is the working fluid. The outlet superheat from both evaporators is set to 4.3 °C. Table 6.4 shows the simulation conditions of the ORC and EORC.

Table 6.4 Simulation conditions of the EORC system.

Term	Unit	Value
Environment pressure (P_{oc})	kPa	101.32
Environment temperature (T_{oc})	°C	20
Pressure drop in all heat exchangers	kPa	30
Turbine isentropic efficiency ($\eta_{is,exp}$)	%	70
Pinch temperature difference	°C	5
Pump isentropic efficiency ($\eta_{is,p}$)	%	90
Chevron angle	°	60
Ejector primary efficiency ($\eta_{Pol,pr}$)	%	0.975

Ejector secondary efficiency ($\eta_{Pol,sec}$)	%	0.97
Ejector diffuser efficiency ($\eta_{Pol,d}$)	%	0.621

Table 6.5 shows the calculated thermodynamic performance and a comparison between EORC and ORC. Integrating the ejector into an organic Rankine cycle decreased the expander outlet pressure by 51.5 kPa, compared to the ORC system. This leads to an increase in power output capacity by 15%. This result agrees with the previous studies that integrate an ejector into an organic Rankine cycle [15] [111] [16] [112].

In contrast to previous studies of Li et al. [15] and Kheiri et al. [112] on the EORC system, where the ejector entrainment ratio was more than 1 (about 2), in the current study the calculated value is about 0.41. In general, it is unrealistic to have the entrainment ratio more than 1 for an ejector that works in the double-choking regime inside an EORC system. It should be noted that the best performance of the ejector always occurs in the double-choking regime in which secondary mass flow rate is constant. Fig. 6.4. compares the ORC and EORC performances.

Table 6.5 Performance comparison between EORC with ORC in the condition of the same outlet point from the first-stage evaporation.

		Unit	ORC	EORC
1. Heat source's parameters				
Heat source mass flowrate		kg/s	11.2	11.2
First-stage evaporator	Inlet	°C	100.8	100.8
	Outlet	°C	89.35	89.35
Second-stage evaporator	Inlet	°C	-	89.35
	Outlet	°C	-	63.8
2. Cycle parameters by R245fa				
Outlet from First-stage evaporator (Expander inlet)		kg/s	2.38	2.38
		°C	91.06	91.06
		kPa	934	934
Outlet from Second-stage evaporator (Primary fluid of ejector)		kg/s	-	5.79
		°C	-	62.14
		kPa	-	434
Expander outlet (Secondary fluid of ejector)		kg/s	2.38	2.38
		°C	58.76	54.01
		kPa	230	178.5
Condenser inlet (Ejector outlet)/Condenser outlet		kg/s	2.38	8.16
		°C	58.76/29.6	55.01/33.45
		kPa	230/200	230/200
Ejector entrainment ratio (ER)		-	-	0.411
Ejector pressure ratio (PR)		-	-	1.289
3. Cycle performance				
Total cycle capacity (W_{net})		kW	42.28	48.86
Pumping work (pump 1)		kW	1.52	1.53
Pumping work (pump 2)		kW	-	1.29
Expander output capacity (W_{exp})		kW	43.81	51.69
Increment of total output capacity		%	-	15.55

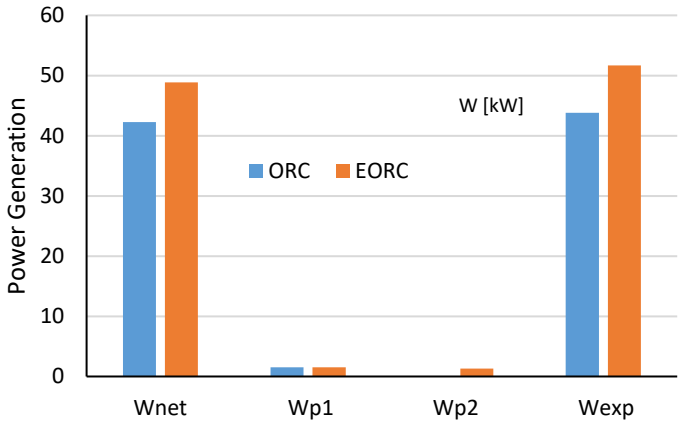

Figure 6.4 Comparison between ORC and EORC performance

6.7 Parametric study

Ejector geometry and working characteristics, as well as some cycle properties, can influence the net power output of the EORC system. Therefore, it is necessary to examine the effects of each of these key parameters to optimize system performance. In the parametric analysis, one parameter is varied, whereas others are kept constant [117].

By applying the validated EORC thermodynamic model, based on the fixed input parameters of table 6.4, a parametric study is carried out. For all the assessed cases, the ejector works in the double-choking regime, meaning that the secondary mass flowrate remains constant for all cases. For a robust parametric analysis, twelve parameters of the EORC system are considered. The most important input parameters for the EORC model are some ejector geometry such as D_{th}, D_{7p}, D_8 and AR, the ejector primary inlet conditions (P_4, T_4), secondary mass flow rate ($\dot{m}_{sec}$), ejector back pressure (P_1), expander inlet properties (P_5, T_5), and ejector polytropic efficacies ($\eta_{pol,pr}$, $\eta_{pol,sec}$, $\eta_{pol,d}$). The effects of these input parameters on the cycle performance such as expander power (W_{exp}), system efficiency (η_s), and exergy efficiency (η_{exe}) are investigated for the base case. All results of the parametric study are summarized in table 6.10.

6.7.1 Effect of ejector dimensions on EORC performance

The effects of some ejector dimensions on the performance of EORC, particularly the expander output power, are analyzed. By considering various input geometries, the results from the thermodynamic model are calculated. In each case, one of the ejector dimensions is changed while the others are fixed. Table 6.6 illustrates these effects on the EORC performance.

The results reveal that the expander back pressure (P_6) and consequently the expander work (W_{exp}) are significantly affected by changing ejector dimensions due to variations in the fluid

flow characteristics and the internal exergy losses related to different parts of the ejector. By increasing the primary throat diameter (D_{th}), the value of the expander back pressure (P_6) significantly increases and consequently the power output (W_{exp}) decreases.

Increasing the nozzle exit diameter (D_{7p}) and the constant area duct diameter (D_8) augment the expander power and the cycle performance due to the decreasing expander back pressure (P_6). Results show that the constant area duct diameter (D_8) is the most influential geometrical parameter affecting the power output and the cycle performance. By increasing the value of D_8 from 93 to 99 mm (about 6.4%), the expander power capacity, the cycle energy efficiency, and exergy efficiency are increased by 12.7%, 13.7%, and 9.8% respectively.

In general, by considering the variation in D_{th} and D_8, it can be concluded that any increment in the ejector area ratio $(D_8/D_{th})^2$ leads to a rise in the value of power output capacity. Effects of ejector diameters on the power output capacity are demonstrated in fig. 6.5.

According to the aforementioned results, the proper design of the ejector geometry can have a very significant effect on the performance of an EORC system, where the equipment size of the other components is the same as the ORC system. For example, by decreasing the value of the D_{th}=65 related to designed ejector (table 6.3) to D_{th}=62, the expander power output will increase from 50.08 to 51.69 kW.

Table 6.6 Effects of ejector dimensions on EORC performance.

	D_{th} [mm]			D_{7p} [mm]			D_8 [mm]		
	62	**63**	**65**	**65**	**70**	**72**	**93**	**96**	**99**
W_{exp} [kW]	51.69	51.53	50.08	48.19	51.81	52.87	51.09	54.92	57.58
η_s [%]	2.81	2.73	2.57	2.61	2.81	2.877	2.77	2.99	3.15
η_{exe} [%]	6.31	6.29	6.21	5.96	6.4	6.41	6.24	6.6	6.85
ΔE_{exp} [kW]	20.15	20.08	19.76	18.64	20.65	20.66	19.89	21.55	22.73
ΔE_{eje} [kW]	40.36	42.71	48.07	46.47	38.47	38.38	41.38	34.88	30.35
ΔE_{tot} [kW]	1410	1411	1412	1415	1408	1407	1411	1405	1402
P_6 [kPa]	178.5	179.4	183.7	199.8	177.8	171.8	182	160.8	147.5

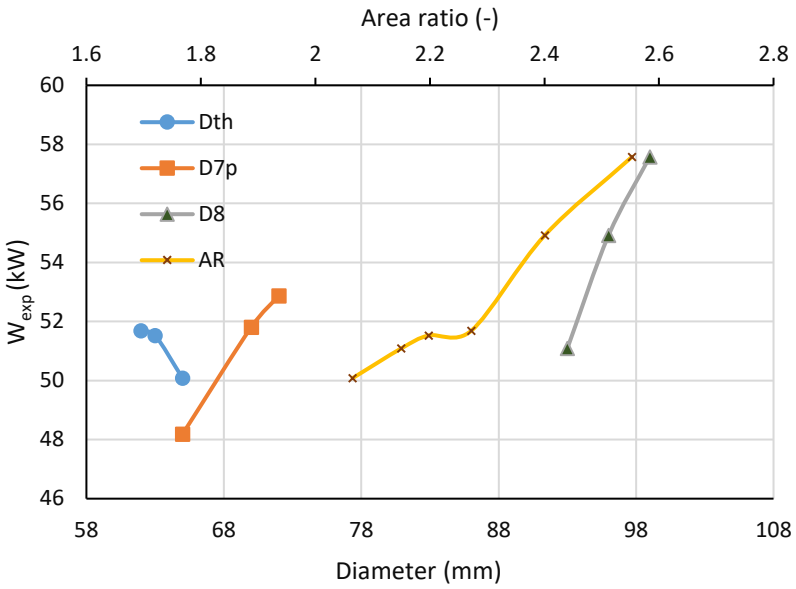

Figure 6.5 Effects of ejector diameters on power output capacity

6.7.2 Effect of ejector operating conditions on EORC performance

Table 6.7 shows the effects of the inlet and outlet ejector properties as well as the secondary mass flow rate on EORC performance. It is found that by increasing ejector primary properties (P_4, T_4), the expander back pressure (P_6) augments and consequently the expander power output (W_{exp}) decreases. In addition, the system energy and exergy efficiencies (η_s, η_{exe}) also reduces due to a noticeable increase in the exergy losses, related to the ejector and the new components such as the second-stage evaporator.

Increasing the secondary mass flow rate ($\dot{m}_{sec}$) has a significant impact on the power output (W_{exp}) based on equation 6.2 even though the expander back pressure (P_6) significantly rises. The results show that by increasing the ejector back pressure (P_1), the value of W_{exp} and P_6 stay constant, meaning that these values are independent of the back pressure. In other words, the upstream of the normal shock is not influenced by back pressure when the ejector is in the double-choking regime (constant secondary mass flow rate ($\dot{m}_{sec}$)). Effects of ejector operating conditions on the power output capacity are depicted in Fig. 6.6 and fig. 6.7.

Table 6.7 Effects of ejector operating conditions on EORC performance.

	P_4 [kPa]			T_4 [°C]		
	412	**430**	**520**	**58**	**61**	**64**
$\dot{W}_{exp}$ [kW]	52.15	51.71	50.52	51.95	51.76	51.59
η_s [%]	2.95	2.83	2.34	2.85	2.82	2.79
η_{exe} [%]	7.419	6.315	5.99	8.108	6.84	5.58
ΔE_{exp} [kW]	20.34	20.15	19.64	20.26	20.18	20.1
ΔE_{eje} [kW]	17.32	38.77	77.31	30.89	37.47	44.41

ΔE_{tot} [kW]	1393	1410	1415	1383	1402	1421
P_6 [kPa]	175.9	178.4	185.4	177	178.1	179.1
	P_1[kPa]			$\dot{m}_{sec}$ [kg/s]		
	190	**200**	**210**	**1**	**2**	**2.5**
$\dot{W}_{exp}$ [kW]	51.69	51.69	51.69	26.95	47.17	52.94
η_s [%]	2.69	2.72	2.75	1.75	2.7	2.83
η_{exe} [%]	5.05	5.33	5.64	4.35	5.98	7.06
ΔE_{exp} [kW]	20.15	20.15	20.15	10.79	18.56	20.58
ΔE_{eje} [kW]	67.11	59.9	53.06	43.49	37.34	32.53
ΔE_{tot} [kW]	1429	1425	1420	1438	1415	1399
P_6 [kPa]	178.5	178.5	178.5	119	154.6	186.1

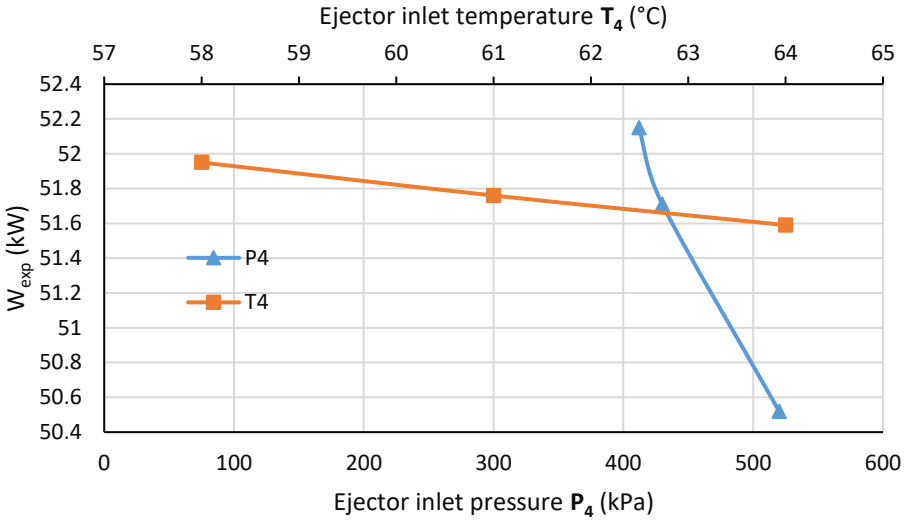

Figure 6.6 Effects of inlet ejector properties on power output capacity

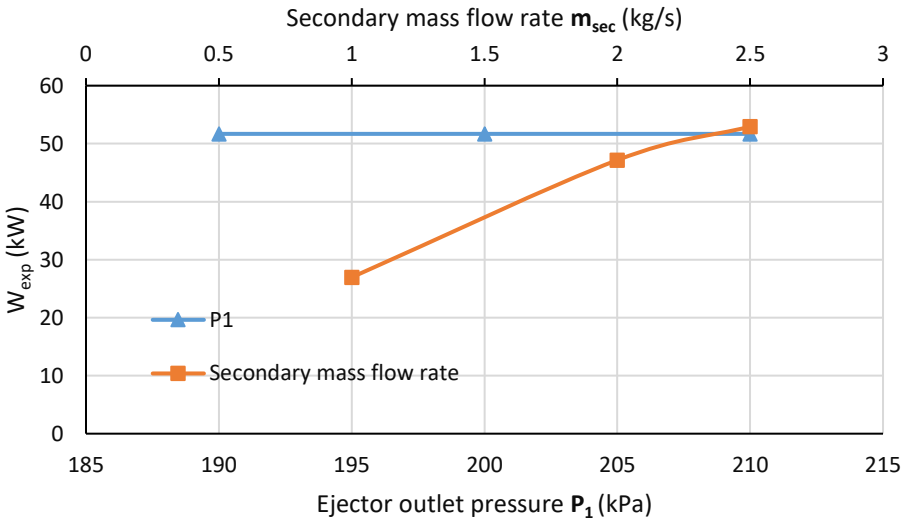

Figure 6.7 Effects of ejector back pressure and secondary mass flow rate on power output capacity

6.7.3 Effect of ejector polytropic efficiencies on EORC performance

Table 6.8 displays the effects of polytropic efficiencies on EORC performance. It is found that $\eta_{Pol,sec}$ has the most impact on expander back pressure and consequently W_{exp}, as decreasing $\eta_{Pol,sec}$ by 15.2 % leads to more than 4.7% increase in W_{exp} because of the increase in the expander pressure difference. Effects of ejector polytropic efficiencies on power output capacity are depicted in fig. 6.8.

It is also shown that by increasing the polytropic diffuser efficiency ($\eta_{Pol,d}$), the value of W_{exp} and other cycle properties remain constant. In other words, these values are independent of the $\eta_{Pol,d}$ in the double-choking mode. It should be mentioned that the acceleration/deceleration ejector processes become isentropic when the polytropic efficiency is equal to 1.

Table 6.8 Effects of the polytropic efficiencies on EORC performance

	$\eta_{Pol,pr}$			$\eta_{Pol,sec}$			$\eta_{Pol,d}$		
	0.94	**0.97**	**0.98**	**0.85**	**0.9**	**0.98**	**0.5**	**0.6**	**0.7**
$\dot{W}_{exp}$ [kW]	51.64	51.69	51.71	49.51	50.5	51.85	51.69	51.69	51.69
η_s [%]	2.84	2.81	2.8	2.68	2.74	2.82	2.809	2.809	2.809
η_{exe} [%]	6.16	6.28	6.32	6.303	6.304	6.305	6.304	6.304	6.304
ΔE_{exp} [kW]	21.12	20.15	20.1	19.21	19.63	20.22	20.15	20.15	20.15
ΔE_{eje} [kW]	41.13	40.46	40.26	41.3	40.87	40.29	40.36	40.36	40.36
ΔE_{tot} [kW]	1412	1410	1409	1410	1409.5	1409	1410	1410	1410
P_6 [kPa]	178.8	178.5	178.4	191.5	185.5	177.6	178.5	178.5	178.5

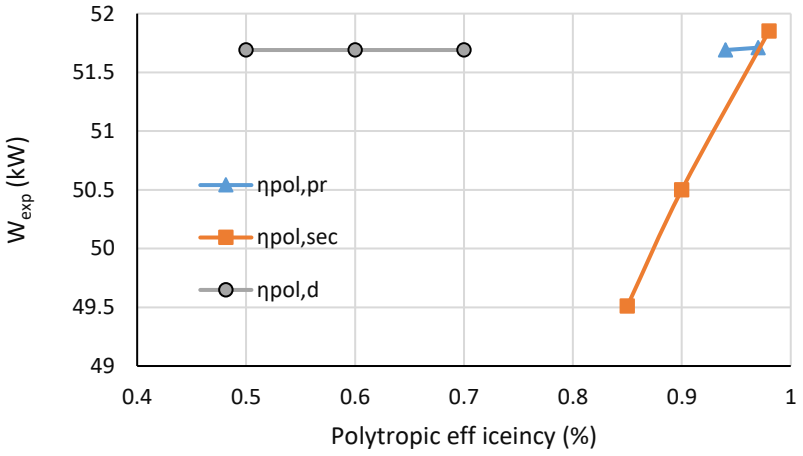

Figure 6.8 Effects of ejector polytropic efficiencies on power output capacity

6.7.4 Effect of expander inlet properties on the performance of EORC

Effects of two key thermodynamic parameters, expander inlet temperature, and expander inlet pressure are shown in table 6.9. The variation of the power output capacity with expander inlet properties is demonstrated in fig. 6.9. Increasing the expander inlet properties leads to an

increase in the enthalpy drop across the expander and consequently a rise in power output [114]. Furthermore, the energy and exergy cycle efficiencies rise gradually with an increase in expander inlet properties due to decreasing total exergy destruction [118].

Table 6.9 Effects of the expander inlet properties on EORC performance.

	T_5 [°C]			P_5 [kPa]		
	96.5	**99.8**	**102.5**	**920**	**940**	**960**
$\dot{W}_{exp}$ [kW]	50.61	51.2	51.95	51.2	51.9	52.58
η_s [%]	2.765	2.79	2.82	2.78	2.81	2.85
η_{exe} [%]	5.51	5.94	6.5	6.24	6.33	6.42
ΔE_{exp} [kW]	20.01	20.09	20.18	19.97	20.22	20.47
ΔE_{eje} [kW]	50.16	44.81	37.99	40.81	40.17	39.54
ΔE_{tot} [kW]	1422	1415	1407	1411	1410	1408
P_6 [kPa]	178.5	178.5	178.5	178.5	178.5	178.5

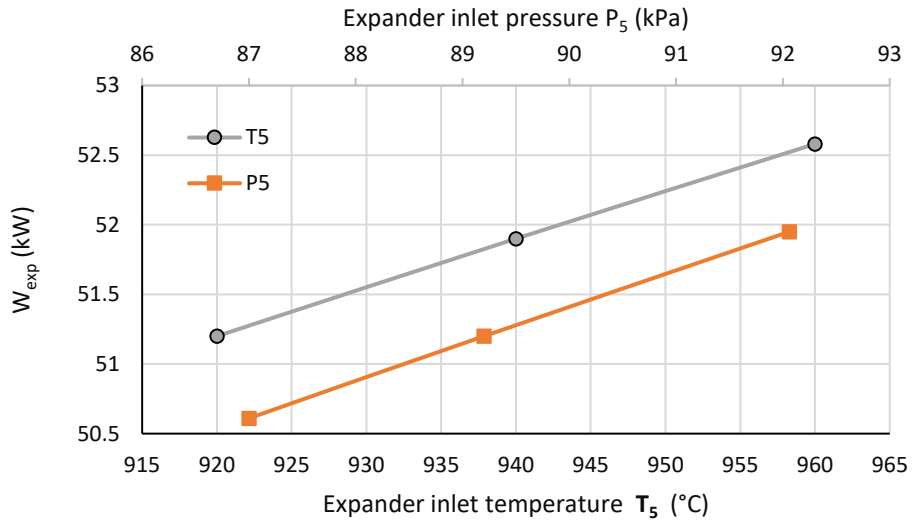

Figure 6.9 Effects of expander inlet properties on power output capacity

6.7.5 A summary of the results of the parametric study

The parametric analysis results of the EORC system are summarized in table 6.10. The system performance in terms of expander power generation and exergy efficiency, as well as the cycle efficiency, strongly depend on the ejector working characteristics. The overall observations can be summarized as follows:

- Expander power output is independent of the ejector outlet properties such as back pressure (P_1), and secondary efficiency ($\eta_{Pol,sec}$) in the double-choking mode.
- Increasing the secondary mass flow rate, primary and secondary polytropic efficiencies, constant area duct diameter, nozzle exit diameter, or inlet expander properties leads to a considerable increase in the system power output.

- Decreasing the throat diameter or inlet ejector properties results in a significant rise in the system power output.
- As expected, the exergetic cycle efficiency (η_{exe}) decreases when the total exergy destruction increases, due to their inverse relationship in the definition of this metric.

Table 6.10 A summary of the results of the parametric study

Parameter	$\dot{W}_{exp}$	η_s	η_{exe}	ΔE_{exp}	ΔE_{eje}	ΔE_{tot}	P_6
D_{th} (↑)	↓	↓	↓	↓	↑	↑	↑
D_{7p} (↑)	↑	↑	↑	↑	↓	↓	↓
D_8 (↑)	↑	↑	↑	↑	↓	↓	↓
AR (↑)	↑	↑	↑	↑	↓	↓	↓
P_4 (↑)	↓	↓	↓	↓	↑	↑	↑
T_4 (↑)	↓	↓	↓	↓	↑	↑	↑
P_1 (↑)	C	↑	↑	C	↓	↓	C
$\dot{m}_s$ (↑)	↑	↑	↑	↑	↓	↓	↑
$\eta_{Pol,pr}$ (↑)	↑	↓	↑	↓	↓	↓	↓
$\eta_{Pol,sec}$ (↑)	↑	↑	↑	↑	↓	↓	↓
$\eta_{Pol,d}$ (↑)	C	C	C	C	C	C	C
P_5 (↑)	↑	↑	↑	↑	↓	↓	C
T_5 (↑)	↑	↑	↑	↑	↓	↓	C

Increase (↑), Decrease (↓), Constant (C)

6.8 Conclusion

In the present study, a modified organic Rankine cycle is studied with a view to augmenting the power generation capacity. To this aim, a supersonic ejector is integrated into the basic ORC and its impact is investigated. The thermodynamic performance of the EORC system is examined for low-temperature heat sources. A parameter sensibility analysis of the EORC system is performed on different ejector working parameters, with the system performance evaluated with indicators such as the expander power, cycle efficiency, and exergy losses.

It is found that increasing the ejector area ratio or the secondary mass flow rate, or decreasing the throat diameter or the inlet ejector properties (T_4, P_4), can increase the power generation considerably. The results show that when the ejector works in double-choking mode, the expander power output is independent of the ejector outlet properties (P_1, $\eta_{Pol,d}$). The constant area duct diameter (D_8) is the most influential geometrical parameter affecting the power output and the cycle performance, as an increase in D_8 by 6% improves the EORC power output by 13%. It is also shown that the ejector secondary polytropic efficiency ($\eta_{Pol,sec}$) has the most impact on the power generation among the ejector component efficiencies.

6.9 Acknowledgements

The authors wish to thank Hydro-Québec laboratory in Shawinigan for their valuable contribution during this research study. This project is a part of the Collaborative Research and Development (CRD) Grants Program at the Université de Sherbrooke. The authors also acknowledge the support of the Natural Sciences and Engineering Research Council of Canada, Rio Tinto Alcan and CanmetENERGY Research Center of Natural Resources Canada.

CHAPTER 7 : CONCLUSION AND PERSPECTIVES

7.1 Conclusion

The main objective of this research project is the performance analysis and optimization of an organic Rankine cycle with ejector (EORC). To achieve this purpose, in the first stage of this thesis, as you may see in chapters 3, 4 and 5, a comprehensive numerical and experimental investigation on the supersonic ejectors has been carried out. These studies are comprised of developing a new 1D model of ejectors, CFD simulation of two different type of ejectors based on available experimental test benches, ejector geometry improvement, determination of the best normal shock assumption and the selection of the efficiencies that are two of the greatest sources of error in the 1D models, effect of ejector pressure ratio in a refrigeration system, and using polytropic conception in the ejector 1D modeling.

Experimental test bench located at Hydro-Quebec was used to validate the results obtained from CFD and 1D modeling. Comparisons were made for CFD and one-dimensional predictions to the corresponding experimental data. The results show that there is a good agreement between models. Therefore, the 1D model presented in this study is ideal for integration into overall system models to accurately predict the performance of the ejector in power cycles, especially in ORC systems.

In chapter 3, a thermodynamic model applicable for two types of ejectors, constant area mixing (CAM) ejectors and constant pressure mixing (CPM) ejectors, is developed and validated against experimental data. The model is based on the application of the polytropic efficiency concept. The reference values of polytropic efficiencies are extracted from CFD models of two ejector types. Compared to experimental data, the model accurately predicts the ejectors dimensions over the entire range of operation with an average error less than 2%.

The results show that the best agreement with experimental data for both types of ejectors (CPM and CAM) is achieved by polytropic efficiencies. It is illustrated that $\eta_{Pol,p}$ has the most impact on the constant area duct length. The parametric analysis completed through the application of the model shows that an increase in ejector back pressure and $\dot{m}_{sec}$ lead to the decrease of a constant area duct length, the main factor responsible for the ejector's size.

In chapter 4, the relationship between the ejector refrigeration cycle performance and the working characteristics of the ejector is investigated. For this purpose, some important

parameters such as pressure ratio, overall ejector efficiency, component efficiencies, entrainment ratio, ejector exergy efficiency and internal irreversibilities in each part as well as ejector geometry are considered. It aims to get a better understanding of the effects of the external and internal parameters on the ejector behavior in order to improve ejector design and cycle performance.

The results show that the best performance of the R245fa refrigeration cycle is achieved at the maximum pressure ratio (PR) for the critical condenser temperature point (T_c^*), these conditions correspond to the minimum of the internal exergy losses generated in the ejector.

It is found that the primary nozzle diameter (D_{7p}) is the geometrical parameter with the greatest effect on the pressure ratio and ejector performance.

In addition, the results show that most of the exergy losses inside the ejector are located in three regions, namely: the constant area mixing section (m-8), the mixing chamber (7-m) and the primary nozzle (th-7p).

In chapter 5, the effect of the normal shock location on the design of a one-phase supersonic ejector was investigated. It is previously proven that the normal shock assumption and the selection of the efficiencies are two of the greatest sources of error in the 1D models.

CFD technique was first used to evaluate the value of the efficiencies, critical back pressure and also more detailed information about the flow, density and temperature distributions in the ejector. Afterwards, data obtained from the CFD simulations were applied in the 1D thermodynamic models to calculate all ejector dimensions.

It is shown that the effect of normal shock place is only on the constant area length (L_4) and flow properties at sections u and d (before and after normal shock). The results show that when the normal shock assumed at the inlet of constant area duct, obtained dimensions by the 1D model are more accurate for both types of ejectors (CPM and CAM) compared to experimental dimensions.

Lastly, in the second stage of this thesis, as you may see in chapter 6, a modified organic Rankine cycle is proposed to augment the power generation and EORC performance. To this aim, a supersonic ejector is integrated into the basic ORC and its impact is investigated. The thermodynamic performance of both ORC and EORC systems are examined for low-temperature heat sources. The results show that when the ejector works in double-choking mode, the expander power output is independent of the ejector outlet properties (P_1, $\eta_{Pol,d}$). Some important indicators such as expander power output, thermal efficiency, exergy efficiency are considered for parameter optimizations.

It is revealed that increasing the ejector area ratio, secondary mass flow rate as well as decreasing the throat diameter and inlet ejector properties (T_4, P_4) can increase the power generation considerably. It is also shown that the ejector secondary polytropic efficiency has the most impact on the power generation among other component efficiencies. It is found that the constant area duct diameter is the most influential geometrical parameter affecting the power output and the cycle performance as a rise in D_8 by 6% leads to an increase in power output by 13%.

7.2 Conclusion (French)

L'objectif principal de ce projet de recherche est l'analyse des performances et l'optimisation d'un cycle de Rankine organique à éjecteur (EORC). Pour atteindre cet objectif, dans la première étape de cette thèse et comme détaillé dans les chapitres 3, 4 et 5, une étude numérique et expérimentale complète sur les éjecteurs supersoniques a été réalisée. Ces études comprennent le développement d'un nouveau modèle 1D d'éjecteurs, la simulation par CFD de deux types d'éjecteurs différents sur la base des bancs d'essais expérimentaux disponibles, l'amélioration de la géométrie des éjecteurs, la détermination de la meilleure hypothèse de choc normal et la sélection du rendement, principales sources d'erreur dans les modèles 1D, effet du rapport de pression de l'éjecteur dans un système de réfrigération et utilisation de la conception polytropique dans la modélisation 1D de l'éjecteur.

Un banc d'essai expérimental situé à Hydro-Québec a été utilisé pour valider les résultats obtenus par modélisation CFD et 1D. Des comparaisons ont été effectuées avec les prédictions CFD et les données expérimentales correspondantes. Les résultats montrent qu'il existe un bon accord entre les modèles. Par conséquent, le modèle 1D présenté dans cette étude est idéal pour une intégration dans des modèles de système afin de prédire avec précision la performance de l'éjecteur dans les cycles d'alimentation, en particulier dans les systèmes ORC.

Au chapitre 3, un modèle thermodynamique applicable à deux types d'éjecteurs, les éjecteurs à mélange à surface constante (CAM) et les éjecteurs à mélange à pression constante (CPM), est développé et validé par rapport aux données expérimentales. Le modèle est basé sur l'application du concept d'efficacité polytropique. Les valeurs de référence des rendements polytropiques sont extraites de modèles CFD de deux types d'éjecteurs. Par rapport aux données expérimentales, le modèle prédit avec précision les dimensions des éjecteurs sur toute la plage de fonctionnement avec une erreur moyenne inférieure à 2%.

Les résultats montrent que le meilleur accord avec les données expérimentales pour les deux types d'éjecteurs (CPM et CAM) est obtenu par des rendements polytropiques. Il est illustré que $\eta_{Pol,p}$ a le plus grand impact sur la longueur de conduit à surface constante. L'analyse paramétrique réalisée grâce à l'application du modèle montre qu'une augmentation de la contre-pression de l'éjecteur et de la vitesse $\dot{m}_{sec}$ entraînent la diminution de la longueur d'une conduite à surface constante, principal facteur de la taille de l'éjecteur.

Au chapitre 4, la relation entre les performances du cycle de réfrigération de l'éjecteur et les caractéristiques de fonctionnement de l'éjecteur est examinée. À cette fin, certains paramètres importants tels que le rapport de pression, l'efficacité globale de l'éjecteur, l'efficacité des composants, le taux d'entraînement, l'efficacité exergétique de l'éjecteur et les irréversibilités internes de chaque pièce ainsi que la géométrie de l'éjecteur sont pris en compte. Il vise à mieux comprendre les effets des paramètres externes et internes sur le comportement de l'éjecteur afin d'améliorer la conception de l'éjecteur et les performances du cycle.

Les résultats montrent que la meilleure performance du cycle de réfrigération R245fa est obtenue avec le rapport de pression maximal (PR) pour le point de température critique du condenseur (T_c^*), Ces conditions correspondent au minimum des pertes d'exergie internes générées dans l'éjecteur.

On constate que le diamètre primaire de la buse (D_{7p}) est le paramètre géométrique ayant le plus grand effet sur le rapport de pression et les performances de l'éjecteur.

De plus, les résultats montrent que la plupart des pertes d'exergie à l'intérieur de l'éjecteur se situent dans trois régions, à savoir: la section de mélange à surface constante (m-8), la chambre de mélange (7-m) et la buse primaire (th-7p).

Au chapitre 5, l'effet de l'emplacement du choc normal sur la conception d'un éjecteur supersonique à une phase a été étudié. Il a déjà été prouvé que l'hypothèse de choc normale et le choix des rendements sont deux des plus grandes sources d'erreur dans les modèles 1D.

La technique CFD a été utilisée dans un premier lieu pour évaluer la valeur exacte des rendements, la contre-pression critique et également des informations plus détaillées sur les distributions de flux, de densité et de température dans l'éjecteur. Ensuite, les données obtenues à partir des simulations CFD ont été appliquées dans les modèles thermodynamiques 1D pour calculer toutes les dimensions de l'éjecteur.

Il a été démontré que l'effet de l'emplacement du choc normal n'est exercé que sur la longueur de la surface constante (L_4) et les propriétés d'écoulement aux sections u et d (avant et après du choc normal). Les résultats montrent que lorsque le choc normal supposé à l'entrée du conduit

à surface constante, les dimensions obtenues par le modèle 1D sont plus précises pour les deux types d'éjecteurs (CPM et CAM) par rapport aux dimensions expérimentales.

Enfin, dans la seconde étape de cette thèse, un cycle organique modifié de Rankine est proposé pour augmenter la production d'énergie et les performances des EORC. À cette fin, un éjecteur supersonique est intégré à la ORC et son impact est étudié. Les performances thermodynamiques des systèmes ORC et EORC sont examinées pour les sources de chaleur à basse température. Les résultats montrent que lorsque l'éjecteur fonctionne en mode à double étranglement, la production d'énergie par turbine est indépendante des propriétés de la sortie de l'éjecteur (P_1, $\eta_{Pol,\ d}$). Certains indicateurs importants, tels que la puissance de sortie du détendeur et l'efficacité thermique, sont pris en compte pour l'optimisation des paramètres.

il est révélé que l'augmentation AR de l'éjecteur, les propriétés de l'éjecteur à l'entrée (T_4 et P_4) peut augmenter considérablement la production d'énergie. Il est également montré que l'efficacité polytropique secondaire de l'éjecteur a le plus grand impact sur la puissance des autres composants. On constate que la surface constante du diamètre du conduit est le paramètre géométrique le plus influant sur la puissance de sortie et que le cycle de performance en hausse de 6% en D_8 entraîne une augmentation de 13% de la puissance de sortie.

7.3 Perspectives

The greatest opportunity for future work in the field of ejector technology seems to be on how to incorporate the ejector cycle into real systems. Since 1858, ejectors have been intensively studied for a large number of various applications. In the past, ejectors have mostly been used in different cycles for refrigeration purposes. In recent decades, they are used in power cycles.

The investigation on power cycles including ORC such as cascade organic Rankine cycles, and ORC with ejector requires further attention.

As discussed in this thesis, the design of the ejector can have a very significant effect on the performance of ejector cycles, since more studies on how to design an appropriate ejector for various ejector cycles is essential. Future research should also investigate how do design other system components in addition to the ejector for use in ejector cycles.

According to the findings from chapter 6, a single and multi-objective optimization can also be suggested. As previously mentioned, it is confirmed that the thermodynamic parameters and ejector dimensions have significant effects on the net power output and the EORC system efficiency. In order to obtain the optimum design parameters, a single and multi-objective optimization can be conducted with the net power output and energy and exergy efficiencies as

the objective function by means of Genetic algorithm method (GA). To maximize the objective function, the turbine inlet and outlet pressure, the turbine inlet temperature, the pinch temperature difference and main dimensions of the ejector can be selected as the decision variables. Physical constraints should be considered to satisfy the acceptable cycle conditions. The turbine inlet must be saturated vapor or superheated vapor state. In the heat exchangers, the temperature of hot fluid must be higher than the temperature of the cold fluid. Area ratio (AR) of the ejector should be between 2 to 8 and also $((L_4+NXP)/D_8)$ should be between 9 to 16. Ejector must work in the double-choking regime to have a higher performance. The decision variables and their ranges for working fluid and control parameters in GA must be determined. The ranges of pinch temperature difference can be respectively set to 5–20 °C according to engineering experience.

In addition, thermodynamic modeling of a CRMC ejector based on component polytropic efficiencies as well as its CFD modeling. Integrating a CRMC ejector into an ORC system and comparing to a traditional ejector.

It is also proposed more investigation on the effect of normal shock location in ejector thermodynamic models. In particular, a place between the inlet and outlet of constant area duct. Experimental and CFD simulation can be used for validation. This study also can be conducted for different procedures of ejector thermodynamic models based on outlets. (Ejector geometry, entrainment ratio, ejector back pressure). Our study only included the ejector geometry as well as inlet and outlet assumptions for the normal shock location in the contestant area duct.

As the last suggestion, in chapter 3, it is proven that the 1D model based on polytropic efficiencies is more accurate than that based on component isentropic efficiencies. This result is obtained from a comparison between ejector geometry calculated by 1D model and experimental one. To have a double checking of this result we can develop a thermodynamic model with outputs of the secondary mass flow rate and the ejector back pressure rather than ejector dimensions. In this case, we can compare the entrainment ratio and compression ratio based on polytropic and isentropic efficiencies with experimental data.

LISTE DES RÉFÉRENCES

[1] S. Quoilin, V. Lemort, and J. Lebrun, “Experimental study and modeling of an Organic Rankine Cycle using scroll expander,” *Appl. Energy*, vol. 87, no. 4, pp. 1260–1268, 2010.

[2] S. Quoilin, M. Orosz, H. Hemond, and V. Lemort, “Performance and design optimization of a low-cost solar organic Rankine cycle for remote power generation,” *Sol. Energy*, vol. 85, no. 5, pp. 955–966, 2011.

[3] S. Quoilin, M. Van Den Broek, S. Declaye, P. Dewallef, and V. Lemort, “Techno-economic survey of Organic Rankine Cycle (ORC) systems,” *Renew. Sustain. Energy Rev.*, vol. 22, pp. 168–186, 2013.

[4] H. Müller-Steinhagen and F. Trieb, “Concentrating solar power,” *Rev. Technol. Ingenia Inf. QR Acad Eng*, vol. 18, pp. 43–50, 2004.

[5] S. Shaaban, “Analysis of an integrated solar combined cycle with steam and organic Rankine cycles as bottoming cycles,” *Energy Convers. Manag.*, vol. 126, pp. 1003–1012, 2016.

[6] G. Ford, “CSP: bright future for linear fresnel technology?,” *Renew. Energy Focus*, vol. 9, no. 5, pp. 48–51, 2008.

[7] Kranz S., “Market Survey—Germany, Low-Bin project. Available from: 〈 http://www.lowbin.eu/documentation.php〉 [accessed 14.04.12].” 2007.

[8] A. Lazzaretto, A. Toffolo, G. Manente, N. Rossi, and M. Paci, “Cost evaluation of Organic Rankine Cycles for low temperature geothermal sources,” *Proc. ECOS*, pp. 4–7, 2011.

[9] R. Moro, P. Pinamonti, and M. Reini, “ORC technology for waste-wood to energy conversion in the furniture manufacturing industry,” *Therm. Sci.*, vol. 12, no. 4, pp. 61–73, 2008.

[10] P. S. Bundela and V. Chawla, “Sustainable development through waste heat recovery.,” *Am. J. Environ. Sci.*, vol. 6, no. 1, pp. 83–89, 2010.

[11] O. Bailey and E. Worrell, “Clean Energy Technologies: A Preliminary Inventory of the Potential for Electricity Generation,” *Lawrence Berkeley Natl. Lab.*, 2005-08-03, LBNL-57451 .

[12] T. Engin and V. Ari, “Energy auditing and recovery for dry type cement rotary kiln systems––A case study,” *Energy Convers. Manag.*, vol. 46, no. 4, pp. 551–562, 2005.

[13] V. Minea, “Power generation with ORC machines using low-grade waste heat or renewable energy,” *Appl. Therm. Eng.*, vol. 69, no. 1, pp. 143–154, 2014.

[14] C. Sprouse and C. Depcik, “Review of organic Rankine cycles for internal combustion engine exhaust waste heat recovery,” *Appl. Therm. Eng.*, vol. 51, no. 1, pp. 711–722, 2013.

[15] X. Li, C. Zhao, and X. Hu, “Thermodynamic analysis of organic Rankine cycle with ejector,” *Energy*, vol. 42, no. 1, pp. 342–349, 2012.

[16] X. Li, X. Li, and Q. Zhang, “The first and second law analysis on an organic Rankine cycle with ejector,” *Sol. Energy*, vol. 93, pp. 100–108, 2013.

[17] X. Li, Q. Zhang, and X. Li, “A Kalina cycle with ejector,” *Energy*, vol. 54, pp. 212–219, 2013.

[18] X. Li, H. Huang, and W. Zhao, “A supercritical or transcritical Rankine cycle with ejector using low-grade heat,” *Energy Convers. Manag.*, vol. 78, pp. 551–558, 2014.

[19] A. Habibzadeh, M. M. Rashidi, and N. Galanis, “Analysis of a combined power and ejector-refrigeration cycle using low temperature heat,” *Energy Convers. Manag.*, vol. 65, pp. 381–391, 2013.

[20] K. Zhang, X. Chen, C. N. Markides, Y. Yang, and S. Shen, "Evaluation of ejector performance in an organic Rankine cycle," *Appl. Energy*, vol. 184, pp. 404–412, 2016.
[21] A. Soroureddin, A. S. Mehr, S. M. S. Mahmoudi, and M. Yari, "Thermodynamic analysis of employing ejector and organic Rankine cycles for GT-MHR waste heat utilization: A comparative study," *Energy Convers. Manag.*, vol. 67, pp. 125–137, 2013.
[22] M. Yari, A. S. Mehr, and S. M. S. Mahmoudi, "Thermodynamic analysis and optimization of a novel dual-evaporator system powered by electrical and solar energy sources," *Energy*, vol. 61, pp. 646–656, 2013.
[23] J. Chen, H. Havtun, and B. Palm, "Parametric analysis of ejector working characteristics in the refrigeration system," *Appl. Therm. Eng.*, vol. 69, no. 1, pp. 130–142, 2014.
[24] B. Gil and J. Kasperski, "Efficiency analysis of alternative refrigerants for ejector cooling cycles," *Energy Convers. Manag.*, vol. 94, pp. 12–18, 2015.
[25] K. Banasiak, A. Hafner, and T. Andresen, "Experimental and numerical investigation of the influence of the two-phase ejector geometry on the performance of the R744 heat pump," *Int. J. Refrig.*, vol. 35, no. 6, pp. 1617–1625, 2012.
[26] K. Cizungu, M. Groll, and Z. G. Ling, "Modelling and optimization of two-phase ejectors for cooling systems," *Appl. Therm. Eng.*, vol. 25, no. 13, pp. 1979–1994, 2005.
[27] S. Elbel and P. Hrnjak, "Experimental validation of a prototype ejector designed to reduce throttling losses encountered in transcritical R744 system operation," *Int. J. Refrig.*, vol. 31, no. 3, pp. 411–422, 2008.
[28] M. Nakagawa, A. R. Marasigan, T. Matsukawa, and A. Kurashina, "Experimental investigation on the effect of mixing length on the performance of two-phase ejector for CO 2 refrigeration cycle with and without heat exchanger," *Int. J. Refrig.*, vol. 34, no. 7, pp. 1604–1613, 2011.
[29] S. Elbel and N. Lawrence, "Review of recent developments in advanced ejector technology," *Int. J. Refrig.*, vol. 62, pp. 1–18, 2016.
[30] K. P. Tyagi and K. N. Murty, "Ejector-compression systems for cooling: utilising low grade waste heat," *J. Heat Recovery Syst.*, vol. 5, no. 6, pp. 545–550, 1985.
[31] N. H. Aly, A. Karameldin, and M. M. Shamloul, "Modelling and simulation of steam jet ejectors," *Desalination*, vol. 123, no. 1, pp. 1–8, 1999.
[32] I. W. Eames, S. Aphornratana, and H. Haider, "A theoretical and experimental study of a small-scale steam jet refrigerator," *Int. J. Refrig.*, vol. 18, no. 6, pp. 378–386, 1995.
[33] B. J. Huang and J. M. Chang, "Empirical correlation for ejector design," *Int. J. Refrig.*, vol. 22, no. 5, pp. 379–388, 1999.
[34] S. Varga, A. C. Oliveira, and B. Diaconu, "Numerical assessment of steam ejector efficiencies using CFD," *Int. J. Refrig.*, vol. 32, no. 6, pp. 1203–1211, 2009.
[35] G. Grazzini and A. Rocchetti, "Numerical optimisation of a two-stage ejector refrigeration plant," *Int. J. Refrig.*, vol. 25, no. 5, pp. 621–633, 2002.
[36] N. Galanis and M. Sorin, "Ejector design and performance prediction," *Int. J. Therm. Sci.*, vol. 104, pp. 315–329, 2016.
[37] D.G. Shepherd, *Principles of turbomachinery*. Prentice Hall, 1956.
[38] O. Samaké, N. Galanis, and M. Sorin, "On the design and corresponding performance of steam jet ejectors," *Desalination*, vol. 381, pp. 15–25, 2016.
[39] M. Khennich, N. Galanis, and M. Sorin, "Effects of design conditions and irreversibilities on the dimensions of ejectors in refrigeration systems," *Appl. Energy*, vol. 179, pp. 1020–1031, 2016.

[40] B. J. Huang, J. M. Chang, C. P. Wang, and V. A. Petrenko, "A 1-D analysis of ejector performance," *Int. J. Refrig.*, vol. 22, no. 5, pp. 354–364, 1999.
[41] H. El-Dessouky, H. Ettouney, I. Alatiqi, and G. Al-Nuwaibit, "Evaluation of steam jet ejectors," *Chem. Eng. Process. Process Intensif.*, vol. 41, no. 6, pp. 551–561, 2002.
[42] X. Chen, S. Omer, M. Worall, and S. Riffat, "Recent developments in ejector refrigeration technologies," *Renew. Sustain. Energy Rev.*, vol. 19, pp. 629–651, 2013.
[43] K. Chunnanond and S. Aphornratana, "An experimental investigation of a steam ejector refrigerator: the analysis of the pressure profile along the ejector," *Appl. Therm. Eng.*, vol. 24, no. 2, pp. 311–322, 2004.
[44] Y.-M. Chen and C.-Y. Sun, "Experimental study of the performance characteristics of a steam-ejector refrigeration system," *Exp. Therm. Fluid Sci.*, vol. 15, no. 4, pp. 384–394, 1997.
[45] S. He, Y. Li, and R. Z. Wang, "Progress of mathematical modeling on ejectors," *Renew. Sustain. Energy Rev.*, vol. 13, no. 8, pp. 1760–1780, 2009.
[46] J. T. Munday and D. F. Bagster, "A new ejector theory applied to steam jet refrigeration," *Ind. Eng. Chem. Process Des. Dev.*, vol. 16, no. 4, pp. 442–449, 1977.
[47] P. Haghparast, M. V. Sorin, and H. Nesreddine, "Effects of component polytropic efficiencies on the dimensions of monophasic ejectors," *Energy Convers. Manag.*, vol. 162, pp. 251–263, 2018.
[48] D.-W. Sun, "Comparative study of the performance of an ejector refrigeration cycle operating with various refrigerants," *Energy Convers. Manag.*, vol. 40, no. 8, pp. 873–884, 1999.
[49] Y. Tang, Z. Liu, Y. Li, C. Shi, and H. Wu, "Performance improvement of steam ejectors under designed parameters with auxiliary entrainment and structure optimization for high energy efficiency," *Energy Convers. Manag.*, vol. 153, pp. 12–21, 2017.
[50] C. Vereda, R. Ventas, A. Lecuona, and M. Venegas, "Study of an ejector-absorption refrigeration cycle with an adaptable ejector nozzle for different working conditions," *Appl. Energy*, vol. 97, pp. 305–312, 2012.
[51] A. Omidvar, M. Ghazikhani, and S. M. R. M. Razavi, "Entropy analysis of a solar-driven variable geometry ejector using computational fluid dynamics," *Energy Convers. Manag.*, vol. 119, pp. 435–443, 2016.
[52] G. Besagni, R. Mereu, and F. Inzoli, "Ejector refrigeration: a comprehensive review," *Renew. Sustain. Energy Rev.*, vol. 53, pp. 373–407, 2016.
[53] L. Zheng and J. Deng, "Research on CO 2 ejector component efficiencies by experiment measurement and distributed-parameter modeling," *Energy Convers. Manag.*, vol. 142, pp. 244–256, 2017.
[54] H. Zhang, L. Wang, L. Jia, and X. Wang, "Assessment and prediction of component efficiencies in supersonic ejector with friction losses," *Appl. Therm. Eng.*, 2017.
[55] S. Taslimitaleghani, M. Sorin, and S. Poncet, "Modeling of two-phase transcritical CO 2 ejectors for on-design and off-design conditions," *Int. J. Refrig.*, 2017.
[56] Keenan, E.P. Neumann, and F. Lustwerk J.H., "An investigation of ejector design by analysis and experiment," vol. J Appl Mech Trans ASME, 72 (1950), pp. 299–309, 1950.
[57] W. Chen, C. Shi, S. Zhang, H. Chen, D. Chong, and J. Yan, "Theoretical analysis of ejector refrigeration system performance under overall modes," *Applied Energy, 185, pp.2074-2084*.
[58] H. Nesreddine, A. Bendaoud, Z. Aidoun, M. Ouzzane, And B. Le Lostec, "Experimental investigation of an ejector-compression cascade system activated with low-grade waste heat," in *The proceedings of the 24 th IIR International Congress of Refrigeration, Yokohama, Japan, August*, 2015, pp. 16–22.

[59] S. Croquer, S. Poncet, and Z. Aidoun, "Turbulence modeling of a single-phase R134a supersonic ejector. Part 2: Local flow structure and exergy analysis," *Int. J. Refrig.*, vol. 61, pp. 153–165, 2016.
[60] G. Besagni and F. Inzoli, "Computational fluid-dynamics modeling of supersonic ejectors: Screening of turbulence modeling approaches," *Appl. Therm. Eng.*, vol. 117, pp. 122–144, 2017.
[61] "ANSYS FLUENT 17.0." ANSYS FLUENT Theory Guide release 17.0, ANSYS Inc., 2017.
[62] S. L. Dixon and C. Hall, *Fluid mechanics and thermodynamics of turbomachinery*. Butterworth-Heinemann, 2013.
[63] Klein, S., "Engineering Equation Solver.(EES)." Engineering Equation Solver. F-Chart Software., 2011.
[64] G. K. Alexis, "Estimation of ejector's main cross sections in steam-ejector refrigeration system," *Appl. Therm. Eng.*, vol. 24, no. 17, pp. 2657–2663, 2004.
[65] Y. Zhu, W. Cai, C. Wen, and Y. Li, "Shock circle model for ejector performance evaluation," *Energy Convers. Manag.*, vol. 48, no. 9, pp. 2533–2541, 2007.
[66] G. Besagni, R. Mereu, P. Chiesa, and F. Inzoli, "An Integrated Lumped Parameter-CFD approach for off-design ejector performance evaluation," *Energy Convers. Manag.*, vol. 105, pp. 697–715, 2015.
[67] X. Wang and J. Yu, "An investigation on the component efficiencies of a small two-phase ejector," *Int. J. Refrig.*, vol. 71, pp. 26–38, 2016.
[68] F. Liu and E. A. Groll, "Study of ejector efficiencies in refrigeration cycles," *Appl. Therm. Eng.*, vol. 52, no. 2, pp. 360–370, 2013.
[69] P. Haghparast, M. V. Sorin, and H. Nesreddine, "The impact of internal ejector working characteristics and geometry on the performance of a refrigeration cycle," *Energy*, vol. 162, pp. 728–743, 2018.
[70] K. Sumeru, H. Nasution, and F. N. Ani, "A review on two-phase ejector as an expansion device in vapor compression refrigeration cycle," *Renew. Sustain. Energy Rev.*, vol. 16, no. 7, pp. 4927–4937, 2012.
[71] K. J. Chua, Sk. Chou, and W. M. Yang, "Advances in heat pump systems: A review," *Appl. Energy*, vol. 87, no. 12, pp. 3611–3624, 2010.
[72] Y. Zhu, Y. Li, and W. Cai, "Control oriented modeling of ejector in anode gas recirculation solid oxygen fuel cell systems," *Energy Convers. Manag.*, vol. 52, no. 4, pp. 1881–1889, 2011.
[73] M. M. Rashidi, A. Aghagoli, and R. Raoofi, "Thermodynamic analysis of the ejector refrigeration cycle using the artificial neural network," *Energy*, vol. 129, pp. 201–215, 2017.
[74] E. Bellos and C. Tzivanidis, "Optimum design of a solar ejector refrigeration system for various operating scenarios," *Energy Convers. Manag.*, vol. 154, pp. 11–24, 2017.
[75] C. Lin, W. Cai, Y. Li, J. Yan, and Y. Hu, "Pressure recovery ratio in a variable cooling loads ejector-based multi-evaporator refrigeration system," *Energy*, vol. 44, no. 1, pp. 649–656, 2012.
[76] Y. Wu, H. Zhao, C. Zhang, L. Wang, and J. Han, "Optimization analysis of structure parameters of steam ejector based on CFD and orthogonal test," *Energy, 151, pp.79-93*.
[77] M. Haida *et al.*, "System model derivation of the CO 2 two-phase ejector based on the CFD-based reduced-order model," *Energy, 144, pp.941-956*.
[78] L. I. Bing, P. ZHeng, and J. Qin, "CFD simulation of two-phase ejector performance influenced by different operation conditions," *Energy, 155, pp.1129-1145*.

[79] S. Varga, A. C. Oliveira, X. Ma, S. A. Omer, W. Zhang, and S. B. Riffat, "Experimental and numerical analysis of a variable area ratio steam ejector," *Int. J. Refrig.*, vol. 34, no. 7, pp. 1668–1675, 2011.
[80] K. Banasiak and A. Hafner, "1D Computational model of a two-phase R744 ejector for expansion work recovery," *Int. J. Therm. Sci.*, vol. 50, no. 11, pp. 2235–2247, 2011.
[81] D. Scott, Z. Aidoun, and M. Ouzzane, "An experimental investigation of an ejector for validating numerical simulations," *Int. J. Refrig.*, vol. 34, no. 7, pp. 1717–1723, 2011.
[82] F. Mazzelli, F. Giacomelli, and A. Milazzo, "CFD modeling of condensing steam ejectors: Comparison with an experimental test-case," *Int. J. Therm. Sci.*, vol. 127, pp. 7–18, 2018.
[83] J. Chen, H. Havtun, and B. Palm, "Conventional and advanced exergy analysis of an ejector refrigeration system," *Appl. Energy*, vol. 144, pp. 139–151, 2015.
[84] B. M. Ziapour and A. Abbasy, "First and second laws analysis of the heat pipe/ejector refrigeration cycle," *Energy*, vol. 35, no. 8, pp. 3307–3314, 2010.
[85] H. Ghaebi, T. Parikhani, H. Rostamzadeh, and B. Farhang, "Thermodynamic and thermoeconomic analysis and optimization of a novel combined cooling and power (CCP) cycle by integrating of ejector refrigeration and Kalina cycles," *Energy*, vol. 139, pp. 262–276, 2017.
[86] I. W. Eames, A. E. Ablwaifa, and V. Petrenko, "Results of an experimental study of an advanced jet-pump refrigerator operating with R245fa," *Appl. Therm. Eng.*, vol. 27, no. 17, pp. 2833–2840, 2007.
[87] M. Trela, R. Kwidzinski, D. Butrymowicz, and J. Karwacki, "Exergy analysis of two-phase steam–water injector," *Appl. Therm. Eng.*, vol. 30, no. 4, pp. 340–346, 2010.
[88] A. Arbel, A. Shklyar, D. Hershgal, M. Barak, and M. Sokolov, "Ejector irreversibility characteristics," *J. Fluids Eng.*, vol. 125, no. 1, pp. 121–129, 2003.
[89] S. Croquer, S. Poncet, and Z. Aidoun, "Turbulence modeling of a single-phase R134a supersonic ejector. Part 1: Numerical benchmark," *Int. J. Refrig.*, vol. 61, pp. 140–152, 2016.
[90] M. Khennich, M. Sorin, and N. Galanis, "Exergy Flows inside a One Phase Ejector for Refrigeration Systems," *Energies*, vol. 9, no. 3, p. 212, 2016.
[91] M. Hamzaoui, H. Nesreddine, Z. Aidoun, and M. Balistrou, "Experimental study of a low grade heat driven ejector cooling system using the working fluid R245fa," *International Journal of Refrigeration, 86, pp.388-400.*
[92] F. Mazzelli and A. Milazzo, "Performance analysis of a supersonic ejector cycle working with R245fa," *Int. J. Refrig.*, vol. 49, pp. 79–92, 2015.
[93] P. Petr and G. Raabe, "Evaluation of R-1234ze (Z) as drop-in replacement for R-245fa in Organic Rankine Cycles–From thermophysical properties to cycle performance," *Energy*, vol. 93, pp. 266–274, 2015.
[94] S. Elbel and P. Hrnjak, "Experimental validation of a prototype ejector designed to reduce throttling losses encountered in transcritical R744 system operation," *Int. J. Refrig.*, vol. 31, no. 3, pp. 411–422, 2008.
[95] Palacz, M., Smolka, J., Kus, W., Fic, A., Bulinski, Z., Nowak, A.J., Banasiak, K. and Hafner, A., 2016. CFD-based shape optimisation of a CO2 two-phase ejector mixing section. Applied Thermal Engineering, 95, pp.62-69.
[96] N. B. Sag, H. K. Ersoy, A. Hepbasli, and H. S. Halkaci, "Energetic and exergetic comparison of basic and ejector expander refrigeration systems operating under the same external conditions and cooling capacities," *Energy Convers. Manag.*, vol. 90, pp. 184–194, 2015.

[97] Banasiak, K., Palacz, M., Hafner, A., Buliński, Z., Smołka, J., Nowak, A.J. and Fic, A., 2014. A CFD-based investigation of the energy performance of two-phase R744 ejectors to recover the expansion work in refrigeration systems: an irreversibility analysis. International Journal of Refrigeration, 40, pp.328-337.

[98] D. A. Dokandari, A. S. Hagh, and S. M. S. Mahmoudi, "Thermodynamic investigation and optimization of novel ejector-expansion CO_2/NH_3 cascade refrigeration cycles (novel CO_2/NH_3 cycle)," *Int. J. Refrig.*, vol. 46, pp. 26–36, 2014.

[99] Y. Bartosiewicz, Z. Aidoun, P. Desevaux, and Y. Mercadier, "Numerical and experimental investigations on supersonic ejectors," *Int. J. Heat Fluid Flow*, vol. 26, no. 1, pp. 56–70, 2005.

[100] T. Sriveerakul, S. Aphornratana, and K. Chunnanond, "Performance prediction of steam ejector using computational fluid dynamics: Part 1. Validation of the CFD results," *Int. J. Therm. Sci.*, vol. 46, no. 8, pp. 812–822, 2007.

[101] A. Selvaraju and A. Mani, "Analysis of an ejector with environment friendly refrigerants," *Appl. Therm. Eng.*, vol. 24, no. 5, pp. 827–838, 2004.

[102] M. Boulenouar and A. Ouadha, "CFD-Exergy analysis of the flow in a supersonic steam ejector," in *Journal of Physics: Conference Series*, 2015, vol. 574, p. 012123.

[103] G. Besagni, R. Mereu, G. Di Leo, and F. Inzoli, "A study of working fluids for heat driven ejector refrigeration using lumped parameter models," *Int. J. Refrig.*, vol. 58, pp. 154–171, 2015.

[104] P. Haghparast, M. V. Sorin, and H. Nesreddine, "Effects of component polytropic efficiencies on the dimensions of monophasic ejectors," *Energy Convers. Manag.*, vol. 162, pp. 251–263, 2018.

[105] P. Haghparast, M. V. Sorin, and H. Nesreddine, "Effect of Assumptions of Normal Shock Location on the Design of Supersonic Ejectors for Refrigeration," *Int. J. Mech. Mechatron. Eng.*, vol. 12, no. 3, pp. 255–264, 2018.

[106] Bao, J., Lin, Y. and He, G., 2017. Working fluids comparison and thermodynamic analysis of a transcritical power and ejector refrigeration cycle (TPERC). International Journal of Refrigeration, 82, pp.262-272.

[107] J. Lee, C. Lee, S. Baek, and S. Jeong, "Investigation of ejector-equipped Joule–Thomson refrigerator operating below 77 K," *Int. J. Refrig.*, vol. 78, pp. 93–107, 2017.

[108] Z. Ma, H. Bao, and A. P. Roskilly, "Thermodynamic modelling and parameter determination of ejector for ejection refrigeration systems," *Int. J. Refrig.*, vol. 75, pp. 117–128, 2017.

[109] G. Besagni, R. Mereu, F. Inzoli, and P. Chiesa, "Application of an integrated lumped parameter-CFD approach to evaluate the ejector-driven anode recirculation in a PEM fuel cell system," *Appl. Therm. Eng.*, vol. 121, pp. 628–651, 2017.

[110] NIST-REFPROP, v9.1., "NIST (2013). NIST Reference Fluid Thermodynamic and Transport Properties -REFPROP, v9.1." 2013.

[111] W. Sun, X. Yue, and Y. Wang, "Exergy efficiency analysis of ORC (Organic Rankine Cycle) and ORC-based combined cycles driven by low-temperature waste heat," *Energy Convers. Manag.*, vol. 135, pp. 63–73, 2017.

[112] R. Kheiri, H. Ghaebi, M. Ebadollahi, and H. Rostamzadeh, "Thermodynamic modeling and performance analysis of four new integrated organic Rankine cycles (A comparative study)," *Appl. Therm. Eng.*, vol. 122, pp. 103–117, 2017.

[113] G. Besagni, R. Mereu, and F. Inzoli, "Ejector refrigeration: a comprehensive review," *Renew. Sustain. Energy Rev.*, vol. 53, pp. 373–407, 2016.

[114] J. Wang, Z. Yan, M. Wang, S. Ma, and Y. Dai, "Thermodynamic analysis and optimization of an (organic Rankine cycle) ORC using low grade heat source," *Energy*, vol. 49, pp. 356–365, 2013.

[115] Y. Dai, J. Wang, and L. Gao, "Parametric optimization and comparative study of organic Rankine cycle (ORC) for low grade waste heat recovery," *Energy Convers. Manag.*, vol. 50, no. 3, pp. 576–582, 2009.

[116] S. Seyedkavoosi, S. Javan, and K. Kota, "Exergy-based optimization of an organic Rankine cycle (ORC) for waste heat recovery from an internal combustion engine (ICE)," *Appl. Therm. Eng.*, vol. 126, pp. 447–457, 2017.

[117] J. Wang, Z. Yan, M. Wang, M. Li, and Y. Dai, "Multi-objective optimization of an organic Rankine cycle (ORC) for low grade waste heat recovery using evolutionary algorithm," *Energy Convers. Manag.*, vol. 71, pp. 146–158, 2013.

[118] J. Sun and W. Li, "Operation optimization of an organic Rankine cycle (ORC) heat recovery power plant," *Appl. Therm. Eng.*, vol. 31, no. 11, pp. 2032–2041, 2011.